Institut für Theoretische Teilchenphysik

Fakultät für Physik

Karlsruher Institut für Technologie

Extra doublets

Global analyses of Standard Model extensions
in the fermionic or scalar sector

Des is wia bei jeda Wissenschaft,
am Schluss stellt sich dann heraus,
dass alles ganz anders war.

(Karl Valentin)

Contents

CHAPTER 1

Introduction

In the first half of the past century, progress in particle physics was driven by experimental results which physicists struggled to explain with one fundamental theory. In the second half, local gauge symmetries emerged as guiding principle to construct renormalisable relativistic quantum field theories, which finally led to the Standard Model of particle physics (SM). The SM describes three of the four fundamental interactions: the strong and weak nuclear force as well as electromagnetism. Only gravity, the weakest of the interactions, could not be embedded into the framework of a renormalisable quantum field theory up to now. The SM as formulated in the 1970s relies on a special mechanism for generating the masses of the elementary particles [1–3]. However, this mechanism requires at least one particle that had not been discovered until recently [4, 5]: the Higgs boson. Even though most experiments in the following decades featured an impressive consistency with the SM, it remained incomplete without the detection of this postulated particle.

In 2011, when I started working on this PhD thesis, the detectors at the Large Hadron Collider (LHC) at CERN had started to take data, but there was no evidence of the Higgs boson so far. However, several results obtained at the Tevatron collider and other experiments seemed to hint at deviations from the SM, e.g. the measurement of the top quark forward-backward asymmetry, the like-sign dimuon charge asymmetry or the magnetic dipole moment of the muon, to mention some of them. Also cosmological observations like dark matter, the baryon asymmetry in the universe or dark energy cannot be explained within the framework of the SM. Furthermore, the SM does not offer solutions to theoretical issues like the hierarchy problem, the unification of the gauge couplings or the origin of the fermion mass hierarchy. On the search for alternatives, many new models have been discussed. They need to have the SM as an effective "low energy" limit in order to describe experimental findings. On the other hand a new model has to solve one or more of the shortcomings of the SM. Most of these SM extensions involve additional particles, which have large masses or small couplings to the SM particles to avoid effects on the measured observables that agree with the SM. These properties, however, make it difficult to verify or falsify the theories beyond the SM, especially if many free parameters are introduced.

In the first part of this thesis I examine a model that stands out not due to its elegance from theoretical perspective but rather due to its simplicity: the Standard Model extended by a perturbative fourth fermion generation (SM4). Contrary to more complex models like supersymmetry, the SM4 is comparably easy to assess because it only has few additional free parameters, which could potentially be determined at the LHC. Compared to the SM, the SM4 features additional $\mathcal{CP}$ violating phases, which were discussed as possible contributions to the asymmetry between the existing matter and antimatter in our universe [6].
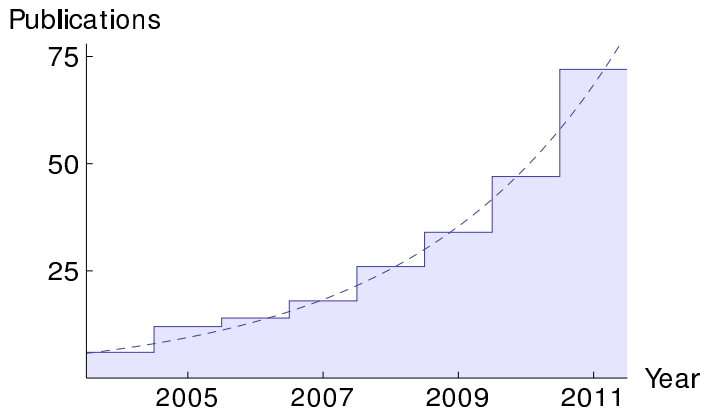
Figure 1.1: The yearly amount of publications about the SM4 between 2004 and 2011 can be described by an exponential function (dashed line).

There have been attempts to explain certain flavour measurements with fourth generation particles [7, 8], and the SM4 neutrinos could even contribute to dark matter [9, 10]. The increased interest in the SM4 since 2004 is illustrated in Fig. 1.1: For each year, I show the number of particle physics publications containing either "fourth generation", "4th generation", "fourth family", or "4th family" in their title [11]. The popularity growth can be approximated by an exponential function.

But then the first LHC results in 2011 and 2012 revealed that the missing piece of the SM had been found: the discovery of a bosonic resonance in the $\gamma\gamma$ and *ZZ* invariant mass distribution was probably the most exciting event in particle physics in many years. The properties of this new particle are in good agreement with the predictions for the SM Higgs boson, which imposes strong constraints on many SM extensions. The SM4 happens to be the first popular model that can even be ruled out on the basis of these measurements. To quantify whether a model is excluded or not, one has to carry out a global analysis of its possible parameter constellations, taking into account all relevant experimental constraints, and compare it with the SM using a likelihood ratio test. Due to the interplay of different observables this comparison is usually non-trivial; for the SM4 it is even more complicated, because it does not decouple from the SM. Therefore, my collaborators and I have performed a likelihood ratio test for non-nested models combining Higgs observables and electroweak precision data, and eventually excluding the SM4 [12].

Similar to the extension of the fermionic SM content by a quark and a lepton doublet, one can add a second scalar doublet to its Higgs sector. This so-called Two-Higgs-Doublets model (2HDM) can arise as effective theory from several models, like for instance supersymmetry. I will explain in the second part of this thesis that the 2HDM parameters are also severely constrained by electroweak precision observables as well as LHC and flavour measurements. However, the 2HDM has a decoupling limit and cannot be ruled out completely like the SM4.

The SM4 and the 2HDM are comparably simple modifications of the SM; nevertheless, the correct statistical treatment of a model comparison is non-trivial. Therefore, I first want to explain the statistical tools that I need in Chapter 2, and discuss the Standard Model of particle physics in Chapter 3. Only then I am prepared to introduce new models

and to compare them with the SM. This is done in Chapter 4 for the SM4 and in Chapter 5 for the 2HDM, before I conclude in Chapter 6.

CHAPTER 2

Statistics

The challenge of theoretical particle physics is to develop a model that describes all observed phenomena as well as possible and serves to predict the outcome of future experiments. With the Standard Model we already have a powerful theory, but there are a few aspects that indicate that it is only an effective limiting case of a more fundamental theory. Many SM extensions with different virtues have been formulated, of which one might be realized, whereas the others sooner or later will be ruled out by experiments. When we now consider one of these new theoretical models, we want to make a statement on how compatible experimental measurements are with it, and furthermore we want to test the new model against the conventional model, which in our case is the SM. In the frequentist approach – the statistical method that I have chosen for this work – this model comparison is done by means of a likelihood ratio test. It provides us with a *p*-value (also called statistical significance) which tells us to which level a model is excluded. After reviewing the foundations of frequentist statistics following [13–16], I will introduce the likelihood ratio test (referring to the discussion in [15]) and its statistical interpretation in Sect. 2.3, and then address two important aspects in our analyses, the treatment of systematic errors and non-nested model comparisons, in Sect. 2.4 and 2.6.

2.1 The likelihood

A theoretical model is characterized by its model parameters ξ_j $(j = 1, ..., N_\xi)$, which can only be determined by experimental observations. Let us assume that there are N_X observables X_i $(i = 1, ..., N_X)$ with a certain probability density function (p.d.f.) $f_i(x_i^{\text{exp}}, \xi)$. Let us further assume that we have the measurements x_i^{exp} of the observables X_i. The probability that one measurement is between x and $x + \mathrm{d}x$ is given by $f_i(x, \xi)\mathrm{d}x$. Adopting vector notation, I can write the joint p.d.f. of all measurements as $f(\mathbf{x}^{\text{exp}}, \xi)$. For a certain set of measurements $\mathbf{x}_0^{\text{exp}}$, we can define the likelihood as

$$L(\xi) = f(\mathbf{x}_0^{\text{exp}}, \xi).\qquad(2.1)$$

If all measurements are statistically independent, we can write the likelihood as the product of the individual p.d.f.s:

$$L(\xi) = \prod_{i=1}^{N_X} f_i(x_{0,i}^{\text{exp}}, \xi)$$

In order to test the compatibility of the model with the experimental results, we must try to bring the theoretical predictions into agreement with the measurements by adapting the parameters. The most popular method to do this is the maximization of the likelihood with respect to the model parameters. I want to refer to this procedure as *fit* in the following and call the parameters which maximize the likelihood *best-fit parameters* $\boldsymbol{\xi}_{\mathsf{bf}}$.

2.2 Gaussian distributions

One essential property of experiments in particle physics is that we cannot obtain reliable information from a single measurement, but rather have to measure many times to extract the p.d.f. of an observable. If it is an average of a large number of measurements, the observable X_i will commonly have a Gaussian p.d.f. with the statistical error σ_i as standard deviation around the central value μ_i. If there are n different measurements $x_{i,k}^{\mathsf{exp}}$ for one observable X_i, where k is between 1 and n, this corresponds to n draws of the same random variable. They can be combined to the average $x_{i,\mathrm{comb}}^{\mathsf{exp}}$. This average itself can be interpreted as Gaussian distributed random variable with error $\sigma_{i,\mathrm{comb}}$. The average and its error can be computed in the following way [13]: To each $x_{i,k}^{\mathsf{exp}}$, we assign a *weight* $w_{i,k}$, which is defined as the inverse squared error:

$$w_{i,k} = \frac{1}{\sigma_{i,k}^2}$$

The combined statistical error shrinks according to

$$\sigma_{i,\mathrm{comb}} = \left(\sum_{k=1}^{n} w_{i,k} \right)^{-\frac{1}{2}}, \tag{2.2}$$

which means that the combined standard deviation decreases by $1/\sqrt{n}$, if the number of equivalent measurements with equal weights is increased by the factor n. For an estimate of the central value of this combination, all individual $x_{i,k}^{\mathsf{exp}}$ are weighted:

$$x_{i,\mathrm{comb}}^{\mathsf{exp}} = \sigma_{i,\mathrm{comb}}^2 \sum_{k=1}^{n} w_{i,k} x_{i,k}^{\mathsf{exp}} \tag{2.3}$$

Inverting these relations, one can also reconstruct information about parts of the combination.

On the theory side, the true value of the observable X_i can be described by the function $x_i^{\mathsf{theo}}(\boldsymbol{\xi})$, assuming the realization of a particular theory. If this assumption is correct, $x_i^{\mathsf{theo}}(\boldsymbol{\xi})$ will coincide with the central value μ_i of the p.d.f. In the N_X-dimensional space of observables the images of the expressions $\mathbf{x}^{\mathsf{theo}}(\boldsymbol{\xi})$ form the so-called theory manifold $\mathcal{M}$.

For every Gaussian distributed observable, we can calculate the *deviation*, which is the difference between the measured value and the theoretical expression around the best-fit point, normalized to the experimental error:

$$\chi_i(\boldsymbol{\xi}) = \frac{x_i^{\mathsf{exp}} - x_i^{\mathsf{theo}}(\boldsymbol{\xi})}{\sigma_i} \tag{2.4}$$

With this definition a one-dimensional Gaussian distribution (normal distribution) is given by the function

$$f_G(x_i^{exp}, x_i^{theo}(\xi), \sigma_i) = \frac{1}{\sqrt{2\pi}\sigma_i} \exp\left[-\frac{1}{2}\chi_i^2\right]. \tag{2.5}$$

This p.d.f. is depicted in Fig. 2.1(a) for $x_i^{theo} = 0$ and $\sigma_i = 1$. Some experiments also have an asymmetric Gaussian distribution, which is characterized by different lower and upper Gaussian errors σ_l and σ_u:

$$f_{aG}(x^{exp}, x^{theo}(\xi), \sigma_l, \sigma_u) = \begin{cases} \dfrac{2\sigma_l}{\sigma_l + \sigma_u} f_G(x^{exp}, x^{theo}(\xi), \sigma_l), & \text{if } x^{exp} < x^{theo}(\xi) \\ \dfrac{2\sigma_u}{\sigma_l + \sigma_u} f_G(x^{exp}, x^{theo}(\xi), \sigma_u), & \text{if } x^{exp} \geq x^{theo}(\xi) \end{cases}$$

An example is shown in Fig. 2.1(b). If we want to determine the deviation of an observable with an asymmetric Gaussian, we have to choose the appropriate error in the denominator of Eq. (2.4) according to the sign of the difference $x^{exp} - x^{theo}(\xi)$.
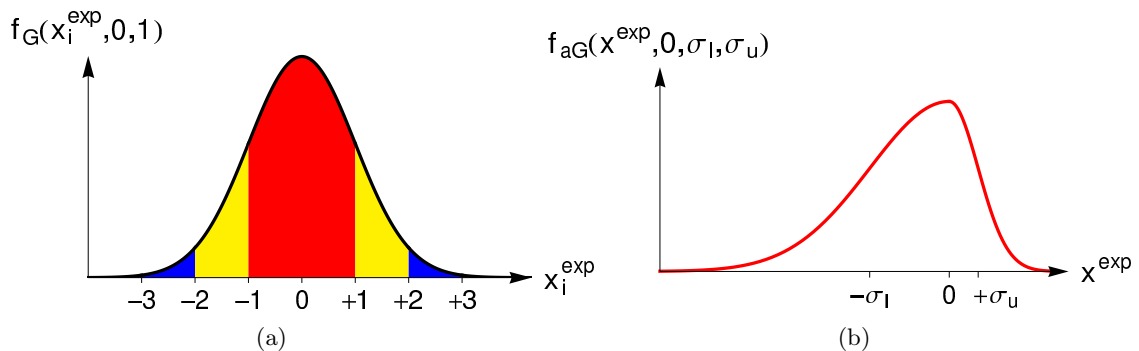
Figure 2.1: The symmetric Gaussian distribution is shown with a standard deviation of 1 (a). The lower standard deviation σ_l and the upper standard deviation σ_u of an asymmetric Gaussian distribution have different values (b). The central value was chosen to be 0 for both.

For multi-dimensional Gaussian distributions, we need to take into account the correlations between different observables: In general, all observables x_i^{theo} depend on the same set of parameters. Changing the value of a parameter to diminish the squared deviation of one observable and to increase the total likelihood also affects the other observables and their deviations. Around the best-fit point, this correlation is quantified by the covariance matrix V_c, which is the inverse of the Hessian matrix of the negative logarithm of the likelihood:

$$(V_c^{-1})_{nm} = -\left.\frac{\partial^2 \ln L(\xi)}{\partial \xi_n \partial \xi_m}\right|_{\xi_{bf}}.$$

The quadratic expansion of the likelihood around the maximum is proportional to

$$\chi^2(\boldsymbol{\xi}, \mathbf{x}^{\mathsf{exp}}) = \boldsymbol{\chi}^T(\boldsymbol{\xi}) V_c^{-1} \boldsymbol{\chi}(\boldsymbol{\xi}),$$

which can be minimized instead of maximizing the likelihood. For independent observables, $V_c = \mathbb{1}$, the χ^2 is equal to the sum of the squared deviations, and the likelihood is the product of the individual Gaussian p.d.f.s.

The minimal χ^2 of a fit, which I will call χ^2_{min}, is a common measure of how well $\boldsymbol{\xi}$ describes the data $\mathbf{x}^{\mathsf{exp}}$. Often, a first estimate of how well a theory performs is given by the minimal χ^2 per degree of freedom, $\chi^2_{\mathsf{min}}/N_{\mathsf{dof}}$. The number of degrees of freedom N_{dof} is given by the difference $N_X - N_\xi$ if we do not artificially constrain $\boldsymbol{\xi}$ in the fit. By definition, N_{dof} is only positive if we have more observables than fit parameters; a system like that is called overconstrained and all parameters can be fixed by the experimental inputs in a fit. Since the expectation value of the deviation is 1, the expected outcome of the fit will be $\chi^2_{\mathsf{min}}/N_{\mathsf{dof}} \approx 1$ if we have many observables which are described well by the theory. The best-fit parameter values $\boldsymbol{\xi}_{\mathsf{bf}}$ for which the χ^2 is minimal will become important in the next section. Moreover, it is of interest how large the "allowed" ranges for the parameters and observables around their best-fit values are. I will also come back to these so-called confidence intervals in the next section.

As defined in Eq. (2.4), the deviation is the minimal difference between $x_i^{\mathsf{theo}}(\boldsymbol{\xi})$ and x_i^{exp}, i.e. the deviation of the best-fit point of a *complete* fit using all N_X measurements x_i^{exp}. One can also use the first $N_X - 1$ observables to predict the last one; I will refer to this method as *prediction*. The χ^2_{min} difference $\Delta\chi^2$ between the complete fit and the prediction fit gives us a measure of how large the impact of the measurement of X_{N_X} on the model fit is. Note that $\Delta\chi^2$ and the squared deviation $\chi^2_{N_X}$ are not the same because other observables will in general have a different best-fit deviation in the prediction fit and in the complete fit.

An example in particle physics for a parameter determination with the help of a prediction fit is the Higgs boson mass: Before this last missing parameter of the SM was measured directly in 2012 as mentioned in the introduction, there had been fits that could exclude the Higgs mass outside a certain confidence interval. So under the assumption that the Standard Model was true, experimentalists knew in which mass region to search.

2.3   The likelihood ratio test

Instead of leaving out or adding information on the experimental side, we can also add new parameters or fix existing ones, hence change the theory. This is especially useful, if we have a model that we do not doubt in general, and we want to check whether a particular realization could exist. Let us define a *constrained* theory B which differs from the *full* theory A by fixing ν of the parameters of A. To quantify the viability of B or to exclude it we need to perform a hypothesis test. Let us assume that B is realized for a given set of measurements $\mathbf{x}_0^{\mathsf{exp}}$ ("null hypothesis"). To compare the compatibility of the two models with these measurements we could use the ratio of their maximized likelihoods L_B^{max} and L_A^{max}.

Instead we can also use

$$S(\mathbf{x}^{\mathsf{exp}}) = -2 \ln \frac{L_B^{\mathsf{max}}}{L_A^{\mathsf{max}}}. \tag{2.6}$$

If $S(\mathbf{x}^{\mathsf{exp}})$ is greater than a predefined value S_0, we will reject the null hypothesis and accept A as realized. Therefore, this hypothesis test is called *likelihood ratio test*. $S(\mathbf{x}^{\mathsf{exp}})$ is a random variable called *test statistic* and is itself characterized by a p.d.f. Since A has more free parameters, L_A^{max} cannot be smaller than L_B^{max}, and $S(\mathbf{x}^{\mathsf{exp}})$ is positive semi-definite. Usually, one chooses the rejection condition S_0 to be $S(\mathbf{x}_0^{\mathsf{exp}})$, i.e. the value the test statistic would take if B was realized with its best-fit parameters $\boldsymbol{\xi}_{\mathsf{bf},B}$ for $\mathbf{x}_0^{\mathsf{exp}}$ and if A was realized with the best-fit parameters of B and the last ν parameters fitted to $\mathbf{x}_0^{\mathsf{exp}}$. If we denote the p.d.f. of the test statistic by $f_{\mathsf{ts}}(\mathbf{x}^{\mathsf{exp}}, \boldsymbol{\xi}_{\mathsf{bf},B})$, we can calculate the probability for wrongly rejecting B, which is called the *p*-value, by the integration of $f_{\mathsf{ts}}(\mathbf{x}^{\mathsf{exp}}, \boldsymbol{\xi}_{\mathsf{bf},B})$ over the observable regions where B is rejected:

$$p = \int f_{\mathsf{ts}}(\mathbf{x}^{\mathsf{exp}}, \boldsymbol{\xi}_{\mathsf{bf},B}) \, \Theta \left(S(\mathbf{x}^{\mathsf{exp}}) - S_0 \right) \mathrm{d}^{N_X} x^{\mathsf{exp}} \tag{2.7}$$

Θ denotes the Heaviside step function. In our calculations, the measurements $\mathbf{x}^{\mathsf{exp}}$ will be simulated toy measurements, and the integration is done numerically.

If we want to depict the calculation of the *p*-value, it is convenient to modify the observable space: In the N_X dimensional observable space we can always find a transformation such that in the new coordinate system $\mathbf{x}_0^{\mathsf{exp}} - \mathbf{x}^{\mathsf{theo},B}(\boldsymbol{\xi}_{\mathsf{bf},B})$ is mapped to the origin with $\sigma_i^{\mathsf{exp}} = 1$ and $V_c = \mathbb{1}$. $\mathcal{M}_A'$ and $\mathcal{M}_B'$ are the theory manifolds of A and B in the transformed space of observables. By definition, $\mathcal{M}_A' \supset \mathcal{M}_B'$ (because B is A with ν parameters fixed), and both contain the origin. If $\mathbf{y}$ is the transformed vector of observables $\mathbf{x}^{\mathsf{exp}}$, we can write the transformed test statistic as $S(\mathbf{y})$. Under the assumption that $\mathcal{M}_A'$ and $\mathcal{M}_B'$ are hyperplanes, $|\mathbf{y}|^2$ is simply the squared distance between the (toy) measurements and the best-fit value of model B, corresponding to the squared deviation χ_i^2 in one dimension. Defining $\mathbf{y}_2$ as the orthogonal part to $\mathcal{M}_B'$ of the projection of $\mathbf{y}$ on $\mathcal{M}_A'$, the test statistic reads $S(\mathbf{y}) = |\mathbf{y}_2|^2$. The *p*-value is now the integral over the $\mathbf{y}$ regions, where $S(\mathbf{y}) > S_0$, i.e. outside an infinitely long "hyper-cylinder" around $\mathcal{M}_B'$. As illustration I show a three-dimensional projection of the observable space with a two-dimensional $\mathcal{M}_A'$ and a one-dimensional $\mathcal{M}_B'$ in Fig. 2.2.

I will resort to this picture of the transformed observable space in Sect. 2.6 when I want to discuss the case where B does not emerge from A by fixing some parameters.

If all measurements have a Gaussian p.d.f., the test statistic directly translates into the difference $\chi_{\mathsf{min},B}^2 - \chi_{\mathsf{min},A}^2$ of the respective minimal χ^2 values of the models:

$$S(\mathbf{x}^{\mathsf{exp}}) = \chi_{\mathsf{min},B}^2 - \chi_{\mathsf{min},A}^2 \tag{2.8}$$

The test statistic is distributed according to a χ^2 distribution, and

$$p = \frac{1}{\Gamma(\nu/2)} \int\limits_{S(\mathbf{x}_0^{\mathsf{exp}})}^{\infty} \varsigma^{\frac{\nu}{2}-1} e^{-\varsigma} \mathrm{d}\varsigma. \tag{2.9}$$
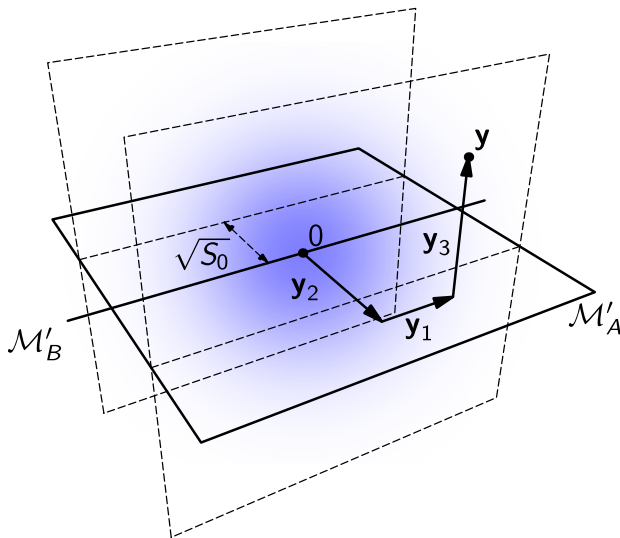
Figure 2.2: Nested models in three dimensions (graphic from [15]). The blue shaded region indicates the p.d.f. of the toy measurements. The dashed planes are the boundaries for the model rejection of *B*.

Commonly, the *p*-value is calculated analytically with this formula in theoretical particle physics. This implies three assumptions [15]: The theory expressions should be linear in the vicinity of the measurements, i.e. the theory manifold should be approximately a hyperplane, such that the closest point to some $\mathbf{x}^{\text{exp}}$ is unique. Next, the p.d.f.s should be of Gaussian shape. And the last important condition, which I want to discuss in Sect. 2.6, is that the constrained theory *B* should be embedded in the full theory *A*. Only if these requirements are met, $S(\mathbf{x}_0^{\text{exp}})$ is given by Eq. (2.8) and can be converted into a *p*-value by Eq. (2.9). This is known under the name Wilks' theorem [17]. In the following, I will refer to this simplification as *naive p*-value. The use of Wilks' theorem is common practice in theoretical particle physics even though the applicability in some cases is questionable. Visualizing Eq. (2.9) in one dimension in the observable space, the *p*-value can be identified with the integral over the "tails" of a (Gaussian) distribution. On the contrary, the regions that are not part of the tails, cannot be excluded; they are the above-mentioned confidence intervals. This is illustrated by the different shaded regions of Fig. 2.1: while the red region corresponding to deviations smaller than 1 constitutes more than 68% of the integral over $f_G(x_i^{\text{exp}}, x_i^{\text{theo}}, \sigma_i)$, scenarios with large deviations only contribute little to the total integrated surface. According to their maximal deviation the red, yellow and blue shaded regions are referred to as 1σ, 2σ and 3σ regions. I will use the same colour coding in the figures of the next chapters. Stating that a parameter value is excluded at a certain confidence level CL – where CL is between 0% and 100% – connotes that the corresponding *p*-value is less than $1-$CL. But this does not only hold for single parameters. By analogy with the one-dimensional Gaussian case, the *p*-value for multi-dimensional problems is also commonly translated into a "σ" statement: One can claim to exclude model *B* at $n\sigma$ if its *p*-value corresponds to the one-dimensional picture of the integrated area under the Gaussian tails where $|\chi_i| > n$.

Observations in particle physics are also based on the hypothesis test idea: Defining a "background" model and a "signal plus background" model, one can also exclude the

former, hence claiming an observation. Over the last decades, certain exclusion and discovery levels evolved as a rule of thumb for particle physicists [16]: If a particular point is outside the 2σ boundary (which roughly corresponds to a confidence level of 95%), it is considered to be disfavoured; everything outside the 3σ region appears to be excluded. For the decision between "signal plus background" and "background only", the criteria are a bit different: If a signal has a deviation of 3 from the background expectation, one speaks of an *evidence*; only if its deviation is 5 or more, one can claim a *discovery* (or *observation*).

The naive definition of the *p*-value usually gives a good approximation and I will use it to illustrate the confidence intervals of single observables and parameters throughout this thesis; however, for the comparison of two models differing in multiple aspects we rely on the correct formulation from Eq. (2.7), which holds for non-Gaussian p.d.f.s as well as non-linear theory manifolds. The only requirement that we maintain at this point is that *B* is *nested* in *A*, meaning that it is a constrained version of *A*. In Chapter 5, we will find exactly these circumstances when comparing the Two-Higgs-Doublets model to the SM. However, in Chapter 4, we will also need to calculate the *p*-value for non-nested theories. Before we discuss non-nested model comparisons, I want to go into detail about the treatment of systematic uncertainties.

2.4   Systematic uncertainties

Up to this point, we have only treated p.d.f.s of a Gaussian shape with statistical errors as standard deviation in detail. However, there are as well uncertainties which cannot be diminished by increasing the number of measurements according to Eq. (2.2). They can originate from the detectors, as for example detector calibration errors, and thus be part of the experimental error, but they also result from theory, as for instance uncertainties on lattice calculations. All these errors are offsets between the true value x_i^{theo} and the measured value x_i^{exp} of an observable which do not average out when the experiment is repeated. Irrespective of their origin, they can be subsumed under the name *systematic uncertainties*. In the *R*fit scheme [14], one introduces additional fit parameters, the so-called *nuisance parameters*, which account for systematic uncertainties in the following way: to each observable X_i with a systematic error σ_i^{syst}, we assign the nuisance parameter ξ_i^{ν}, which is allowed to float between -1 and 1, and add $\xi_i^{\nu} \cdot \sigma_i^{\mathsf{syst}}$ to x_i^{theo}. In Fig. 2.3, three different profile likelihood function are shown: the left one is an ordinary Gaussian distribution, the red line displays an observable without statistical error but with a systematic error, and the right curve illustrates the resulting profile likelihood of an observable which has both, statistical and systematic errors, when maximizing with respect to all ξ_i^{ν}.

The notation implies that all systematic errors (including experimental uncertainties) are converted into bounded theory parameters, where several systematic uncertainties adherent to one observable can be combined by adding them linearly.

The *R*fit method can also be used to limit parameters by relating them to an artificial observable with only a systematic error like in Fig. 2.3(b). On the one hand this can be useful to prevent masses from becoming negative or to limit angles to take values between 0 and 2π, but on the other hand this smears the definition of N_{dof} because the number of parameters can be arbitrarily increased with this method [16].
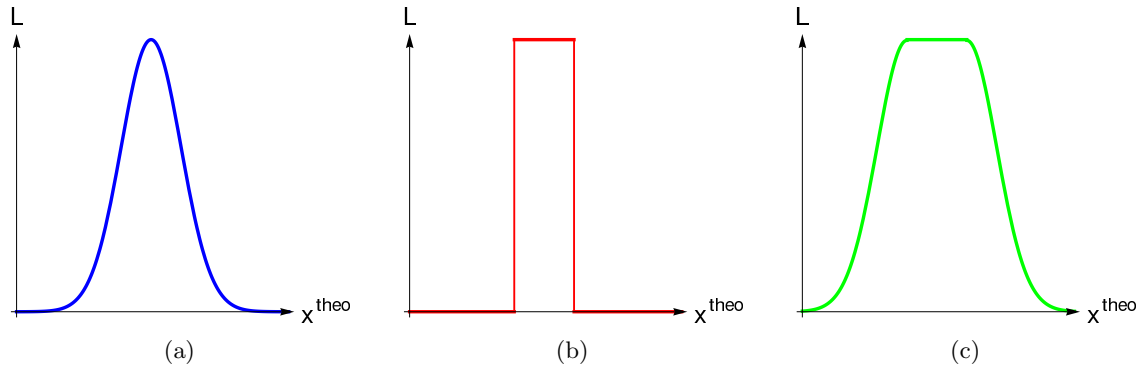
Figure 2.3: Three different likelihood profiles: the blue curve (a) is a Gaussian distribution, like in Fig. 2.1(a), the red line (b) displays a range of likelihood (Rfit with systematic error), and the green function (c) is the profile of a quantity with both, statistical and systematic errors.

2.5 CKMfitter

For the fits in this thesis I used the CKMfitter package [14], which is based on the Rfit method. The package is written in WOLFRAM Mathematica files; the minimization is outsourced to Fortran subroutines. A global parameter fit with CKMfitter usually involves two steps: the first is minimizing the χ^2 with respect to all parameters, and the optional second part is the scan over one or two parameters or observables. For the initial minimization, all parameters are treated as free within their allowed ranges, a certain number of starting points is randomly generated, and the χ^2 minimum is searched for using numerical gradients. (Analytical gradients are in principle supported but not applicable if the external routines come into play that I want to use.) For the one-dimensional scans, the specified range for the scan quantity is divided into N equally spaced points for each of which a "constrained" minimization is performed, in which the scan quantity is fixed. (N is the granularity defined by the user.) The same applies for two-dimensional scans, respectively. One important feature is that the scans do in general not start at one end of the scan range(s) but at the scan point that is closest to the best-fit point. All following scan steps use the χ^2 information of the previous step. Hence, one usually gains better convergence of the "constrained" fits in the sense that the minimum is found more reliably. Especially in two-dimensional fits this behaviour can be an advantage compared to plain "left-to-right" scanning. In spite of this virtue I wrote a program that parallelizes 2D scans by partitioning them into 1D scans, which reduces the scan time by a factor $1/N$, provided that one has the possibility to execute the parallelized scans on N processors at the same time. For details, see App. D. The duration of one fit plus scan procedure is from a second to several days, depending on the complexity of the theory expressions, on the external routines attached to the fitter, and on whether parallelization was used or not. I will comment on the performance of the single CKMfitter model implementations when discussing the combined fit results of the following chapters.

2.6   Non-nested models

If two models A and B are not nested, the determination of the p-value becomes more complicated. Like in Sect. 2.3, I will follow [15] to construct a definition based on a geometrical picture: Non-nestedness directly translates into the fact that one theory manifold is not a subset of the other. Let us again take B as the null hypothesis. The test statistic as defined in (2.6) is not positive semi-definite any longer, so we set $S = 0$ if $L_B^{max} > L_A^{max}$. Assuming Gaussian p.d.f.s, one can find a mapping of the observable space like in Sect. 2.3 such that in the new coordinate system $\mathbf{x}_0^{exp} - \mathbf{x}^{theo,B}(\xi_{bf,B})$ corresponds to the origin with $\sigma_i^{exp} = 1$ and $V_c = \mathbb{1}$. If we approximate $\mathcal{M}_B'$, the transformed theory manifold of model B, by its tangent hyperplane H_B' in the new observable space, the tangent hyperplane H_A' of $\mathcal{M}_A'$ will now not be a subset of it, nor vice versa. We can decompose the transformed vector of a (toy) measurement $\mathbf{y}$ into a parallel part $\mathbf{y}_\parallel$ and an orthogonal part $\mathbf{y}_3$ with respect to H_B' and further divide $\mathbf{y}_\parallel$ into $\mathbf{y}_1$ and $\mathbf{y}_2$, of which the latter is defined to be orthogonal to H_A'. Let Y_1, Y_2 and Y_3 be the corresponding subspaces and let $\mathbf{c}$ be the projection of $\mathbf{y}_A$ on Y_2, where $\mathbf{y}_A$ is any point on H_A'; then the distance of H_A' from the subspace Y_1 is given by $|\mathbf{c}|$. In Fig. 2.4, a three-dimensional example is given with H_A' being one-dimensional and a two-dimensional H_B'.
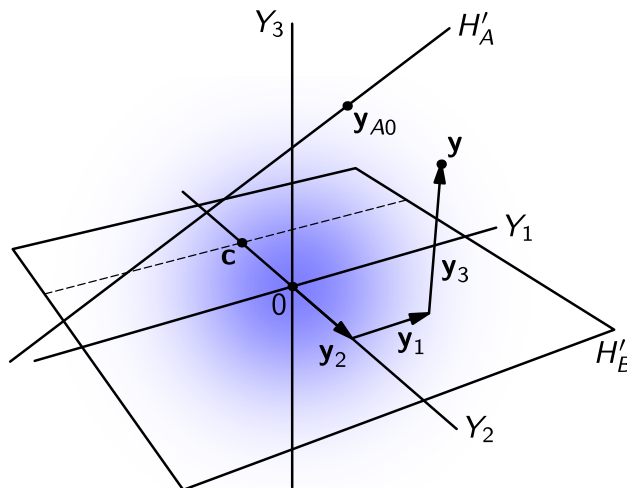
Figure 2.4: Non-nested models in three dimensions (graphic from [15]). The blue shaded region indicates the p.d.f. of the toy measurements.

The $\chi^2_{min,B}$ of theory B is now $|\mathbf{y}_3|^2$, but where in the nested case we would have $\chi^2_{min,A} = |\mathbf{y}_2|^2 + |\mathbf{y}_3|^2$, we now only get the lower bound of $|\mathbf{y}_2 - \mathbf{c}|^2$ for the minimal χ^2 of A, which is realized if $\mathbf{y} - (\mathbf{y}_2 - \mathbf{c})$ is on H_A'. So again requiring $S(\mathbf{y})$ to be smaller than some reference value S_0 we need to integrate over the regions where $|\mathbf{y}_3|^2 < S_0 + |\mathbf{y}_2 - \mathbf{c}|^2$, but this time there are also contributions of toy measurements with $|\mathbf{y}_3|^2 > S_0 + |\mathbf{y}_2 - \mathbf{c}|^2$ to the p-value integral in (2.7) because we only have a lower bound for $\chi^2_{min,A}$. (For instance, take the point $\mathbf{y}_{A0}$ on H_A' in Fig. 2.4: if the Y_3 components of $\mathbf{y}_{A0}$ have a different sign than the ones of a toy measurement $\mathbf{y}$, and at the same time their Y_1 and Y_2 components agree, the point will always be closer to H_B' than to H_A', regardless of whether $|\mathbf{y}_3|^2$ is smaller or greater than S_0.) The difficulty now is that these "special" regions are not as easy to

identify since their boundaries (where $S(\mathbf{y}) = S_0$) are curved, even though we made use of the linear approximation with hyperplanes. Therefore we need to specify a sampling density $\rho(\mathbf{x}_k^{\text{exp}})$ that is tuned to generate Monte Carlo integration points inside and outside the boundaries; the p-value expression for the original observable space then reads

$$p = \frac{1}{N} \sum_{k=1}^{N} \frac{f(\mathbf{x}_k^{\text{exp}}, \boldsymbol{\xi}_{\text{bf,B}})}{\rho(\mathbf{x}_k^{\text{exp}})} \, \Theta \left(S(\mathbf{x}_k^{\text{exp}}) - S_0 \right).$$

As our final formulation only depends on $S(\mathbf{x}_k^{\text{exp}})$ and not on χ^2 values, it is also valid if the p.d.f.s are not Gaussian. And dismissing the hyperplane approximation makes the problem harder to picture, but will not pose a problem to the numerical integration. To obtain a trustworthy result with small uncertainties within reasonable time, it is crucial how $\rho(\mathbf{x}_k^{\text{exp}})$ is chosen. In our fits we use a customized sampling density which is adjusted during the calculation.

The SM4 model, which I will discuss in Chapter 4, and the SM are not nested; furthermore, linearity is not satisfied and there are systematic errors involved. For our hypothesis test, we used Martin Wiebusch's program myFitter [15] to calculate the p-value. To test the performance of the SM4, we need to define our standard first. In particle physics this standard is the Standard Model which will be analyzed thoroughly in the following chapter. Only then we are able to discuss its extensions, where we will need to apply our knowledge about nestedness and linearity.

CHAPTER 3

The Standard Model

The Standard Model of particle physics (SM) describes three of the four fundamental interactions of all elementary particles we know. (A summary can e.g. be found in [18] and in [19].) It is based on an $SU(3) \otimes SU(2) \otimes U(1)$ gauge symmetry. The corresponding quantum numbers are the colour, the weak isospin I and the hypercharge Y, respectively. The gauge couplings are the strong coupling g_3, the weak coupling g_2, and the hypercharge coupling g_1. The particle content of the SM consists of elementary fermions and bosons, which transform according to the representations of the gauge groups shown in Table 3.1. The fermions can be divided into quarks and leptons, which transform in the fundamental and singlet representation of $SU(3)$, respectively. Left-handed quarks and leptons transform as $SU(2)$ doublets Q_j and L_j. For the right-handed fields, which are singlets under $SU(2)$ transformations, we differentiate between up-type quarks u_j on the one hand and down-type quarks d_j and the charged leptons ℓ_j on the other hand, which correspond to the $SU(2)$ isospin up and down components of the left-handed doublets. Originally, the neutrinos ν_j, which are the right-handed equivalent of the isospin up component of L_j, do not belong to the SM fields. However, I will treat them just like the other fermions as massive Dirac particles. The index j denotes the generation the fields are attributed to; the SM has three generations, which each consist of an $SU(2)$ doublet of an up-type and a down-type quark, and one containing a charged lepton and a neutrino, as well as the right-handed partners.

$$
\begin{array}{cccc}
 & j = 1 & j = 2 & j = 3 \\[4pt]
\text{Quark doublets:} & \begin{pmatrix} u \\ d \end{pmatrix}, & \begin{pmatrix} c \\ s \end{pmatrix}, & \begin{pmatrix} t \\ b \end{pmatrix} \\[14pt]
\text{Lepton doublets:} & \begin{pmatrix} \nu_e \\ e \end{pmatrix}, & \begin{pmatrix} \nu_\mu \\ \mu \end{pmatrix}, & \begin{pmatrix} \nu_\tau \\ \tau \end{pmatrix}
\end{array}
$$

To every fermion one can attribute a specific quantum number called *flavour*. Whereas the first generation would be sufficient to describe the constituents of atoms and thus explain most aspects of nature as we know it, for this work about high-energy physics primarily the heaviest fermions are of interest: the top quark t, the bottom quark b and the τ lepton.

In addition to the elementary fermions, the SM also contains elementary bosons: The gauge vector bosons G_3^a, G_2^a and G_1 transform as adjoint representations under $SU(3)$, $SU(2)$ and $U(1)$, respectively; they can be combined with the generators T_n^a of the nth

gauge group to form linear operators $\mathbf{G}_n = G_n^a T_n^a$ on some arbitrary representations. Finally, the Higgs field Φ is a complex scalar $SU(2)$ doublet.

Fermion	Representation	Boson	Representation
Q_j	$(\mathbf{3}, \mathbf{2}, 1/3)$	G_3^a	$(\mathbf{8}, \mathbf{1}, 0)$
u_j	$(\mathbf{3}, \mathbf{1}, 4/3)$	G_2^a	$(\mathbf{1}, \mathbf{3}, 0)$
d_j	$(\mathbf{3}, \mathbf{1}, -2/3)$	G_1	$(\mathbf{1}, \mathbf{1}, 0)$
L_j	$(\mathbf{1}, \mathbf{2}, -1)$	Φ	$(\mathbf{1}, \mathbf{2}, 1)$
ν_j	$(\mathbf{1}, \mathbf{1}, 0)$		
ℓ_j	$(\mathbf{1}, \mathbf{1}, -2)$		

Table 3.1: The elementary particles of the SM and their $SU(3)$ and $SU(2)$ representations and hypercharge.

The SM Lagrangian can be split into four parts:[1]

$$\mathcal{L}_{\mathrm{SM}} = \mathcal{L}_G + \mathcal{L}_F + \mathcal{L}_H + \mathcal{L}_Y$$

The first term contains the Yang-Mills Lagrangians of the gluons G_3^a, the weak bosons G_2^a, and G_1:

$$\mathcal{L}_G = -\frac{1}{4} \sum_{n=1}^{3} \mathrm{tr}\left[(\mathbf{F_n})_{\mu\nu}(\mathbf{F_n})^{\mu\nu}\right],$$

where the field strength tensors $(\mathbf{F}_n)^{\mu\nu}$ are defined as

$$(\mathbf{F}_n)^{\mu\nu} = \partial^\mu(\mathbf{G}_n)^\nu - \partial^\nu(\mathbf{G}_n)^\mu - \mathrm{i}g_n[\mathbf{G}_n^\mu, \mathbf{G}_n^\nu],$$

a sum of gauge boson field derivatives and the commutator of the bosons. (The $U(1)$ commutator is zero.)

The next part of the Lagrangian consists of the kinetic terms of the fermions:

$$\mathcal{L}_F = \mathrm{i}\gamma_\mu \sum_{j=1}^{3} \left(\overline{Q}_j\mathbf{D}^\mu Q_j + \bar{L}_j\mathbf{D}^\mu L_j + \bar{u}_j\mathbf{D}^\mu u_j + \bar{d}_j\mathbf{D}^\mu d_j + \bar{\ell}_j\mathbf{D}^\mu \ell_j + \bar{\nu}_j\mathbf{D}^\mu \nu_j\right) \qquad (3.1)$$

Here, the covariant derivatives

$$\mathbf{D}^\mu = \partial^\mu - \mathrm{i}\sum_{n=1}^{3} g_n \mathbf{G}_n^\mu$$

include the couplings to the gauge bosons.

---

[1]I will not list gauge fixing terms.

After the vector bosons and the fermions and their interactions, we now address the scalar sector of the SM. It contains one $SU(2)$ doublet Φ, the so-called Higgs field:

$$\mathcal{L}_H = (\mathbf{D}_\mu\Phi)^\dagger(\mathbf{D}^\mu\Phi) + \mu^2\Phi^\dagger\Phi - \frac{\lambda}{4}(\Phi^\dagger\Phi)^2 \tag{3.2}$$

All massive elementary particles receive their masses by coupling to the Higgs field. However, Φ needs to have a non-zero, but finite vacuum expectation value v in order to fulfil this feature, which in turn means that the quadratic coupling μ^2 and the quartic coupling λ have to be positive. The fermion mass terms arise from the Yukawa Lagrangian

$$\mathcal{L}_Y = -\sum_{j,k=1}^{3}\left[Y_{jk}^d\left(\overline{Q}_j\Phi\right)d_k + Y_{jk}^u\left(\overline{Q}_j i\sigma_2\Phi^*\right)u_k \right.$$
$$\left. + Y_{jk}^\ell\left(\overline{L}_j\Phi\right)\ell_k + Y_{jk}^\nu\left(\overline{L}_j i\sigma_2\Phi^*\right)\nu_k + \text{h.c.} \right]. \tag{3.3}$$

It describes the interaction between fermions and the Higgs field. Here, the Y_{jk}^f are the Yukawa matrices coupling the Higgs field to the right-handed field f of the generation k and to a left-handed partner from generation j. In order to introduce mass terms in the SM, the vacuum expectation value of the $SU(2)$ doublet Φ has to be non-zero. Exploiting gauge symmetry, it can be brought to the form

$$\langle\Phi\rangle_0 = \frac{1}{\sqrt{2}}\begin{pmatrix}0\\v\end{pmatrix}$$

with $v > 0$. This vacuum expectation value breaks the electroweak symmetry $SU(2)\otimes U(1)$ spontaneously to the electromagnetic symmetry group $U(1)_\text{em}$, with the conserved electric charge given by

$$Q = I_3 + \frac{Y}{2},$$

where I_3 is the third component of the weak isospin. The three arising Goldstone bosons become the longitudinal components of three of the four electroweak gauge bosons. The corresponding charge eigenstates are the electrically charged W^+ and W^- with mass m_W as well as two neutral states which can be rotated to the massive Z boson and to the massless photon γ by the so-called weak mixing angle θ_w. This angle also gives us the electrical charge coupling $e = g_2\sin\theta_w$. The Z and γ boson couplings to left-handed and right-handed fermions can be rearranged into a vector part proportional to γ_μ and an axial part with Dirac structure $\gamma_\mu\gamma_5$. Let g_{Vf} and g_{Af} be the corresponding couplings of the Z to fermion f, which will be used in the following.

Furthermore, we find one real massive Higgs boson H. Such a particle was postulated in 1964 by Peter Higgs [1], but it has been found only in 2012 at the LHC (see Sect. 3.3), thus completing the particle content of the SM from the experimental point of view.

As for the fermions, $\mathcal{L}_Y$ contains the mass terms after electroweak symmetry breaking. Neutrino masses are very small; there are only upper limits on their masses available, however, two neutrino mass eigenvalue differences are known to be non-zero (see e.g. [13] for

a review). Diagonalizing the 3×3 Yukawa couplings matrices yields the mass eigenvalues; the flavour eigenstates are accordingly transformed to mass eigenstates. The price one has to pay are flavour-changing couplings in $\mathcal{L}_F$, generated by non-zero off-diagonal elements of the product of the down-type and the up-type transformation matrices. For the quarks, this product is called quark mixing matrix V or simply CKM matrix, according to its developers Cabibbo, Kobayashi and Maskawa [20, 21]. It is a 3×3 matrix and mixes the quark flavour eigenstates. As a unitary matrix, it has nine degrees of freedom, of which five are unphysical. The remaining four parameters can be expressed as three rotation angles θ_{12}, θ_{13} and θ_{23}, which describe the size of the mixing between two generations each, and one complex phase δ_{13}. With the abbreviations $c_{ij} = \cos\theta_{ij}$ and $s_{ij} = \sin\theta_{ij}$, the standard parametrization of the CKM matrix reads [13]

$$V \equiv \begin{pmatrix} V_{ud} & V_{us} & V_{ub} \\ V_{cd} & V_{cs} & V_{cb} \\ V_{td} & V_{ts} & V_{tb} \end{pmatrix} = \begin{pmatrix} c_{12}c_{13} & s_{12}c_{13} & s_{13}e^{-i\delta_{13}} \\ -s_{12}c_{23} & c_{12}c_{23} & s_{23}c_{13} \\ -c_{12}s_{23}s_{13}e^{i\delta_{13}} & -s_{12}s_{23}s_{13}e^{i\delta_{13}} & \\ s_{12}s_{23} & -c_{12}s_{23} & c_{23}c_{13} \\ -c_{12}c_{23}s_{13}e^{i\delta_{13}} & -s_{12}c_{23}s_{13}e^{i\delta_{13}} & \end{pmatrix}. \tag{3.4}$$

Also in the lepton sector, such a matrix exists, yet throughout this thesis, I will assume it to be diagonal and neglect its parameters.

Apart from its gauge symmetry structure, one can formulate three discrete symmetry transformations for $\mathcal{L}_{\mathrm{SM}}$: replacing particles by their antiparticles is called $\mathcal{C}$ symmetry, the parity operation $\mathcal{P}$ is equivalent to mirroring the space coordinates just as $\mathcal{T}$ inverses the time. $\mathcal{L}_{\mathrm{SM}}$ is not symmetric under these transformations, but as a Lorentz transformation invariant local quantity, the SM Lagrangian must be invariant under the combination $\mathcal{CPT}$. While $\mathcal{P}$ is violated by the weak interaction [22], the combination $\mathcal{CP}$ seemed to be conserved until in 1964 an asymmetry in neutral meson decays showed that $\mathcal{L}_{\mathrm{SM}}$ is not totally $\mathcal{CP}$ symmetric [23]. This result was the original motivation for the postulation of a third generation [21] because $\mathcal{CP}$ violation requires physical complex phases in the Lagrangian. Only if there are at least three fermion generations, the complex phases of the CKM matrix cannot be compensated by phase rotations of the quark fields, and $\mathcal{L}_F$ contains complex quark couplings.

3.1   Parameters

After electroweak symmetry breaking, $\mathcal{L}_{\mathrm{SM}}$ contains 21 real parameters:[2]

- 3 gauge couplings $g_1 = e/\cos\theta_w$, $g_2 = e/\sin\theta_w$, g_3,

- μ and the quartic Higgs coupling λ from $\mathcal{L}_H$, connected via $v = 2\sqrt{\frac{\mu^2}{\lambda}}$,

---

[2]In principle, the $SU(3)$ part of the SM could contain one additional $\mathcal{CP}$ violating parameter θ, but $|\theta|$ is very small and consistent with zero.

- 6 quark masses m_u, m_d, m_s, m_c, m_b, m_t, and 6 lepton masses m_e, m_μ, m_τ, m_{ν_e}, m_{ν_μ}, m_{ν_τ}, which are identified by $\frac{1}{\sqrt{2}} \tilde{Y}^f_{jj} v$, where $\tilde{Y}^f_{jj}$ are the eigenvalues of the diagonalized Yukawa matrices Y^f_{jk} from (3.3), and j is the generation index,

- 3 quark mixing angles θ_{12}, θ_{13}, θ_{23}, and

- 1 quark mixing phase, denoted as δ_{13}.

These parameters are a priori free, but I assume perturbative couplings for the high energy observables that I want to discuss in the following. It is useful to switch to a handier set of parameters; all masses well below the Z scale (i.e. all fermion masses except for the top quark mass) can be treated as fixed since their uncertainties are too small to affect our observables. As next step, I relate v to the well-measured Fermi constant $G_F = 1/(\sqrt{2}v^2)$ and also treat it as fixed. Instead of the electromagnetic coupling e and θ_w, I want to use the Z boson mass and the hadronic contribution to the fine structure constant $\alpha_{\text{em}} \equiv \frac{e^2}{4\pi}$ at the Z scale. They are related to the original parameters by

$$m_Z = \frac{ev}{\sin(2\theta_w)} \sqrt{\frac{1}{1 - \Delta r}}$$

$$\Delta\alpha^{(5)}_{\text{had}}(m_Z) = 1 - \frac{\alpha_{\text{em}}(0)}{\alpha_{\text{em}}(m_Z)} - \Delta\alpha_{\text{lep}} - \Delta\alpha_{\text{top}},$$

where Δr includes higher order corrections, and $\Delta\alpha_{\text{lep}}$ and $\Delta\alpha_{\text{top}}$ denote the leptonic and the t loop contribution to the photon propagator at the Z scale, of which the error is negligible. Also the fine structure constant is very well known at the Z scale as well as for low energy processes; the main error of $\alpha_{\text{em}}(m_Z)$ stems from $\Delta\alpha^{(5)}_{\text{had}}$ [24]. The $SU(3)$ coupling constant is traded for the strong coupling $\alpha_s = g_3^2/(4\pi)$. Next, the Higgs mass can be derived from the quadratic coupling of Φ, $m_H = \sqrt{2}\mu$. Finally, taking the quark mixing parameters as they are, we end up with nine fit parameters:

$$m_t, \quad m_Z, \quad \Delta\alpha^{(5)}_{\text{had}}, \quad \alpha_s, \quad m_H, \quad \theta_{12}, \quad \theta_{13}, \quad \theta_{23}, \quad \delta_{13} \tag{3.5}$$

Now that we have defined the model, we can compare it with experimental results. For all fits in this thesis I used the CKMfitter package which treats systematic errors in the Rfit scheme [14] as introduced in Sect. 2.4. The CKM angles and the phase were constrained by taking mainly the PDG values for the CKM matrix elements and a CKMfitter look-up table for the unitarity triangle angle γ, compare App. A. I will not explicitly mention them in the following. Before discussing the measurements by the detector collaborations at the Large Hadron Collider (LHC), I want to address the results obtained at three preceding colliders: the LEP collider, SLC and the Tevatron. The first two started in the years 1989 and 1992, respectively, to collide electrons and positrons at a centre-of-mass energy of $\sqrt{s} \approx m_Z$ and later at LEP up to $\sqrt{s} = 209$ GeV. The SLC was shut down in 1998 and the LEP collider in 2000 [24]. The Tevatron, a proton-antiproton collider, ran from 1983 to 2011 at maximally $\sqrt{s} = 1.96$ TeV [25].

3.2   Electroweak precision observables

Amongst the main results of the LEP collider and SLC experiments are precision measurements: After the discovery of the W and Z bosons, their fundamental features and decay properties could be determined with relatively small statistical uncertainties due to the large amount of collected data. Measuring electron-positron collisions, the LEP and SLC experiments benefited from the low background, due to which the systematic errors are small. Over the years, a certain set of observables evolved that was used to test the Standard Model parameters at the Z scale; it is commonly referred to as electroweak precision observables (EWPO). As their experimental values are mainly based on LEP measurements, I will only mention the SLC data explicitly, where its contribution is important. (Most of the EWPO description is taken from [24] and [19]). They consist of the following quantities:

The Z mass m_Z is assigned to the peak of the bosonic resonance at approximately 91 GeV. Its total decay width Γ_Z is extracted from a beam energy scan around the centre-of-mass energy $\sqrt{s} = m_Z$. On the theory side, it is the sum of the hadronic decay width $\Gamma_Z^{\mathrm{had}} = \Gamma_Z^u + \Gamma_Z^d + \Gamma_Z^s + \Gamma_Z^c + \Gamma_Z^b$, the width of decays into charged leptons $\Gamma_Z^{\mathrm{lept}} = \Gamma_Z^e + \Gamma_Z^\mu + \Gamma_Z^\tau$, and the invisible decay width $\Gamma_Z^{\mathrm{inv}} = N_\nu^{\mathrm{light}} \Gamma_Z^\nu$ into light neutrinos. Γ_Z^f is the partial decay width of a Z decaying into the final state $f\bar{f}$. It can be related to the real effective vector and axial couplings of fermions to the Z boson, g_{Vf} and g_{Af}:

$$\Gamma_Z^f = N_C^f \frac{G_F m_Z^3}{6\sqrt{2}\pi} \left(g_{Vf}^2 + g_{Af}^2 \right)$$

The colour factor N_C^f of fermion f is 3 for quarks and 1 for leptons. (I do not explicitly show radiator factors or non-factorisable contributions here.) Independent measurements of Γ_Z and all visible partial decay widths were used to fit the number of neutrinos which have a mass smaller than $m_Z/2$ to

$$N_\nu^{\mathrm{light}} = 2.9840 \pm 0.0082. \tag{3.6}$$

The measured total hadronic Z cross section can be compared to the theoretical expectation

$$\sigma_{\mathrm{had}}^0 = \frac{12\pi}{m_Z^2} \frac{\Gamma_Z^e \Gamma_Z^{\mathrm{had}}}{\Gamma_Z^2}.$$

Here and in the following, the index 0 indicates the theoretically corrected pole observables that were extracted from the measurements. (Strictly speaking, these quantities are not observables but merely pseudo-observables, i.e. parameters determined by a fit to the observed cross sections and asymmetries.) Another ratio of decay widths is

$$R_q^0 = \frac{\Gamma_Z^q}{\Gamma_Z^{\mathrm{had}}},$$

the partial width of a Z decaying into a specific quark pair, normalized to the total hadronic decay width. The corresponding leptonic quantity is defined reversely:

$$R_\ell^0 = \frac{\Gamma_Z^{\text{had}}}{\Gamma_Z^\ell}$$

It is the ratio of the total hadronic Z width and the width of a Z decaying into a charged lepton pair. Here, lepton universality is assumed, which means that $g_{V\ell}$ and $g_{A\ell}$ are equal for the charged leptons and thus $R_e^0 = R_\mu^0 = R_\tau^0$.

Further important observables are forward-backward asymmetries. They are defined as the difference between the number of events with the final state particles scattered into forward and backward direction as compared to the incoming electron beam, normalized to the sum of all events:

$$A_{\text{FB}} = \frac{N_F - N_B}{N_F + N_B}$$

At LEP, forward-backward asymmetries have been measured for decays into c and b quarks as well as charged leptons (again assuming lepton universality). On the theory side, they can be related to the asymmetry parameters $\mathcal{A}_e$ and $\mathcal{A}_f$ stemming from the tree-level differential cross-section expression for the process $e^+ e^- \to f\bar{f}$:

$$\frac{\mathrm{d}\sigma_{f\bar{f}}}{\mathrm{d}\cos\theta} = \frac{3}{8}\sigma_{f\bar{f}}^{\text{tot}} \left[\left(1 - \mathcal{P}_e \mathcal{A}_e \right) \left(1 + \cos^2\theta \right) + 2 \left(\mathcal{A}_e - \mathcal{P}_e \right) \mathcal{A}_f \cos\theta \right],$$

where θ is the scattering angle between the incoming electron and the decay product f, and $\mathcal{P}_e$ is the electron beam polarization. The fermionic asymmetry $\mathcal{A}_f$ can be expressed in terms of the ratio of the above-mentioned effective couplings of fermions to the Z:

$$\mathcal{A}_f = \frac{2 g_{Vf}/g_{Af}}{1 + (g_{Vf}/g_{Af})^2}$$

$\mathcal{A}_e$ can also be identified with the left-right asymmetry of electrons, which is defined as the difference of the cross sections of left-handed and right-handed electrons in the initial state, normalized to their sum. Once again assuming lepton universality, I take the effective leptonic asymmetry $\mathcal{A}_\ell$ from [26], which is the combination of all three leptonic asymmetries from the LEP detectors as well as the left-right asymmetry measured by the SLD detector at the SLC. In terms of these asymmetries, the expression for the forward-backward asymmetries reads

$$A_{\text{FB}}^{0,f} = \frac{3}{4} \mathcal{A}_e \mathcal{A}_f. \tag{3.7}$$

Another asymmetry is the hadronic forward-backward charge flow: The difference between charged jet events in forward and backward direction with respect to the incoming electron

beam allows us to extract the squared sine of the effective weak mixing angle, which can be written as

$$\sin^2\theta_\ell^{\text{eff}} = \frac{1}{4}\left(1 - \frac{g_{V\ell}}{g_{A\ell}}\right) \tag{3.8}$$

Apart from the Z pole observables, I also take into account the W boson mass, which at tree level can be expressed by $m_W = g_2 v/2$. It is the first of the mentioned EWPO for which the Tevatron combination is competitive with the LEP value. I also use the total W boson decay width Γ_W in my fit, even if its measurement is not precise enough to yield a strong constraint. Furthermore, I take the Tevatron combination of the top quark pole mass m_t^{pole}, the $\Delta\alpha_{\text{had}}^{(5)}(m_Z)$ determination from [27] and the $\alpha_s(m_Z)$ extraction from tau decays [28] as inputs.

In short, that amounts to a total of 18 observables, of which the first four coincide with parameters from our above parametrization (3.5):

$$m_t^{\text{pole}}, \quad m_Z, \quad \Delta\alpha_{\text{had}}^{(5)}, \quad \alpha_s, \quad \Gamma_Z, \quad \sigma_{\text{had}}^0, \quad R_b^0, \quad R_c^0, \quad R_\ell^0,$$

$$A_{\text{FB}}^{0,b}, \quad A_{\text{FB}}^{0,c}, \quad A_{\text{FB}}^{0,\ell}, \quad \mathcal{A}_b, \quad \mathcal{A}_c, \quad \mathcal{A}_\ell, \quad m_W, \quad \Gamma_W, \quad \sin^2\theta_\ell^{\text{eff}}$$

For the fits, I linked the subroutine DIZET from the Zfitter code [29–31] to CKMfitter. DIZET calculates the EWPO including higher order corrections. Moreover, I created a general multi-purpose interface which can be used to connect any external programs to the CKMfitter program, see App. D. (Even if Zfitter includes a minimization routine, in my fits the minimization of the parameters was performed by CKMfitter.) The two-loop electroweak corrections for R_b^0 from [32], which are not implemented in Zfitter, have been included. They increase the deviation of R_b^0 from less than 1 to more than 2. Aside from the four CKM matrix parameters, I used m_Z, $\alpha_s(m_Z)$, $\Delta\alpha_{\text{had}}^{(5)}(m_Z)$, m_t^{pole} and m_H as fit parameters. The Higgs mass is not constrained by direct measurements in this section, reproducing the pre-LHC status. All numerical inputs for the electroweak precision observables that I used can be found in App. A. The best-fit values of the single quantities as well as their deviations in the SM fit can be found in Fig. 3.1. I also list the difference $\Delta\chi^2$ between the minimal χ^2 values of the complete fit and the prediction fit as defined in Sect. 2.2. The b quark forward-backward asymmetry and the R_b^0 ratio exhibit the largest deviations with absolute values greater than 2. They also yield the largest contributions to the total χ_{min}^2 of the EWPO fit, which is 21.21.

Here the difference between the squared deviation from the best-fit point and the $\Delta\chi^2$ is obvious: While Γ_Z and $\mathcal{A}_b$ have the very same $\Delta\chi^2$, the best-fit deviation of the Z width is smaller than the one of the b asymmetry. This means that the larger discrepancy between experiment and theory of $\mathcal{A}_b$ is accommodated just as well by shifts of the other observables when comparing the prediction fit with the complete fit.

Due to their small uncertainties, the EWPO yield strong constraints to physics beyond the SM, because effects of heavy particles in loop corrections have not been measured. Often when new physics models are analyzed, the electroweak precision fit is taken into account using the so-called oblique parameters S, T and U, introduced by Peskin and Takeuchi [33, 34]. In the SM, they are zero by definition. They can be used for heavy non-SM

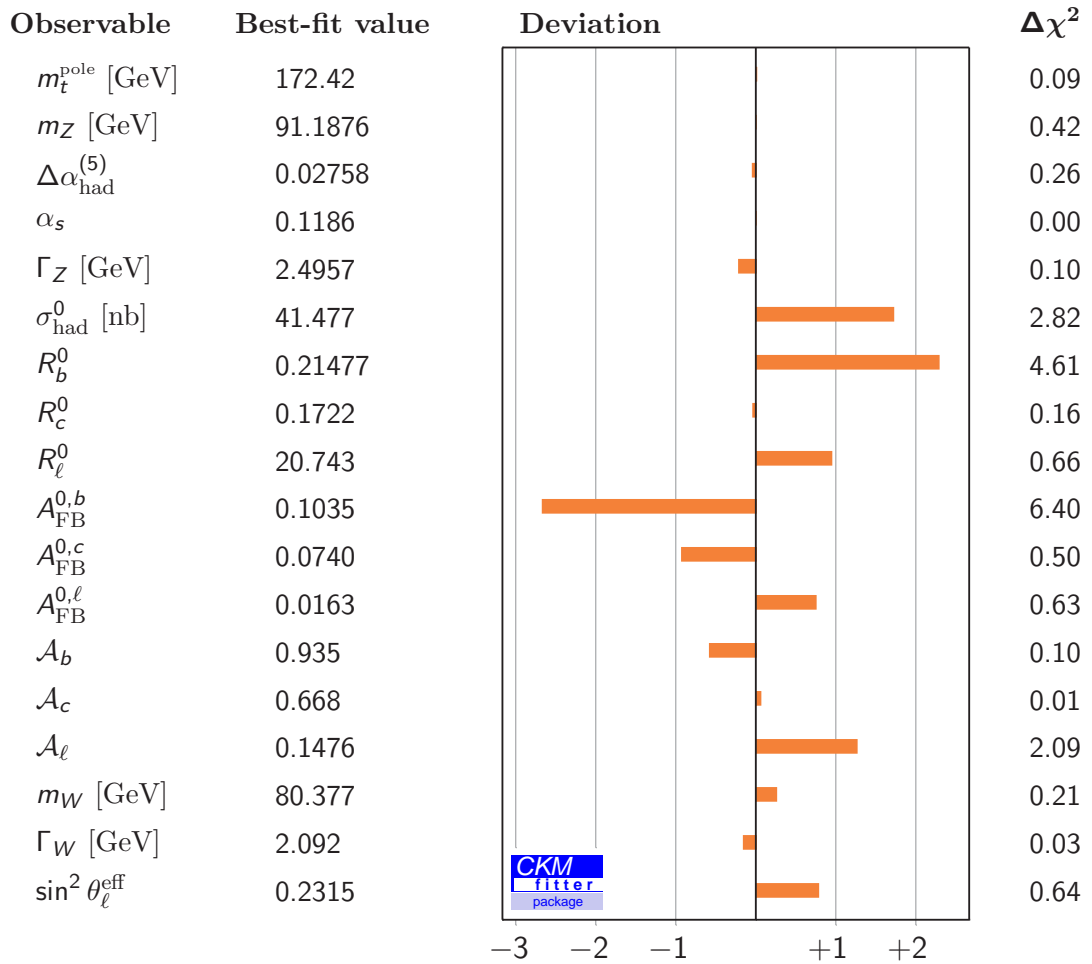| Observable	Best-fit value	Deviation	$\Delta\chi^2$
m_t^{pole} [GeV]	172.42		0.09
m_Z [GeV]	91.1876		0.42
$\Delta\alpha_{\mathrm{had}}^{(5)}$	0.02758		0.26
α_s	0.1186		0.00
Γ_Z [GeV]	2.4957		0.10
σ_{had}^0 [nb]	41.477		2.82
R_b^0	0.21477		4.61
R_c^0	0.1722		0.16
R_ℓ^0	20.743		0.66
$A_{\mathrm{FB}}^{0,b}$	0.1035		6.40
$A_{\mathrm{FB}}^{0,c}$	0.0740		0.50
$A_{\mathrm{FB}}^{0,\ell}$	0.0163		0.63
$\mathcal{A}_b$	0.935		0.10
$\mathcal{A}_c$	0.668		0.01
$\mathcal{A}_\ell$	0.1476		2.09
m_W [GeV]	80.377		0.21
Γ_W [GeV]	2.092		0.03
$\sin^2\theta_\ell^{\mathrm{eff}}$	0.2315		0.64

Figure 3.1: Deviations of the EWPO from the best-fit point in the SM fit before the Higgs discovery. (As defined in Eq. (2.4), the deviation of the observable X_i is $\left(x_i^{\mathrm{exp}} - x_i^{\mathrm{theo}}\right)/\sigma_i$.) The experimental inputs can be found in App. A. I also present the individual χ^2 contributions in the last column.

particles, if three requirements are met: the electroweak gauge part of the new theory has to be SM-like ($SU(2) \otimes U(1)$ before spontaneous symmetry breaking), the new particles must be heavier than the Z scale, and there must be no vertex corrections from the heavy particles. I will discuss their applicability in the next two chapters in the respective EWPO section.

As already stated, until last year the only unknown SM parameter, which could only be roughly extracted from the EWPO, was the Higgs mass. Even if the EWPO depend only logarithmically on m_H [35], they constituted the strongest available upper bounds on it. This was usually presented in the so-called "blue-band plot", the minimal χ^2 value as a function of m_H resulting from a global fit with m_H fixed. The plot before the Higgs discovery from [24] and my own fit are displayed in Fig. 3.2(a) and 3.2(b), respectively. Using inputs from [24], I could reproduce the old blue-band plot. I also show the more restrictive fit including the latest inputs for the EWPO from Table A.2 in App. A. Its Higgs mass prediction is $m_H = 93^{+35}_{-21}$ GeV. The historic blue-band plot is also based on `Zfitter` fits; but since no Rfit method was used, the theoretical uncertainty is overlaid in the blue band, while in Fig. 3.2(b) the theoretical uncertainty is contained in the $\Delta\chi^2$ value.

(a)

(b)
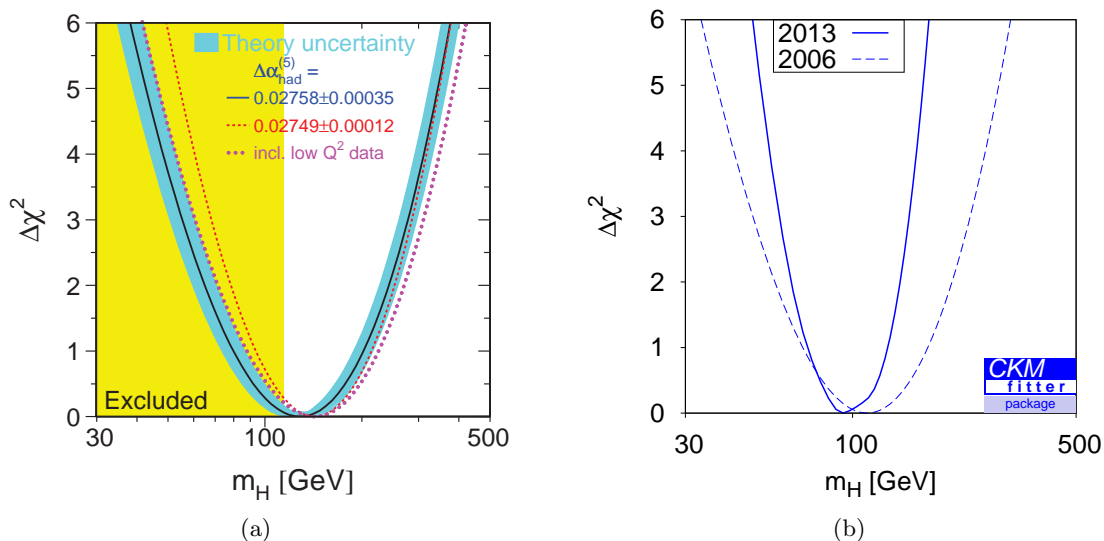
Figure 3.2: The blue-band plot from [24] on the left shows the χ^2 dependence of the Higgs mass m_H in a global fit to the EWPO. The theoretical errors determine the width of the blue band. The yellow range is excluded by direct Higgs searches at the LEP collider. In my fit on the right, the theoretical errors were taken into account using the Rfit scheme (cf. Sect. 2.4). The dashed line is a fit using the old inputs from [24].

The LEP detectors could only set a lower bound of 114.4 GeV at 95% CL to m_H [36], corresponding to the yellow-shaded excluded region in Fig. 3.2(a). In the year 2010, Tevatron Higgs searches could also exclude a Higgs mass range between 162 and 166 GeV at 95% CL [37]. The actual discovery, however, could be achieved by the LHC detectors ATLAS and CMS.

3.3   Higgs searches

On 4th July 2012, the ATLAS and CMS collaborations announced the discovery of a new boson "at a mass near 125 GeV", for which they claimed a local significance of $5.9\,\sigma$ and $5.0\,\sigma$, respectively, in the corresponding publications [4, 5]. This statement was based on the evaluation of the 2011 data set of around $5\,\mathrm{fb}^{-1}$, taken at a centre-of-mass energy of $\sqrt{s} = 7\,\mathrm{TeV}$, as well as up to $5\,\mathrm{fb}^{-1}$ from the 2012 run at $\sqrt{s} = 8\,\mathrm{TeV}$. The complete 2011 and 2012 Higgs search data were presented at the Moriond conferences in 2013 and comprise up to $25\,\mathrm{fb}^{-1}$. Also the Tevatron collaborations of the CDF and D∅ detectors declared a statistical significance of 3.1σ at 125 GeV in their latest combined analysis [38] which uses up to $10\,fb^{-1}$ of integrated luminosity. In the context of the SM, this new boson is interpreted as the Higgs boson H introduced at the beginning of this chapter. More detailed analyses concentrating on further characteristics like the spin are also in good agreement with SM expectations [39–41]. Therefore, I will refer to this discovery as the Higgs discovery in this work. Whereas the Tevatron was a proton-antiproton collider with a maximal centre-of-mass energy of $\sqrt{s} = 1.96\,\mathrm{TeV}$, the LHC used two proton beams with $\sqrt{s} = 7\,\mathrm{TeV}$ in 2011 and with $\sqrt{s} = 8\,\mathrm{TeV}$ in the 2012 run. At LHC and Tevatron, the main Higgs production processes are gluon-gluon fusion (ggF), vector boson fusion (VBF), W and Z associated production (WH and ZH, sometimes combined to VH), as well as $t\bar{t}$ associated production (ttH). I subsume WW and ZZ fusion in one VBF category but mostly consider WH and ZH separately, because in contrast to the two fusion processes the vector boson associated Higgs productions have distinguishable signatures in the final state and hence can be separated into different observables. The five final states of a Higgs decay that are separable from background are $b\bar{b}$, WW^*, ZZ^*, $\tau\tau$ as well as $\gamma\gamma$. Since m_W and m_Z are greater than $m_H/2$, only one of the produced massive bosons can be on the mass shell; the other one is virtual, which is denoted by the asterisk. The overview in Fig. 3.3 shows the leading order processes and also assigns the relative size of the individual production cross sections and the partial decay widths.

Due to different initial states and different collision centre-of-mass energies, the LHC production fractions differ from the ones at Tevatron; at both colliders, the gluon-gluon fusion is dominant. Almost 8.5% of the produced Higgs bosons decay into two gluons; however, those decays cannot be separated from the background. The missing 3% of the decays (e.g. $H \to Z\gamma$) are also not (yet) separable from background events. In the SM, gluons and photons couple to the Higgs boson only via loop processes; the main contributions originate from top quark and W boson loops at leading order. In other models, however, also other particles could be involved already at one-loop level. This fact makes the Higgs particle an excellent probe for physics beyond the SM.

As already explained in Chapter 2, a discovery is defined as a signal that has a statistical significance of at least 5σ. For the Higgs searches, the "signal" is quantified by the signal strength μ, the ratio of measured and theoretically expected signal events and can be translated into the ratio of the specific process cross sections $\sigma(X \to H \to Y)$ of a certain initial state X producing a Higgs H which then decays into the specific final state Y:

$$\mu(X \to H \to Y) \equiv \frac{N_{\mathrm{observed}}}{N_{\mathrm{expected}}} = \frac{\sigma_{\mathrm{observed}}(X \to H \to Y)}{\sigma_{\mathrm{SM}}(X \to H \to Y)} \qquad (3.9)$$
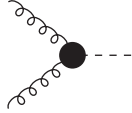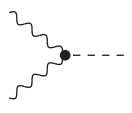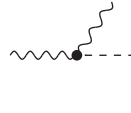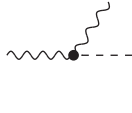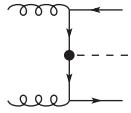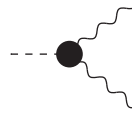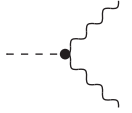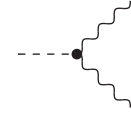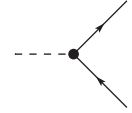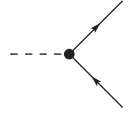
Figure 3.3: The most important Higgs production and decay modes with corresponding relative contributions and branching ratios in the SM at leading order. Gluons and photons only couple via loop processes to the Higgs boson, which are illustrated as inclusive vertices. The LHC values are taken from [42] for a centre-of-mass energy of 8 TeV, the Tevatron values are for 1.96 TeV [43], both assuming $m_H \approx 126$ GeV. the branching ratios and [44]

$\mu(X \to H \to Y)$ is mass dependent and should be 1 at the Higgs mass and 0 everywhere else in the SM, if one neglects the Higgs decay width. The signal cross section $\sigma(X \to H \to Y)$ factorizes in narrow-width approximation:

$$\sigma(X \to H \to Y) = \sigma(X \to H) \cdot \epsilon_{XY} \cdot \mathcal{B}(H \to Y), \qquad (3.10)$$

where $\sigma(X \to H)$ is the Higgs production cross section of the production mode X, and $\mathcal{B}(H \to Y)$ is the branching ratio of a Higgs boson decaying into the final state Y. The efficiencies ϵ_{XY} incorporate all detector, selection and reconstruction efficiencies; they are different for each $X \to H \to Y$ process. Effective Higgs couplings to fermions and vector bosons, like e.g. in [45–48], can be used to test the details of the SM, but for our SM extension fits they are not applicable; therefore, I will not use them in this thesis. A combination of the four best Higgs mass measurements in the decays $H \to \gamma\gamma$ and $H \to ZZ^*$ at ATLAS and CMS gives us $m_H = 125.96^{+0.18}_{-0.19}$. The inputs can be found in Table A.4. All available relevant Higgs signal strengths that were used in the fits were measured at the LHC, where the initial state is pp, and Tevatron with $p\bar{p}$ in the initial state, and can be found in Fig. A.1 in App. A together with a detailed description. Combining them yields a Higgs signal strength of $1.007^{+0.099}_{-0.098}$ at $m_H \approx 126$ GeV. If one is especially interested in the decay properties, the experimental results can be combined for the five decay channels from Fig. 3.3.

Table 3.2 is only for illustration; in the fits, I used all individual observables rather than these combinations. However, when discussing particular features of one of the decay

Decay channel	μ_{comb}	Number of observables	$\Delta\chi^2$	Deviation from 0
$H \to \gamma\gamma$	1.16 ± 0.18	39	53.94	6.44
$H \to WW^*$	0.75 ± 0.16	5	7.77	4.69
$H \to ZZ^*$	1.13 ± 0.24	4	2.03	4.71
$H \to b\bar{b}$	$1.30^{+0.45}_{-0.44}$	6	2.26	2.95
$H \to \tau\tau$	1.12 ± 0.29	9	8.57	3.86
all channels	$1.007^{+0.099}_{-0.098}$	63	72.76	10.17

Table 3.2: Higgs signal strength combinations at $m_H \approx 126\,\text{GeV}$, ordered by decay products. The N_{dof} and the compatibility with signal and background are given in the third, fourth and fifth column.

channels, this picture will be useful.

The inclusion of Higgs mass measurements to the precision SM fit means at the same time basically fixing the last unknown parameter of the SM; it raises the χ^2 of the EWPO fit from 21.21 to 26.93. The CKMfitter performance of a fit with 100 minimizations and a 1D scan with granularity 20 was 9 to 14 minutes. The impact on the single electroweak observables can be seen in Fig. 3.4, where I show the deviations with and without Higgs mass input.

Before the Higgs discovery, $A_{\text{FB}}^{0,b}$ featured the strongest tension between theory and experiment. In the new fit this tension is a bit relaxed, but the deviation is still greater than two and now equal to the slightly increased deviation of R_b^0. In Fig. 3.5(a), I show the measured values and the 1, 2 and 3σ regions surrounding the best-fit point of these two observables. This is the most dramatic illustration of SM incompatibility present in the EWPO. A much weaker discrepancy is exhibited by the comparison of fit and experiment in the m_t^{pole}-m_W plane next to it in Fig. 3.5(b). This figure has always been used to illustrate the EWPO fit and its dependence on the Higgs mass, compare [13, 24, 26]. And indeed, by fixing m_H, the best-fit central values of the top quark mass and the W mass receive the largest shifts of all EWPO with respect to their experimental errors. However, this is only visible for the deviation of the bosonic mass (which nevertheless is smaller than one); while in the "old" fit the central value of m_t^{pole} was set to the lower end of the range assigned by the Rfit treatment due to the systematic uncertainty, it is now fixed at its upper end, so the difference between both best-fit values of almost 3σ does not result in a sizeable change of the deviation nor in a noteworthy increase of the $\Delta\chi^2$.

Also the discrepancy of the $\mathcal{A}_\ell$ measurement with the SM increased. In total, however, all EWPO data are basically consistent with SM expectations. Also the combined signal strengths are in good agreement with the theory. While the first published data on the $H \to \gamma\gamma$ signal strengths seemed to indicate an excess around 126 GeV even too large for the SM and caused a lot of excitement, the deviation of $\mu_{\text{comb}}(H \to \gamma\gamma)$ has dropped below one if we take the latest data into account. Only $\mu_{\text{comb}}(H \to WW^*)$ has a deviation greater than one because less events than expected in the SM have been detected and the experimental uncertainty is the smallest of all combined signal strengths. For all electroweak precision observables and combined signal strengths I also performed predic-

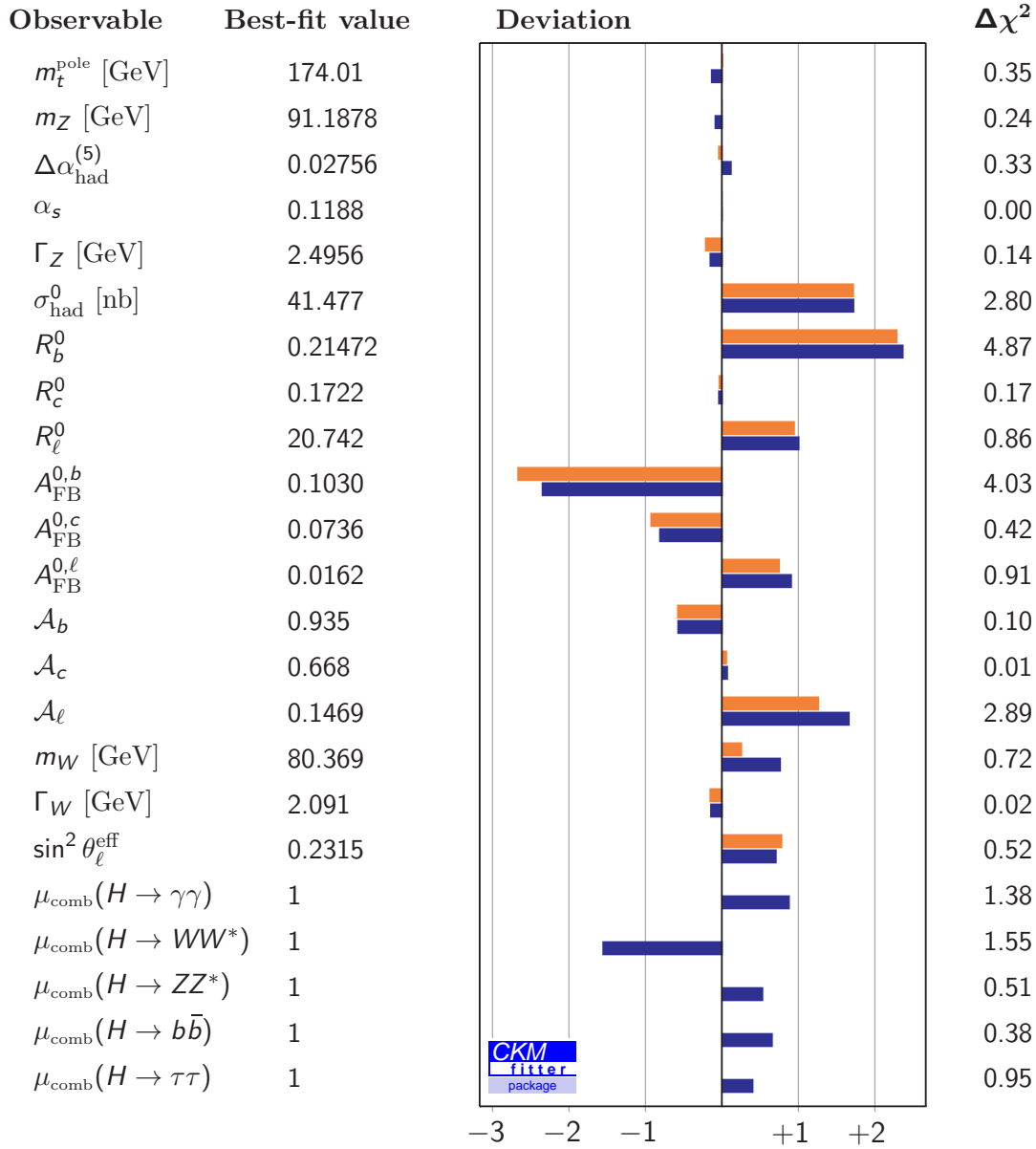| Observable	Best-fit value	Deviation	$\Delta\chi^2$
m_t^{pole} [GeV]	174.01		0.35
m_Z [GeV]	91.1878		0.24
$\Delta\alpha_{\text{had}}^{(5)}$	0.02756		0.33
α_s	0.1188		0.00
Γ_Z [GeV]	2.4956		0.14
σ_{had}^0 [nb]	41.477		2.80
R_b^0	0.21472		4.87
R_c^0	0.1722		0.17
R_ℓ^0	20.742		0.86
$A_{\text{FB}}^{0,b}$	0.1030		4.03
$A_{\text{FB}}^{0,c}$	0.0736		0.42
$A_{\text{FB}}^{0,\ell}$	0.0162		0.91
$\mathcal{A}_b$	0.935		0.10
$\mathcal{A}_c$	0.668		0.01
$\mathcal{A}_\ell$	0.1469		2.89
m_W [GeV]	80.369		0.72
Γ_W [GeV]	2.091		0.02
$\sin^2\theta_\ell^{\text{eff}}$	0.2315		0.52
$\mu_{\text{comb}}(H \to \gamma\gamma)$	1		1.38
$\mu_{\text{comb}}(H \to WW^*)$	1		1.55
$\mu_{\text{comb}}(H \to ZZ^*)$	1		0.51
$\mu_{\text{comb}}(H \to b\bar{b})$	1		0.38
$\mu_{\text{comb}}(H \to \tau\tau)$	1		0.95

Figure 3.4: Deviations of the EWPO and the Higgs signal strengths from the best-fit point in the SM fit before (orange) and after (blue) the Higgs discovery. (The deviations are defined as in Fig. 3.1.) For the individual $\Delta\chi^2$ of the signal strength combinations in the last column, I give the average contribution per observable (compare Table 3.2).

tion fits, where the latter were assumed to have the same efficiencies as the corresponding ATLAS categories at 8 TeV. The predictions illustrate the compatibility with the other observables as well as the effect of adding the respective measurement to the fit. The (naive) p-value scans in the SM can be found in App. B together with the measurements and the prediction fit results in the other models which I want to discuss in the next two chapters.

(a) (b)
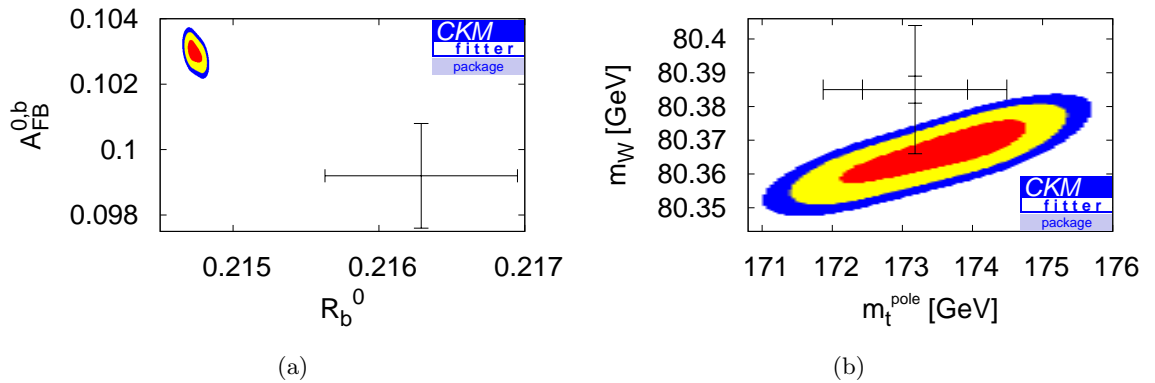
Figure 3.5: The 1, 2 and 3σ regions are shown in the R_b^0-$A_{FB}^{0,b}$ plane (a) and in the m_t^{pole}-m_W plane (b), shaded in red, yellow and blue, respectively. The direct measurements are marked by the cross, where the inner error bars are the theoretical errors, and the outer error bars denote the statistical uncertainties. A plot similar to (b) can be found in [12].

Our analysis is the first global fit to all available EWPO and Higgs data performed after the discovery of the Higgs boson [12]. The results largely agree with the electroweak fit by the Gfitter collaboration [49] and the Bayesian fit by Ciuchini et al. [50].

As the Higgs observables are hardly influenced by little modifications of all SM parameters except for the Higgs mass, and the EWPO only have a logarithmic dependence on m_H [35], both analyses can to a good approximation be performed separately. This in turn means that the individual $\Delta\chi^2$ contributions of the signal strength fit can simply be added to the EWPO fit χ^2, amounting to a total of $\chi^2_{\text{min}} = 99.69$. Four of the best-fit parameters can be found in Fig. 3.4; the remaining values are

$$m_H = 125.96\,\text{GeV}, \quad \theta_{12} = 0.227, \quad \theta_{13} = 0.00405, \quad \theta_{23} = 0.0409, \quad \delta_{13} = 1.15.$$

The Higgs mass is simply the combination of the mass extractions presented in Table A.4, and the mixing angles are mainly constrained by the CKM matrix elements from Table A.1 in App. A.

The consistency of the precisely measured experimental data with the SM is astonishing and gives us the opportunity to severely constrain or even rule out physics models beyond the SM. In the next two chapters, I want to shed light on two of such SM extensions. For both, Higgs search measurements and EWPO depend on the same set of parameters, such that combined fits of the Higgs signal strengths and EWPO are mandatory. The primary goal of this thesis was originally to perform a combined fit of the SM4, which will be discussed in the next chapter.

CHAPTER 4

The Standard Model with four fermion generations

At the beginning of Chapter 3, I mentioned that there are three generations of fermions in the Standard Model. The number of generations, however, cannot be deduced from a fundamental theoretical principle, nor is there a direct indication from the experimental side pointing at exactly three generations. The SM4 is the SM amended by a sequential fermion generation with the same quantum numbers as the knwon three generations. Adding a new generation of four fermions is equivalent to replacing the 3 in (3.1) and (3.3) by a 4, and the complete fermion content ordered in $SU(2)$ doublets looks like the following:

$$\begin{pmatrix} u \\ d \end{pmatrix}, \quad \begin{pmatrix} c \\ s \end{pmatrix}, \quad \begin{pmatrix} t \\ b \end{pmatrix}, \quad \begin{pmatrix} t' \\ b' \end{pmatrix}$$
$$\begin{pmatrix} \nu_e \\ e \end{pmatrix}, \quad \begin{pmatrix} \nu_\mu \\ \mu \end{pmatrix}, \quad \begin{pmatrix} \nu_\tau \\ \tau \end{pmatrix}, \quad \begin{pmatrix} \nu_4 \\ \ell_4 \end{pmatrix}$$

An assumption that I impose on the model I want to analyze in this chapter is the one of *perturbativity*: increasing the mass of a fermion means enlarging its Yukawa coupling, cf. Eq. (3.3). But like for the other couplings we require a converging power series if we want to treat Yukawa interactions perturbatively. It has only been very roughly quantified how large fermion masses can be before perturbativity breaks down. Tree-level partial-wave unitarity arguments limit the quark masses to be lighter than 500 GeV and the lepton masses to be lighter than 1 TeV if we assume that the corresponding doublets are almost mass degenerate [51, 52], meaning that their mass eigenvalues are almost equal. Analyses of electroweak next-to-leading order contributions to Higgs production with a fourth generation also reveal an incipient breakdown of the perturbation expansion at mass scales around 600 GeV [53]. However, a precise value at which perturbativity fails cannot be deduced easily; one might be able to apply perturbative methods well above these scales. Nevertheless, it is important to state clearly that for the fourth generation model discussed in the following perturbative behaviour is assumed. So my definition of a Standard Model with four generations (SM4) is an SM extension by a complete and perturbative generation of chiral fermions.

Now why should I add this fourth fermion generation? As already stated, the number of fermion generations cannot be related to any other parameter of the SM. It was shown that there need to be at least three generations in order to have $\mathcal{CP}$ violation in the Yukawa sector in Eq. (3.3) [21]. From LEP data can be inferred that there are only three

types of neutrinos lighter than $m_Z/2$, cf. Eq. (3.6). However, heavier neutrinos could still exist and were even discussed as possible dark matter candidates [9, 10]. But also the quarks of the fourth generation could possibly contribute to the solution of a cosmological puzzle: the apparent excess of matter in our universe as compared to antimatter discloses a disproportion which cannot be explained by the SM phase δ_{13} alone; further $\mathcal{CP}$ violating mechanisms are necessary to account for baryogenesis in order to satisfy the Sakharov criteria [54]. A sizeable contribution might stem from the two additional phases contained in the 4×4 CKM matrix of the SM4 [6], even if it is not sufficient to account for the entire asymmetry. Furthermore, a fourth generation of fermions could solve some discrepancies between measured and calculated flavour observables, such as $\mathcal{CP}$ violation in B meson measurements [7, 8, 55].

In this chapter, I will introduce the four generations model thoroughly in Sect. 4.1, I will discuss the same constraints as in the previous chapter, and finally show that after combining the most important observables in a global fit, the SM4 can be excluded at a statistically significant level.

4.1   Parameters

In addition to the nine SM parameters from (3.5) we have nine new parameters in the SM4: the four fermion masses $m_{t'}$, $m_{b'}$, m_{ℓ_4} and m_{ν_4}, three more quark mixing angles θ_{14}, θ_{24}, θ_{34}, and two additional quark mixing phases δ_{14} and δ_{24}.

In this work, I will use 800 GeV as somewhat arbitrary upper limit for the fourth generation fermion masses assuming that the mentioned breakdown of perturbativity occurs beyond this threshold. For the lower bounds, the direct searches need to be taken into account. Concerning the quarks, the most powerful constraints to date are bounds from the LHC detectors; the latest measurements state $m_{t'} > 656$ GeV [56] and $m_{b'} > 675$ GeV [57] at 95% CL. However, both analyses assume specific decay properties: the t' (b') is supposed to decay to Wb (Wt) with a branching ratio of 100%. Another analysis shows that mass degenerate fourth generation quarks must be heavier than 685 GeV [58]. The Particle Data Group still lists $m_{t'} > 420$ GeV and $m_{b'} > 372$ GeV at 95% CL as largest exclusion limits in their latest review [13]. Since there are no LHC exclusion bounds without any assumption on the branching ratios or mass degeneracy available a conservative lower mass limit of 400 GeV for the t' and b' quarks seems to be appropriate in order to not exclude any possible scenario from the beginning. The most stringent direct search limits for the fourth generation leptons were obtained at the LEP detectors. They are $m_{\ell_4} > 100.8$ GeV [59] from $W\nu$ decays and $m_{\nu_4} > 45$ GeV from invisible Z decays [60], again at 95% CL. There are no observables that constrain the new CKM matrix parameters directly, so in principle the angles are allowed to take any value between $-\frac{\pi}{2}$ and $\frac{\pi}{2}$ and the phases are varied between 0 and 2π. However, the 4×4 CKM matrix needs to be unitary, which severely constrains its off-diagonal elements in the fourth row and in the fourth column as already the 3×3 SM part satisfies the unitarity conditions to a good approximation. In this context, it is important to stress that the SM parameters of the CKM matrix have to be reinterpreted in the SM4 [61]. The CKM matrix parametrization of Eq. (3.4) is only valid in the SM4 if all extra mixing angles are set to zero; in general the SM 3×3 part of the SM4 4×4 CKM matrix does not have to be unitary. In principle, one could

also parametrize the leptonic Yukawa sector in a similar way; the resulting mixing matrix is called Pontecorvo-Maki-Nakagawa-Sakata (PMNS) matrix [62–64]. However, leptonic mixing effects on the observables that I want to discuss here are of minor importance and only occur in higher order corrections. Therefore, I will assume a diagonal lepton mixing matrix in the following, setting all mixing angles and $\mathcal{CP}$ phases of the PMNS matrix to zero. The neutrinos are supposed to be Dirac particles.

Whereas the EWPO and Higgs measurements in the SM have turned out to be effectively orthogonal in the parameter space, we will see that in the SM4 both sets of observables are entangled with respect to the parameters they depend on. A relation between Higgs mass and heavy fermions is also indicated by lattice studies: analyses of the non-perturbative parameter region up to 1 TeV have shown that for a Higgs mass of 126 GeV fermions with masses of about 300 GeV or more can destabilize the Higgs potential [65, 66]. However, this does not necessarily mean that heavy fermions are excluded, but may merely indicate that "our" vacuum is only metastable. Here, I want to focus on the perturbative part and discuss the interplay of the EWPO and the Higgs signal strengths in the following sections.

4.2 Electroweak precision observables

Many studies have investigated the viable parameter space of the SM4; I will discuss the most prominent ones in Sect. 4.4. The majority of them used the oblique parameters (cf. Sect. 3.2) instead of the full set of electroweak precision observables. It was shown in [67–69] that in the SM4 the oblique parameter U is negligible if one uses S and T; so one ends up with only two pseudo-observables. Only taking into account S and neglecting T, the mass degenerate SM4 was even said to be excluded at 6σ in former PDG reviews [70]. But this approximation has proven to be illegitimate once a non-trivial CKM matrix is assumed [69]. Any way, the preconditions for the use of the oblique parameters are not satisfied: not only could the new leptons be as light as the Z scale, the neutrino could even be lighter. Furthermore, in our general formulation of the model the heavy quarks are allowed to mix with the light species, such that vertex corrections are possible. This is why we decided to use the complete information from the EWPO instead of the oblique parameters.

To this end, we chose the "hybrid" approach introduced in [71]: as in Chapter 3, the SM expressions for the EWPO (except for R_b^0) are calculated with `Zfitter` on the level of the effective Z–fermion couplings g_{Vf} and g_{Af}, while the one-loop SM4 corrections to the effective couplings, $\delta g_{Vf} \equiv g_{Vf}^{\mathsf{SM4}} - g_{Vf}$ and $\delta g_{Af} \equiv g_{Af}^{\mathsf{SM4}} - g_{Af}$ are obtained using `FeynArts`, `FormCalc` and `LoopTools` [72–74]. We can now reduce all SM4 expressions to the SM formulae and correction terms depending on δg_{Vf} and δg_{Af}.

In the SM4, the EWPO fit alone is slightly better than in the SM: the total χ^2_{min} amounts to 20.82 without fixing m_H, and to 26.26 taking its measurement into account. (The SM fit produced χ^2_{min} values of 21.21 and 26.93 respectively.) If the Higgs boson had not been found in the mass region below 200 GeV, the EWPO fit would have been much better in the SM4 than in the SM, compare the prediction fit in Fig. B.3(g). Before the Higgs discovery, this feature was a frequently quoted argument to motivate the SM4. With the Higgs mass around 126 GeV, many deviations of the individual observables do not change

a lot (cf. Fig. 4.3). The deviations of the W and Z boson mass change the sign, and while the largest deviations in the SM, i.e. the ones of $A_{\mathrm{FB}}^{0,b}$ and R_b^0, are diminished in their absolute values, the ones of σ_{had}^0 and $\mathcal{A}_\ell$ are increased. There are two major features of the EWPO fit: The first is that large mass splittings in the fourth generation fermion doublets are excluded: Fig. 4.1(a) shows that the allowed mass difference Δm at 95% CL is between -75 and $82\,\mathrm{GeV}$ for the quarks and between -167 and $109\,\mathrm{GeV}$ for the leptons. This will be important for the combination with the Higgs signal strength fit that I want to present in the next section. The second important result of the electroweak fit is that mixing between the fourth generation and the SM quarks is disfavoured. θ_{34} is smaller than 0.16 at 95% CL with a best-fit value of 0, which can be seen in Fig. 4.1(b), where a p-value scan over θ_{34} is shown. Quark mixing between the fourth and the third generation would even be stronger suppressed if I used a larger central value for V_{tb} (cf. Table A.1). The constraints on the other two angles are even stronger.

(a)　　　　　　　　　　　　　　　　(b)
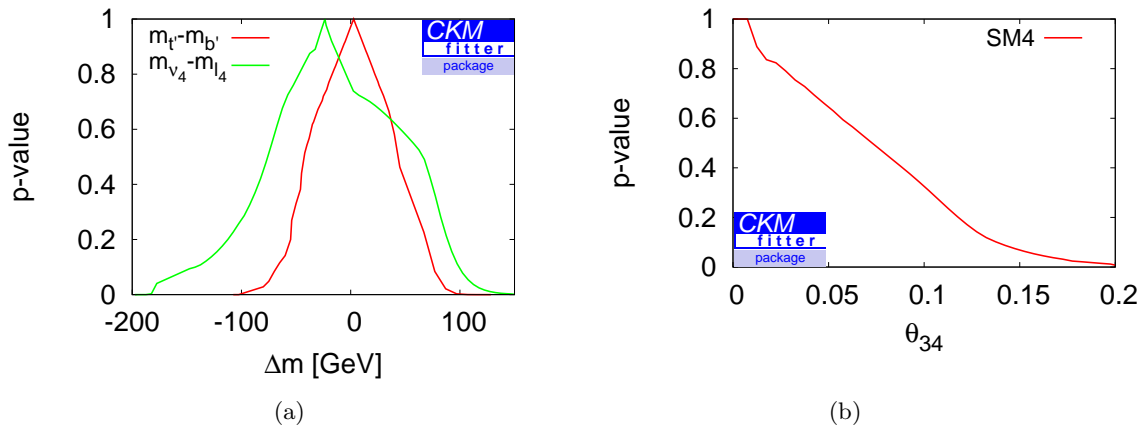
Figure 4.1: The mass splitting of the fourth generation $SU(2)$ doublet partners is strongly constrained by the EWPO: the absolute quark mass difference cannot exceed 82 GeV at 95% CL, while the lepton mass splitting is somewhat less limited to 167 GeV at most at 95% CL (a). The scan over θ_{34} shows that scenarios are favoured where fourth generation quark decays into SM quarks are suppressed.

4.3　Higgs searches

The Higgs content of the SM4 is the same as in the Standard Model: there is one scalar $SU(2)$ doublet that acquires a non-zero vacuum expectation value by electroweak symmetry breaking. The only free parameter of the scalar sector of the SM4 is the Higgs mass m_H. The measured signal strengths are assumed to be the SM4 ones. I consider the same five production mechanisms as in the SM (ggF, VBF, WH, ZH, ttH), but if m_{ν_4} is small enough, we get an additional, invisible decay channel to the five SM decay modes [75]. From Eqns. (3.9) and (3.10) one can see that in narrow-width approximation the SM4 signal strength splits up into a production and a decay ratio, if one attributes the efficiencies ϵ_{XY} to the production part:

$$\mu(X \to H \to Y) = \frac{\sigma_{\mathrm{SM4}}(X \to H) \cdot \epsilon_{XY}}{\sigma_{\mathrm{SM}}(X \to H) \cdot \epsilon_{XY}} \cdot \frac{\mathcal{B}_{\mathrm{SM4}}(H \to Y)}{\mathcal{B}_{\mathrm{SM}}(H \to Y)}$$

I assume that the efficiencies of the SM4 are the same as in the SM. Instead of ϵ_{XY} I use the *percentage contributions* ϱ_{XY} in the following, which incorporate the relative admixture of the respective production process $X \to H$ in a particular decay channel to Y:

$$\varrho_{XY} = \frac{\sigma_{SM}(X \to H)\,\epsilon_{XY}\,\mathcal{B}_{\mathrm{SM}}(H \to Y)}{\sum\limits_i \sigma_{SM}(i \to H)\,\epsilon_{iY}\,\mathcal{B}_{\mathrm{SM}}(H \to Y)} \qquad (4.1)$$

If we sum over the five possible initial states X, the ϱ_{XY} add up to 1. The percentage contributions are convenient when we want to use signal strengths from the proton colliders Tevatron and LHC: as we have no information about the particular production on parton level for an individual process, we have to sum over all possible production channels. For some signal strengths measurements, additional signatures in the final state indicate a predominance of a specific production process. In that case one can simply set all other percentage contributions to zero. The ϱ_{XY} inputs used in this thesis can be found in Tables A.5, A.6 and A.7. If no values were provided by the detector collaborations, I simply take the relative proportions from Fig. 3.3, thus assuming efficiencies of 100%. We can sum over the five production modes, attribute the corresponding ϱ_{XY}, and then trade the production cross sections for the total decay widths and the branching ratios, which gives us the convenient expression

$$\mu(H \to Y) = \left(\sum_i \frac{\mathcal{B}_{\mathrm{SM4}}(H \to i)}{\mathcal{B}_{\mathrm{SM}}(H \to i)} \varrho_{iY} \right) \cdot \frac{\Gamma_H^{\mathrm{SM4}}}{\Gamma_H^{\mathrm{SM}}} \cdot \frac{\mathcal{B}_{\mathrm{SM4}}(H \to Y)}{\mathcal{B}_{\mathrm{SM}}(H \to Y)}. \qquad (4.2)$$

For our fits, we used the publicly available code `HDecay` v. 4.45 [76] to generate branching ratios and total decay width in the SM as well as in the context of the SM4. The program includes higher order corrections from [53, 77–79]. The calculated quantities depend on the Higgs mass and – in case of the SM4 – on the fourth generation fermion masses, but it is implicitly assumed that $\theta_{14} = \theta_{24} = \theta_{34} = 0$. As for the last angle, we have seen in Fig. 4.1(b) that this simplification is supported by the EWPO. Since the matrix elements of the first two rows of the SM CKM matrix have been determined quite precisely, and they fulfil the corresponding 3×3 unitarity conditions, we expect $|V_{ub'}| \ll 1$ and $|V_{cb'}| \ll 1$, and thus also the other two angles to be small, so the suppression of quark mixing between the fourth generation and the SM particles seems to be justified. The `HDecay` output was saved in look-up tables and during the fit procedure an algorithm was used to interpolate their entries. The small interpolation error of this treatment was neglected.

In the SM4, the predominant production and decay channels have quite different attributes: the gluon-gluon fusion, which already in the SM is the main production process at proton colliders, is naively enhanced by roughly a factor of 10 at leading order due to the additional heavy quark contributions in the loop [80]. On the other hand, the decay $H \to \gamma\gamma$ is heavily suppressed: Already in the SM, the diphoton production exhibits a destructive interference; at leading order, the t and W loop enter calculations with a different sign and partially cancel each other. In the SM4, this cancellation is even stronger [81]. Taking into account next-to-leading order corrections, the suppression is almost perfect; the Higgs decay to two photons is very unlikely [53]. However, as discussed in Chapter 3, the LHC detectors at first even measured a larger excess of the signal strengths than they

would have expected in the SM. Even if the latest $\mu(H \to \gamma\gamma)$ values are more SM-like now, their experimental errors have also decreased, and these observables thus strongly contradict the SM4 hypothesis. (The deviation of the diphoton signal strength can roughly be estimated by the deviation from 0 in Table 3.2.) Also the other signal strengths are affected: the fit favours a neutrino mass which is lighter than $m_H/2$, so the total decay width of the Higgs boson Γ_H^{SM4} is larger than in the SM. But if $\mathcal{B}_{\mathrm{SM4}}(H \to \nu_4\nu_4)$ and $\mathcal{B}_{\mathrm{SM4}}(H \to gg)$ are increased, all other branching ratios are diminished at the same time, which in turn means that the Higgs decay into vector bosons is suppressed compared to the SM. This also affects the decay to b quarks because they are assumed to be produced in association with vector bosons, and additionally because $\mathcal{B}_{\mathrm{SM4}}(H \to b\bar{b})$ is also reduced. On the other hand, the $H \to \tau\tau$ signal strength receives such a large boost by the ggF enhancement and the invisible decay width that its predicted value is larger than 4 at 99% CL. This circumstance legitimates the assumption of a diagonal PMNS matrix because lepton mixing effects would additionally increase $\mu(H \to \tau\tau)$.

Next, I briefly comment on effective Higgs couplings approaches in the literature like e.g. [45–48], which for our purposes are not applicable for the SM4 for several reasons: The mentioned higher order corrections have different effects on the effective couplings for different decay products. Some of the approaches are oversimplified in the sense that they do not leave room for invisible decay channels as present in the SM4 case. Apart from the effective couplings, we would furthermore need their correlations. Moreover, the errors on the Higgs signal strengths are relatively large, such that a quadratic χ^2 distribution is only a vague approximation. Finally, the numerical p-value determination with toy-measurements would not be applicable.

4.4   Combined analysis

Before combining the discussed constraints, I want to briefly sum up the most important literature on the SM4, which is a story of premature exclusion and resurrection: After the success of the third fermion generation postulated by Kobayashi and Maskawa [21] a fourth generation was a self-evident next step. However, the SM4 was put under pressure by the oblique parameters in the 1990s as T was fitted to be negative while it is by definition larger than zero in the SM4. This lead to an exclusion statement in the PDG review of 99.2% CL [82]. Around the year 2000, updated EWPO fits hinted at positive T values, and several authors inferred that a fourth generation was no longer excluded by electroweak precision data, see e.g. [67, 83–85]. Furthermore, the Higgs boson was still not found, neither at the LEP detectors nor at the Tevatron, and the fact that in the SM4 the Higgs boson could in principle be much heavier than the upper bound deduced from the blue-band plot of the SM made the fourth generation a quite popular model [68], see also Fig. B.3(g) in App. B. The SM4 analyses became more intricate and also considered quark mixing effects between the SM fermion content and the fourth generation [55, 61, 69, 86, 87]. But as soon as the first LHC data were published, the strong interest in this revived model was damped because the first Higgs search results posed serious problems to the SM4 [88–91]. However, if one wants to exclude the model, all possible realizations need to be analyzed, such as e.g. the possibility of "light" fourth generation neutrinos. Before the ICHEP conference 2012, where the Higgs discovery was proclaimed,

our collaboration presented the first quantitative exclusion statement at 3.1σ, taking into account available Higgs search data and the EWPO and combining them with a newly developed p-value calculation method for non-nested models [92]. The update of this analysis, which belongs to the main achievements presented in this thesis, finally sealed the fate of the SM4, excluding it to more than 5σ [12].

In the following, I want to elaborate on the details of this work. In particular, I will repeat parts of the analyses with up-to-date inputs and show that the constraints from the direct Higgs searches have become even stronger since the Higgs discovery. The SM4 parametrization including the quark mixing matrix was implemented into CKMfitter by Andreas Menzel. On this basis, I added the discussed observables and performed global fits that were cross-checked by Martin Wiebusch using myFitter. One CKMfitter fit with 100 minimizations and a 1D scan with granularity 20 takes between one hour and several hours. The bottleneck is the call of the `Zfitter` subroutine `DIZET` as well as the calculation of the SM4 contributions for the EWPO.

The χ^2_{min} of the SM4 EWPO fit (20.82) is comparable with the one of the SM (21.21); the one of the signal strengths fit alone amounts to 124.05. The combination of both sets of constraints in the fit yields $\chi^2_{\mathsf{min}} = 145.33$, corresponding to a $\chi^2_{\mathsf{min}}/N_{\mathsf{dof}}$ greater than 2.0. The best-fit parameter values that are not listed in Fig. 4.3 are

$$m_H = 125.97\,\mathrm{GeV}, \quad \theta_{12} = 0.227, \quad \theta_{13} = 0.00415, \quad \theta_{23} = 0.0410, \quad \delta_{13} = 1.17,$$
$$m_{t'} = 401\,\mathrm{GeV}, \quad m_{b'} = 407\,\mathrm{GeV}, \quad m_{\nu_4} = 56.7\,\mathrm{GeV}, \quad m_{\ell_4} = 105\,\mathrm{GeV},$$
$$\theta_{14} = 0.01, \quad \theta_{24} = 0.08, \quad \theta_{34} = 0.00.$$

The two mixing phases δ_{14} and δ_{24} are not constrained by the fit. Exploring best-fit point in detail shows that the SM4 Higgs data fit wants to compensate for the large diphoton and the small $\tau\tau$ signal strength by allowing for large fourth generation mass splittings. And exactly this is forbidden by the EWPO: In Fig. 4.2(a), I show the χ^2 depending on m_{ν_4}. One can see that the best-fit value of $56.7\,\mathrm{GeV}$ is slightly below $m_H/2$. This is due to the fine-tuned Higgs decay width, which in this neutrino mass range is highly sensitive to the invisible decay $H \rightarrow \nu_4\bar{\nu}_4$. Above the Higgs threshold, this invisible decay is kinematically excluded; the enormous χ^2 is basically flat. If one leaves away the EWPO in the fit, the strong exclusion of an SM4 without invisible decays is relaxed by the permission of large mass splittings. While this effect was clearly visible in our publications [91, 92], it is hardly recognizable now that the χ^2 has become that huge: The χ^2 difference between a fit without and with EWPO at the best-fit neutrino mass (which is equal in both cases) is about 20; the difference above the Higgs threshold is 40. If one assumes a Majorana character of the fourth neutrino, the result will almost be the same, since the signal strength fit does not change and the effect on the EWPO can be neglected.

The most important parameter of the SM4 exclusion is, of course, the Higgs mass. Whereas in the SM, m_H can be treated as fixed, it is not a priori clear that this also holds for the SM4, so a short comment on this is necessary. For most of the fits in this thesis, I used the four mass extractions from Table A.4, but in [12] we compare the explicit χ^2 dependence of the Higgs mass in the SM and SM4. To this end, I digitalized the plots showing the individual signal strengths as functions of m_H that were provided by the detector collaborations at the ICHEP 2012 conference (see Fig. A.2). Furthermore,
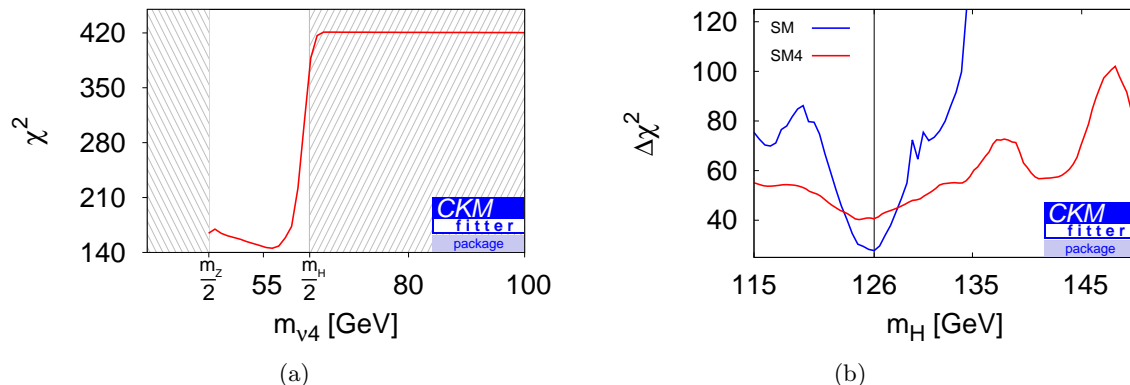
Figure 4.2: On the left side I show a scan over the fourth generation neutrino mass (a); the hatched areas are the regions below the LEP limit on light neutrinos and above $m_H/2$. On the right, the blue-band plot for the SM and the SM4 including the signal strength information from July 2012 is displayed (b). It depicts the best-fit discrepancy between the SM and the SM4: While the SM is compatible with the signal strengths, the χ^2_{min} of the SM4 is much larger.

the signal information was used to disfavour non-signal Higgs mass regions: As already mentioned, the signal strength would be one at the Higgs mass and zero everywhere else, if the experimental errors were negligible and Γ_H^{SM4} is small. To find the signal region, one would have to choose different Higgs mass bins and check for each bin whether the signal strength deviates from zero or not. If we attributed this deviation from zero to each bin, this would translate into a constant shift of the χ^2. Now we would perform several hypothesis tests, each comparing two non-nested models which only differ in their Higgs mass values. Assuming the realization of a specific Higgs mass (our hypothesis) we would have to subtract from the χ^2 the squared deviation from zero and add the squared signal strength deviation for the considered mass bin instead. Finally, the hypothesis with the smallest χ^2 prevails, which in the Higgs case is the mass bin around 126 GeV. (In a more thorough analysis of this problem, one would of course rather determine the *p*-value.) Since for the calculation of the *p*-value only the χ^2 difference with respect to the best-fit point is important, I simply subtracted the squared deviation from zero at the respective Higgs mass value. That is why not the total χ^2, but rather a $\Delta\chi^2$ depending on m_H is shown in Fig. 4.2(b), approximately reproducing the figure from [12]. In both models, the SM and the SM4, the best-fit Higgs mass value is about 126 GeV. Therefore, I will only use the four direct mass measurements from Table A.4 in the following and exclusively discuss signal strengths at 126 GeV.

Another difference between our publications [12, 91, 92] and this work is that I do not set $\theta_{34} = 0$ here because the bounds have relaxed a bit compared to [92]. Nevertheless, a qualitatively different outcome of the fit is not expected; at the best-fit point essentially no mixing between the fourth generation and the SM quarks is favoured.

The deviations at the best-fit point of the SM4 can be found in Fig. 4.3, where they are compared to the SM deviations. Again, the signal strengths from Table 3.2 are represented by the ATLAS 8 TeV quantities. As already mentioned, the EWPO fit is roughly as good as in the SM. An interesting feature is that the top quark mass has the second largest

$\Delta\chi^2$, whereas its deviation is zero. This shows the dependence of the other observables on m_t^{pole}: Other than in the SM, the SM4 fit has the freedom to choose relatively light top quarks in order to compensate for the Higgs mass measurement if direct top quark measurements are not taken into account; the predicted value is even $m_t^{\text{pole}} = 148$ GeV. (All prediction fits can be found in App. B, where they are also compared to the SM.) As soon as the measured t quark mass is included to the fit, m_t^{pole} takes a value at the lower end of the allowed Rfit range. On the contrary, Γ_Z has a larger deviation than in the SM, but its $\Delta\chi^2$ is equally small. While the tensions of $A_{\text{FB}}^{0,b}$ and R_b^0, which feature the largest deviations of the SM, are a bit ameliorated in the SM4, the discrepancy of $\mathcal{A}_\ell$ is enhanced. What poses serious problems on the SM4 fit are the signal strengths: As discussed above, tauonic Higgs decays would be seen more often than expected in the SM, and the decays to two photons or b quarks would hardly be visible. However, exactly the contrary seemed to be the case considering the first published Higgs data. Even if the deficit of $H \to \tau\tau$ events and the apparent excess of the diphoton signal strength seem to converge to their SM expectations with more evaluated and published measurements, more data means at the same time that the experimental errors become smaller, which in turn increases the deviations of the fermionic decay signal strengths. The largest impact is the one on the $H \to \gamma\gamma$ signal strength. The SM4 parameters cannot by any means be adapted in such a way that they can account for the accidental cancellation of fermionic and bosonic contributions to the decay amplitude. The largest potential value for $\mu(H \to \gamma\gamma)$ is 0.18 at 95% CL, and that is by far not enough to explain the measurement. Its best-fit value of 0.08 is even smaller; this is due to the tauonic Higgs decays, which determine the behaviour of the SM4 parameters and have the largest $\Delta\chi^2$ on average. The dilemma of the SM4 is that a small absolute deviation of $\mu(H \to \tau\tau)$ simultaneously means large deviations of $\mu(H \to \gamma\gamma)$ and $\mu(H \to b\bar{b})$ and vice versa. This unsolvable discrepancy finally leads to the exclusion of the SM4.

The SM4 and the SM are not nested. For the calculation of the p-value, we use Martin Wiebusch's program myFitter [15], which deals with all the subtleties described in Sect. 2.6. With the data available after the Higgs discovery, we found a p-value of $1.1 \cdot 10^{-7}$, corresponding to 5.3σ (4.8σ, leaving aside Tevatron data) [12]. Since then, the signal strengths have become even more stringent: On the one hand, the seeming suppression of $\mu(H \to \tau\tau)$ has been lifted, but this fact cannot compensate for the deviations of $\mu(H \to \gamma\gamma)$ and $\mu(H \to b\bar{b})$ on the other hand, which have grown by 1.7 and 2.2, respectively. For the determination of the p-value in [12], the simulations already took several days because one needs to generate a sufficient amount of toy measurements that contribute to the numerical integration of the test statistic to guarantee a small uncertainty on the central value. Considering the fact that the convergence of the numerical integration can only have worsened with the new inputs, I refrained from re-calculating the p-value with the available Higgs data. Naively applying Wilks' theorem today, with ν being the difference in the number of model parameters, we obtain $7.0 \cdot 10^{-7}$ for the p-value, which corresponds to 5.0σ. The correct p-value is expected to be considerably smaller. Altogether we can regard the possibility of additional fermion doublets in a perturbative sequential generation as SM extension as excluded and turn to the analogon in the scalar sector: an additional Higgs doublet.

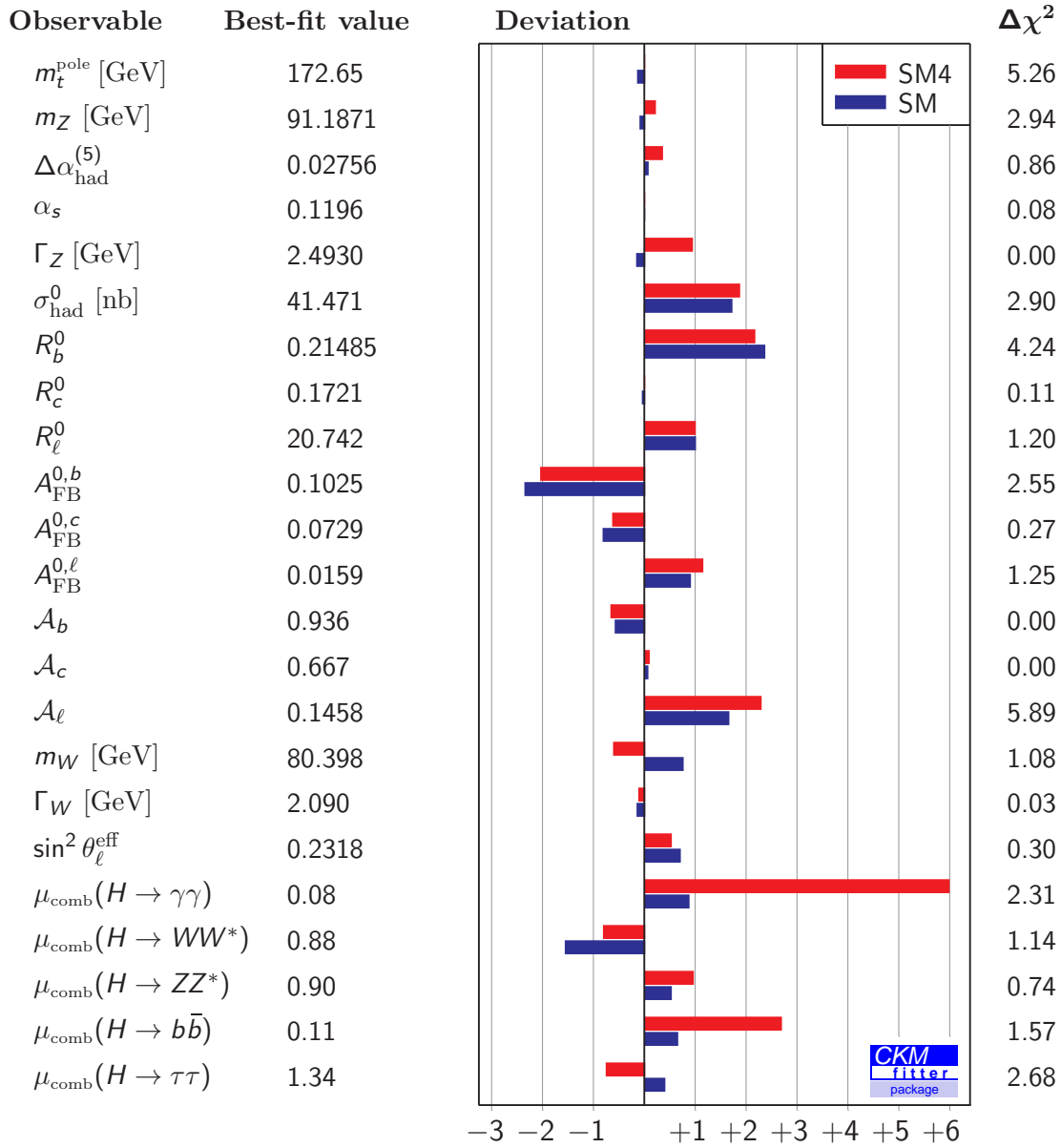| Observable	Best-fit value	Deviation	$\Delta\chi^2$
m_t^{pole} [GeV]	172.65		5.26
m_Z [GeV]	91.1871		2.94
$\Delta\alpha_{\text{had}}^{(5)}$	0.02756		0.86
α_s	0.1196		0.08
Γ_Z [GeV]	2.4930		0.00
σ_{had}^0 [nb]	41.471		2.90
R_b^0	0.21485		4.24
R_c^0	0.1721		0.11
R_ℓ^0	20.742		1.20
$A_{\text{FB}}^{0,b}$	0.1025		2.55
$A_{\text{FB}}^{0,c}$	0.0729		0.27
$A_{\text{FB}}^{0,\ell}$	0.0159		1.25
$\mathcal{A}_b$	0.936		0.00
$\mathcal{A}_c$	0.667		0.00
$\mathcal{A}_\ell$	0.1458		5.89
m_W [GeV]	80.398		1.08
Γ_W [GeV]	2.090		0.03
$\sin^2\theta_\ell^{\text{eff}}$	0.2318		0.30
$\mu_{\text{comb}}(H \to \gamma\gamma)$	0.08		2.31
$\mu_{\text{comb}}(H \to WW^*)$	0.88		1.14
$\mu_{\text{comb}}(H \to ZZ^*)$	0.90		0.74
$\mu_{\text{comb}}(H \to b\bar{b})$	0.11		1.57
$\mu_{\text{comb}}(H \to \tau\tau)$	1.34		2.68

$-3\ -2\ -1 \quad +1\ +2\ +3\ +4\ +5\ +6$

Figure 4.3: Deviations of the EWPO and the Higgs signal strengths from the best-fit point in the SM4 (red) and in the SM (blue).

CHAPTER 5

The Two-Higgs-Doublets model

In generic Two-Higgs-Doublets models, one has two scalar $SU(2)$ Higgs doublets Φ_1 and Φ_2 instead of a single Φ as in the SM [93]. The most general definition of a Two-Higgs-Doublets model as extension of the SM is given by the replacement of $\mathcal{L}_H$ by the Higgs Lagrangian

$$
\begin{aligned}
\mathcal{L}_H^{\text{2HDM}} =& (\mathbf{D}_\mu \Phi_1)^\dagger (\mathbf{D}^\mu \Phi_1) + (\mathbf{D}_\mu \Phi_2)^\dagger (\mathbf{D}^\mu \Phi_2) \\
& - m_{11}^2 \Phi_1^\dagger \Phi_1 - m_{22}^2 \Phi_2^\dagger \Phi_2 + m_{12}^2 \left(\Phi_1^\dagger \Phi_2 + \Phi_2^\dagger \Phi_1 \right) \\
& - \frac{\lambda_1}{2} \left(\Phi_1^\dagger \Phi_1 \right)^2 - \frac{\lambda_2}{2} \left(\Phi_2^\dagger \Phi_2 \right)^2 - \lambda_3 \left(\Phi_1^\dagger \Phi_1 \right) \left(\Phi_2^\dagger \Phi_2 \right) \\
& - \lambda_4 \left(\Phi_1^\dagger \Phi_2 \right) \left(\Phi_2^\dagger \Phi_1 \right) - \left[\frac{\lambda_5}{2} \left(\Phi_1^\dagger \Phi_2 \right)^2 + \text{h.c.} \right] \\
& - \left\{ \left[\lambda_6 \left(\Phi_1^\dagger \Phi_1 \right) + \lambda_7 \left(\Phi_2^\dagger \Phi_2 \right) \right] \left(\Phi_1^\dagger \Phi_2 \right) + \text{h.c.} \right\} .
\end{aligned}
\tag{5.1}
$$

(I adopt the notation of Gunion and Haber [94]. A general discussion can be found e.g. in [95].) If one sets Φ_2 to zero, one reobtains the SM Higgs part from (3.2) identifying $-m_{11}^2$ with μ^2 and λ_1 with $\lambda/2$. However, this general definition, which goes by the name 2HDM of type III, violates $\mathcal{CP}$ symmetry and contains flavour-changing neutral currents at tree level. A sufficient condition for a $\mathcal{CP}$-conserving Higgs sector are real parameters m_{12}^2, λ_5, λ_6 and λ_7. (The other parameters are real by hermiticity of $\mathcal{L}_H^{\text{2HDM}}$.) Flavour-changing neutral currents are strongly constrained by experimental data; therefore we can impose an additional Z_2 symmetry to eliminate the relevant terms from the Lagrangian [96, 97]: If the full model Lagrangian $\mathcal{L}^{\text{2HDM}}$ is invariant under the transformation $\Phi_1 \to -\Phi_1$, Φ_1 does not couple to the SM particles at all. This model is called 2HDM of type I. If the Z_2 symmetry transformation is $\Phi_1 \to -\Phi_1$ and $d_j \to -d_j$, one speaks of the 2HDM of type II. In this scenario, Φ_2 only couples to up-type quarks and neutrinos, whereas Φ_1 exclusively couples to down-type quarks and charged leptons; the Yukawa Lagrangian of the 2HDM of type II takes the following shape:

$$
\begin{aligned}
\mathcal{L}_Y^{\text{2HDM}} = - \sum_{j,k=1}^{3} \Big[& Y_{jk}^d \left(\overline{Q}_j \Phi_1 \right) d_k + Y_{jk}^u \left(\overline{Q}_j i\sigma_2 \Phi_2^* \right) u_k \\
& + Y_{jk}^\ell \left(\overline{L}_j \Phi_1 \right) \ell_k + Y_{jk}^\nu \left(\overline{L}_j i\sigma_2 \Phi_2^* \right) \nu_k + \text{h.c.} \Big]
\end{aligned}
$$

With this Z_2 symmetry, flavour-changing neutral currents are automatically absent at tree level. The m_{12}^2, λ_6 and λ_7 terms in the Higgs Lagrangian violate this symmetry, but we keep m_{12}^2 to permit soft Z_2 breaking without spoiling the desired form of $\mathcal{L}_Y^{2\mathrm{HDM}}$.

In this work, I want to focus on the $\mathcal{CP}$-conserving 2HDM of type II with soft Z_2 breaking term, which I will refer to as 2HDM in the following context. Its Higgs Lagrangian is (5.1) without the last line ($\lambda_6 = \lambda_7 = 0$), and m_{12}^2 and λ_5 are real. The reason why this specific model is very popular is that it could be a limiting case of supersymmetric models, and the discovery of a second Higgs doublet with the characteristics of a 2HDM type II could be an indication for the realization of supersymmetry in nature, see e.g. [98] for a review. Moreover, the 2HDM of type II easily complies with most of the constraints from flavour physics because it lacks flavour-changing neutral currents at tree level.

5.1 Parameters

In the above formulation, the 2HDM is parametrized by the couplings of the quadratic and quartic Higgs field terms in the Lagrangian. These couplings, however, have to fulfil several requirements to describe a consistent theory of the physical nature. It is therefore convenient to change to a more intuitive basis, which sometimes is called *physical* parametrization. If we expand both $SU(2)$ doublets around their vacuum expectation value, we get

$$\Phi_a(x) = \frac{1}{\sqrt{2}} \begin{pmatrix} \phi_a^+ \\ v_a + h_a + i\chi_a \end{pmatrix} \qquad (a = 1, 2). \tag{5.2}$$

Simultaneous diagonalization of the 2×2 squared mass matrices of the charged components ϕ_a^+ and the imaginary parts χ_a is characterized by the rotation angle β. It gives us two zero eigenvalues that are identified by the longitudinal components of the massive W and Z bosons, and two finite mass eigenvalues $m_{H^+}^2$ and $m_{A^0}^2$, corresponding to the eigenstates H^+ and A^0, which are the charged Higgs boson and $\mathcal{CP}$-odd Higgs boson. The vacuum expectation values are related to the diagonalization angle via $\tan\beta = \frac{v_2}{v_1}$. Furthermore, they have to account for electroweak symmetry breaking in the well-known way, so $v_1^2 + v_2^2 = v^2$. The squared mass matrix of the $\mathcal{CP}$-even components h_a are not diagonalized by β, but we have the additional freedom to perform this rotation, and call the corresponding angle α. The mass eigenvalues are called h^0 and H^0, where the former is by definition the lighter one and in this work will be interpreted as the new boson discovered at the LHC. The SM Higgs field would be a linear combination of both of them: $H = -h^0 \sin(\beta - \alpha) - H^0 \cos(\beta - \alpha)$. The ratios of all resulting tree-level couplings of the neutral Higgs bosons to fermions and gauge bosons and the respective SM coupling only depend on α and β, see Table 5.1.

Since in the W and Z coupling ratios only the difference between the two diagonalization angles appears, I will choose $\beta - \alpha$ as the relevant fit parameter. Moreover, I will use the quartic coupling λ_5, which can be related to the soft breaking parameter m_{12}^2. I fix all SM parameters including v to their best-fit values and set $m_{h^0} = 126$ GeV because varying

Higgs boson	$d_j d_j, \ell_j \ell_j$	$u_j u_j$	WW, ZZ
h^0	$-\dfrac{\sin\alpha}{\cos\beta}$	$\dfrac{\cos\alpha}{\sin\beta}$	$\sin(\beta-\alpha)$
H^0	$\dfrac{\cos\alpha}{\cos\beta}$	$\dfrac{\sin\alpha}{\sin\beta}$	$\cos(\beta-\alpha)$
A^0	$\tan\beta$	$\cot\beta$	0

Table 5.1: Neutral Higgs couplings to fermions and vector bosons, normalized to the SM Higgs couplings.

them is not expected to change the 2HDM fit results qualitatively. We then end up with six free parameters in the 2HDM:

$$m_{H^+}, \quad m_{A^0}, \quad m_{H^0}, \quad \beta-\alpha, \quad \tan\beta, \quad \lambda_5$$

The relations between the couplings and the physical parameters of the 2HDM are listed in App. C.

Before completely switching to the physical parametrization, let us explore some theoretical restrictions first: In the SM, the condition that the Higgs potential must be bounded from below can be simply expressed by requiring $\lambda \geq 0$. This feature, called *positivity*, looks a bit more complicated in the 2HDM. Gunion and Haber have showed that the following inequalities must be satisfied if one wants to avoid an unstable Higgs potential [94]:

$$\lambda_1 > 0, \qquad \lambda_2 > 0, \qquad \lambda_3 > -\sqrt{\lambda_1\lambda_2}, \qquad \lambda_4 > |\lambda_5| - \lambda_3 - \sqrt{\lambda_1\lambda_2} \qquad (5.3)$$

Furthermore, we want to guarantee that the minimum of the Higgs potential at 246 GeV is the global minimum. If it was only a local minimum, it would be metastable and the different vacuum expectation value of the global minimum could be attained one day such that all particle masses would change. However, this scenario is strongly constrained by the lifetime of our universe, and therefore I want to make the assumption that we live in the global minimum of the Higgs potential. This topic was extensively discussed in [99]; it was found that requiring that the global minimum is the one around 246 GeV is equivalent to the validity of the following inequality:

$$m_{12}^2 \left(m_{11}^2 - \sqrt{\frac{\lambda_1}{\lambda_2}} m_{22}^2 \right) \left(\tan\beta - \sqrt[4]{\frac{\lambda_1}{\lambda_2}} \right) > 0 \qquad (5.4)$$

I will refer to this property as *stability* condition.

The last aspect on the theoretical side will be a similar one to that in the SM4: as with the fourth generation Yukawa couplings, I want to require perturbativity of the 2HDM quartic couplings. In principle, higher order calculations are necessary to determine the maximal absolute values of the λ_i above which perturbativity fails. Since this is beyond

the scope of this thesis, I simply choose a universal upper limit on the quartic couplings and impose

$$|\lambda_i| \leq 2\pi. \tag{5.5}$$

The most conservative estimate of the perturbative breakdown is $|\lambda_i| \leq 4\pi$, but it was shown in [100] that in the SM $|\lambda| \leq 2\pi$ is a more appropriate upper bound for the quartic coupling λ. Since the same applies in the 2HDM, where we have five λ_i, I adopt this convention. The consequences of a different choice of the perturbativity bound will be discussed in Sect. 5.5. The main effect of the limitation of the $|\lambda_i|$ values is that the mass splitting between m_{H^0}, m_{A^0} and m_{H^+} has to be of order of the vacuum expectation value $v \approx 246$ GeV. In all fits in the following sections, the three constraints of positivity, stability, and perturbativity are implicitly employed.

Like for the SM4 particles we also have to take direct Higgs particle searches into account in the 2HDM. For the neutral heavy Higgs particles almost the same bounds apply as for the SM Higgs. The charged Higgs, however, is of particular interest for experimental searches, as it would contribute to flavour-changing neutral current processes at loop level. At LEP, m_{H^+} has found to be larger than 79.3 GeV at 95% CL [101]. For the lower bounds on the masses of the neutral Higgs bosons, I refer to the discussion in Sect. 5.3. In the fits I use 10 TeV as arbitrary upper mass limit for the heavy Higgs masses. (Heavier Higgs particles would be out of reach for the current LHC even if it ran at its design energy of $\sqrt{s} = 14$ TeV.) In our parametrization, we assume β to be between 0 and $\frac{\pi}{2}$ without loss of generality, which translates into a range from 0 to ∞ for $\tan\beta$. α is supposed to be in the fourth quadrant (between $-\frac{\pi}{2}$ and 0), so $\beta - \alpha$ is in the interval from 0 to π.

In contrast to the SM4, the SM is nested in the 2HDM. The SM can be reobtained by fixing $\beta - \alpha = \frac{\pi}{2}$ and sending all heavy Higgs masses to infinity. This limit is called the *decoupling limit* [94]. As 2HDM realizations in the vicinity of this limiting case are hardly distinguishable from the SM, I want to focus on the parameter regions where the 2HDM phenomenology deviates from the SM, i.e. primarily analyze the low mass scenarios with masses below 1 TeV. Let us again start the discussion of experimental model constraints with the EWPO.

5.2 Electroweak precision observables

As in the SM4, we cannot use the oblique parameters due to Z vertex contributions by the 2HDM particles. Especially for the decay $Z \to b\bar{b}$, heavy Higgs contributions play a role at loop level [102–104], which affects e.g. R_b^0 or $\mathcal{A}_b$. So once more the method from [71] is applied: we obtain the SM values using Zfitter and add the 2HDM contributions calculated at one-loop level with FeynArts, FormCalc and LoopTools. For details, see Sect. 4.2. Compared to the SM4 case we now need to call the Zfitter routine DIZET only once for each fit, since we fixed the SM parameters, and thus avoid the bottleneck that took most of the SM4 fit running time. (Varying SM parameters might have an impact on the 2HDM EWPO fit, but the best-fit parameter region will be near the decoupling limit even without EWPO constraints, so an SM-like EWPO fit outcome is expected.)

The EWPO modify the heavy Higgs mass spectrum of the 2HDM in the following way: While perturbativity of the quartic couplings limits the mass splittings to a few hundred GeV, they now additionally have to fulfil the condition that either the H^0 or the A^0 mass have to be closer to m_{H^+} than about 150 GeV. Since both, the perturbativity bound and the EWPO constrain the heavy Higgs masses, I illuminate the differences in Fig. 5.1 for a fixed charged Higgs mass of 500 GeV with a small Gaussian error of 3 GeV. On the left side I only use the above-mentioned theoretical constraints, which forbid that the neutral Higgs masses exceed m_{H^+} by more than 300 GeV and that the mass difference $m_{H^0} - m_{A^0}$ becomes too large in magnitude. The right figure shows the impact on the same fit if the EWPO are included: For $m_{H^0} < m_{H^+}$, the mass of the $\mathcal{CP}$-odd Higgs is basically also fixed to m_{H^+}. If m_{H^0} is larger than the charged Higgs mass, one of the neutral Higgs particles needs to have a mass which differs from m_{H^+} at most by 150 GeV.
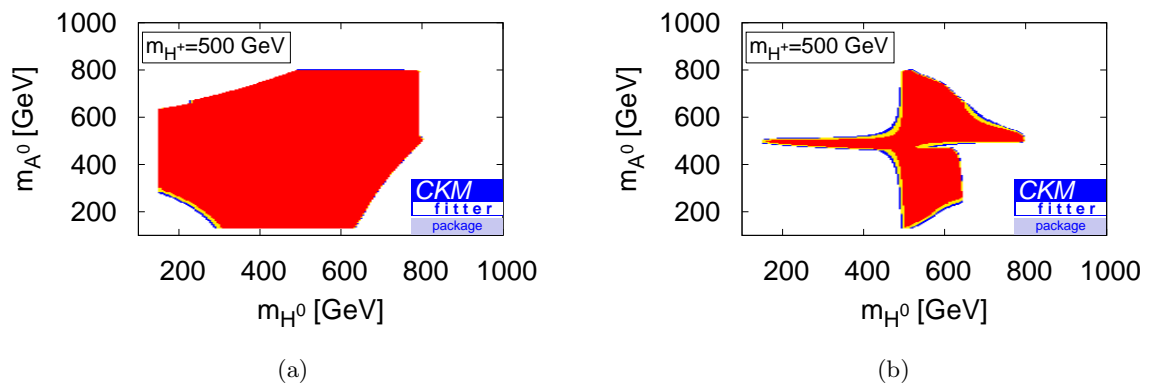
Figure 5.1: I show scans over the m_{H^0}-m_{A^0} plane for $m_{H^+} = 500$ GeV without (a) and with (b) EWPO constraints. The requirement of perturbativity cuts away large mass splitting regions at the edges (a), whereas one of the neutral boson masses is forced to stay closer than 150 GeV to the charged Higgs mass if we add the EWPO to the fit (b).

5.3 Higgs searches

I interpret the new boson discovered at around 126 GeV at the LHC to be the lighter $\mathcal{CP}$-even eigenvalue and thus discard the possibility that it is the heavier H^0 and that the h^0 was not seen at LEP, as discussed in [105]. I also want to dismiss the idea of a mass degenerate Higgs resonance at the LHC implying that $m_{h^0} \approx m_{H^0} \approx 126$ GeV [106]. In order to clearly separate the heavy Higgs bosons from h^0, I impose a lower limit of 150 GeV on their masses.

To make use of the Higgs signal strength information, I want to change notation: Let us define the factor $r_i^{2\text{HDM}}$ as the ratio of the squared 2HDM vertex coupling of a neutral Higgs H to the particle i and the respective squared SM coupling. This ratio corresponds to the ratio of the partial widths in the corresponding models: $\Gamma_H^{i,2\text{HDM}} = r_i^{2\text{HDM}}\Gamma_H^{i,\text{SM}}$. By analogy with the SM4 expression (4.2), and taking the percentage contributions from Eq.

(4.1), we can rewrite the signal strength in a compact way as

$$\mu(H \to Y) = \sum_i r_i^{\text{2HDM}} \cdot \varrho_{iY} \cdot \frac{r_Y^{\text{2HDM}}}{\sum_f r_f^{\text{2HDM}} \mathcal{B}_{\text{SM}}(H \to f)}. \qquad (5.6)$$

So to calculate the theoretical 2HDM expectation for the signal strengths, the only remaining quantities we need are the r_i^{2HDM} factors, the percentage contributions and the SM branching ratios. All information about the 2HDM contributions are encoded in the r_i^{2HDM} if we again assume that the efficiencies and thus the percentage contributions in the 2HDM do not differ from their SM values. We only need to know the couplings of the Higgs boson to the heavy fermions and the massive gauge bosons, for which we take the squared tree-level expressions from Table 5.1, as well as the coupling ratios to g and γ. The latter two couple to H only via loop processes, which also involve the heavy Higgs particles of the 2HDM. In my CKMfitter implementation, r_g^{2HDM} and r_γ^{2HDM} are calculated by an external routine written by Martin Wiebusch that I linked to the rest of the code. The above definition of the signal strength may also be applied to the heavy neutral Higgs particles. In this work, I have only used it for h^0 and H^0. For the latter, I digitalized the 95% confidence level exclusion limits of $H \to ZZ$ searches at CMS up to 1 TeV [107], for details see App. A. Similar exclusion limits are available for the $H \to WW$ decay, but since the 2HDM Higgs couplings to W and Z are the same, I confined myself to using only the $H \to ZZ$ exclusion information.

In the SM4, the combination of the EWPO and the Higgs searches was sufficient to exclude the model. As the 2HDM cannot be excluded because the SM is nested, it is worthwhile to include further observables to the fit. Since we have decided to discuss a flavour conserving Higgs sector, strong constraints can be derived from flavour-changing neutral currents, which can only occur at loop level like in the SM.

5.4 Flavour observables

Many flavour observables are important fit constraints for $\tan\beta < 1$ or in the large $\tan\beta$ region. When $\tan\beta \gtrsim 40$, the heavy Higgs couplings to down-type quarks and charged leptons are enhanced, and observables like the branching ratios of the decays $B \to \tau\nu$, $B \to D\tau\nu$ or $B \to D^*\tau\nu$, which receive sizeable contributions from the charged Higgs boson, would have to be included to the fit [108]. However, I want to concentrate on low $\tan\beta$ scenarios in this thesis for two reasons: I will show that only then sizeable deviations from the decoupling limit condition $\beta - \alpha = \pi/2$ are possible; and furthermore, the measurements of the mentioned (semi-)tauonic B decays are in conflict with each other in the SM, and the disagreement becomes worse in the 2HDM of type II [109]. So the very large $\tan\beta$ regions of the figures in this thesis have to be taken with a grain of salt, in the sense that the p-value of the 2HDM is overestimated.

Yet there are two flavour observables which I want to use in my fits because they are powerful constraints for moderate $\tan\beta$ values: the B_s^0–$\overline{B}_s^0$ mixing frequency Δm_{B_s} and the branching ratio of B mesons decaying into $X_s\gamma$, where X_s is a hadronic state containing an s or $\bar{s}$ quark. Both processes can only be described by flavour-changing neutral currents

at loop level, to which in the 2HDM also the charged Higgs contributes. In Fig. 5.2 I show examples of relevant SM diagrams and possible 2HDM diagrams for B_s^0–$\overline{B}_s^0$ mixing and $b \to s\gamma$ transitions.
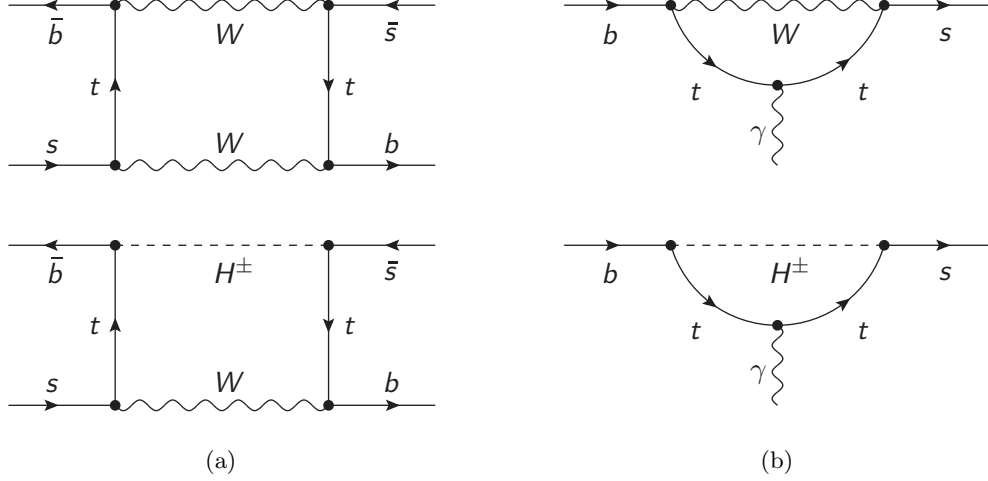
Figure 5.2: Sample diagrams for one-loop B_s^0–$\overline{B}_s^0$ mixing (a) and $b \to s\gamma$ decays (b). The occurring virtual particles include W and t in the SM (upper diagrams) as well as H^+ in the 2HDM (lower diagrams).

The oscillation frequency in the B_d^0 system has also been determined experimentally, how-ever the ratio $\Delta m_{B_d} / \Delta m_{B_s}$ is the same in the 2HDM of type II and in the SM, and since the relative error of Δm_{B_s} is much smaller, B_d^0–$\overline{B}_d^0$ mixing would not additionally constrain our parameters. I now discuss how I include the two flavour observables to my fits and show their impact on the parameter space.

5.4.1 B_s^0–$\overline{B}_s^0$ mixing

The first measurement of the oscillation frequency of a B_s^0 meson changing to its antiparticle $\overline{B}_s^0$ and vice versa dates back to the year 2006 [110]. Of all neutral mesons systems, the B_s^0–$\overline{B}_s^0$ mixing has the highest oscillation frequency and was determined to unprecedented precision only recently [111]. This frequency is equal to the mass difference between the heavier and the lighter mass eigenstate of the B_s^0–$\overline{B}_s^0$ system and in the 2HDM it reads [112–116]

$$\Delta m_{B_s} = \frac{G_F^2}{24\pi^2} \left| V_{ts}^* V_{tb} \right|^2 f_{B_s}^2 \eta_{B_s} \hat{B}_{B_s} m_{B_s} \overline{m}_t^2 \left(S_{WW} + S_{WH} + S_{HH} \right), \quad \text{where}$$

$$S_{WW} = 1 + \frac{9}{1 - x_{tW}} - \frac{6}{(1 - x_{tW})^2} - 6 \frac{x_{tW}^2 \ln(x_{tW})}{(1 - x_{tW})^3},$$

$$S_{WH} = \frac{x_{tH}}{\tan\beta^2} \left(\frac{(2x_{HW} - 8) \ln(x_{tH})}{(1 - x_{HW})(1 - x_{tH})^2} + \frac{6x_{HW} \ln(x_{tW})}{(1 - x_{HW})(1 - x_{tW})^2} + \frac{8 - 2x_{tW}}{(1 - x_{tW})(1 - x_{tH})} \right),$$

$$S_{HH} = \frac{x_{tH}}{\tan\beta^4} \left(\frac{1 + x_{tH}}{(1 - x_{tH})^2} + \frac{2x_{tH} \ln(x_{tH})}{(1 - x_{tH})^3} \right),$$

and $x_{ij} = m_i^2/m_j^2$. In this context, H denotes the charged Higgs boson H^+. The SM part is incorporated in the function S_{WW}. The additional 2HDM diagrams with one or both W bosons exchanged by H^+ lead to the occurrence of S_{WH} and S_{HH}, which both are zero in the limit $m_{H^+} \to \infty$ or $\tan\beta \to \infty$. Apart from the Fermi constant and the CKM matrix elements, the appearing prefactors are the decay constant f_{B_s}, the bag factor $\hat{B}_{B_s}$, the QCD correction η_{B_s}, the B_s^0 mass m_{B_s}, and the $\overline{MS}$ top mass $\overline{m}_t$. Since we fixed the top pole mass to its SM best-fit value, also $\overline{m}_t$ is treated as fixed in my fits; the same applies for the CKM matrix elements. The remaining numerical input values are listed in Table A.9 in App. A. Δm_{B_s} has a sizeable impact on the allowed $\tan\beta$ values and sets a lower limit of 0.17 at 95% CL to it, even if m_{H^+} is at the upper end of its scan range, see Fig. 5.3. For $m_{H^+} < 1\,\mathrm{TeV}$ the corresponding requirement is $\tan\beta > 0.7$.
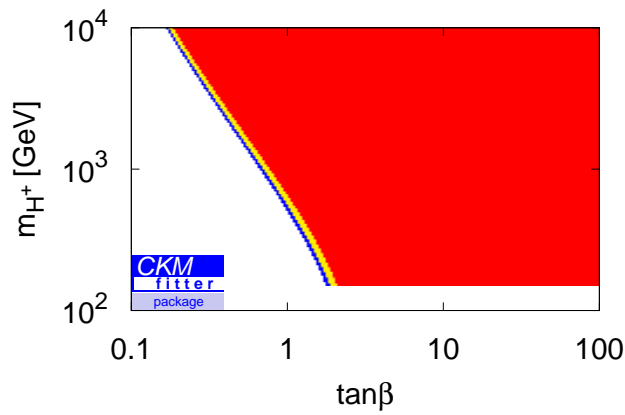
Figure 5.3: B_s^0–$\overline{B}_s^0$ mixing disallows small $\tan\beta$ values. The exact lower bound depends on the mass of the charged Higgs particle. The 1σ, 2σ and 3σ, regions are the coloured in red, yellow and blue, respectively.

Whereas B_s^0 meson mixing provides us with a bound on $\tan\beta$, I will now address an observable for which low m_{H^+} contradicts the experimental measurement – regardless of $\tan\beta$.

5.4.2 $b \to s\gamma$

For the flavour-changing neutral current $b \to s\gamma$ as displayed in Fig. 5.2(b) I included to my fit the branching ratio of $\overline{B}$ mesons decaying into hadrons containing an $\bar{s}$ quark and a photon with an energy larger than $1.6\,\mathrm{GeV}$. Since for these processes also three-loop effects are important, the analytical formulae are quite complicated. Therefore, I parametrized the most up-to-date next-to-next-to-leading order result available [117]:

$$\mathcal{B}(\overline{B} \to X_s\gamma) = \mathcal{B}(\overline{B} \to X_c e^-\bar{\nu})_{\mathrm{exp}} \left| \frac{V_{ts}^* V_{tb}}{V_{cb}} \right|^2 \frac{6\,\alpha_{\mathrm{em}}}{\pi\,C}$$

$$\cdot \left\{ 0.1271 + 2.884\,(\cosh(3.097 - 1.345L) + 15.17)^{-1} \right.$$

$$+ \frac{1}{\tan^2 \beta} \Big[\left(0.05342 + 1.210 \left(0.4343L - 1 \right)^{1.9} + 9.125 \left(0.4343L - 1 \right)^5 \right)$$

$$\left(\cosh(6.696 - 2.908L) \right)^{-1} \Big]$$

$$+ \frac{1}{\tan^4 \beta} \Big[\left(186.3 - 810.0L + 1605L^2 - 1909L^3 \right.$$

$$+ 1501L^4 - 811.8L^5 + 303.9L^6$$

$$- 77.49L^7 + 12.86L^8 - 1.252L^9$$

$$\left. + 0.05439L^{10} \right) \left(\cosh(13.24 - 5.750L) \right)^{-1} \Big] \Big\}$$

$L = \log(m_{H^+}/\mathrm{GeV})$ is the logarithm[1] of the charged Higgs mass in units of GeV and $\mathcal{B}(\overline{B} \to X_c e^- \bar{\nu})_{\mathrm{exp}}$ is the measured branching ratio of semileptonic B to D decays, which is corrected with the factor C to account for its charm quark mass dependence [118]. The used values can be found in Table A.9 in App. A. This parametrized approximation is valid for all $\tan \beta > 0.1$ and m_{H^+} up to 10 TeV; its error σ^{par} is around 2% at most for small $\tan \beta$, compare Fig. 5.4(a). But we are only interested in scenarios which are compatible with the Δm_{B_s} bound, for which σ^{par} is well below 1%. Together with the uncertainties from the prefactors, which were estimated according to [117], I obtain a total theoretical error of 14%. When including $\mathcal{B}(\overline{B} \to X_s \gamma)$ to the fit, the main effect is that the lower charged Higgs mass bound is increased to $m_{H^+} > 250$ GeV at 95% CL for all $\tan \beta$, compare Fig. 5.4(b). This limit is slightly different from the one obtained in [108], because my error estimation is a bit more conservative.

(a)

(b)
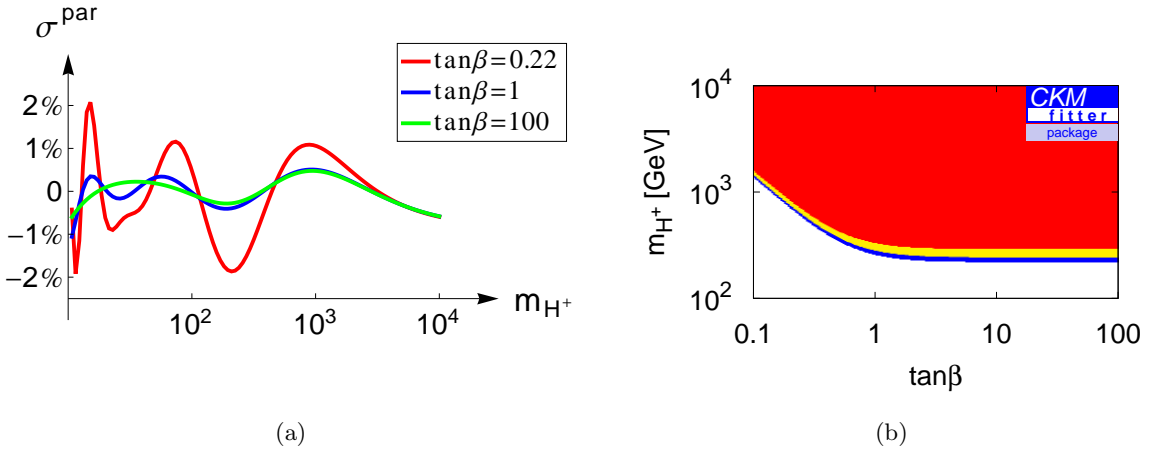
Figure 5.4: The left figure displays the normalized error for my $\mathcal{B}(\overline{B} \to X_s \gamma)$ approximation depending on m_{H^+} for three different values of $\tan \beta$. On the right, the effect of $\mathcal{B}(\overline{B} \to X_s \gamma)$ on the charged Higgs mass fit is shown: $m_{H^+} < 230$ GeV is excluded at 3σ.

Similar figures like 5.3 and 5.4(b) can be found in the CKMfitter analysis of 2HDM effects on flavour observables [116].

---

[1]Note that "log" is the decadic logarithm whereas I denote the natural logarithm by "ln" throughout this work.

5.5 Combined analysis

Like in the previous chapter, I first want to list the relevant literature in order to compare my results with them. The original formulation of the 2HDM dates back to the 1970s, but comprehensive analyses have only been performed in the past years, because only now, we are equipped with observables that can sizeably constrain the 2HDM parameter space. Since it is almost impossible to go into detail about all of these studies, I want to restrict myself to a small selection:

In 2008, the Gfitter collaboration published a 2HDM fit of $\tan\beta$ and the charged Higgs mass, using observables that depend – apart from SM parameters – only on those two parameters. With R_b^0, $\mathcal{B}(\overline{B} \to X_s\gamma)$ and $B \to \tau\nu$ as their strongest constraints, they found $m_{H^+} > 240\,\mathrm{GeV}$ at 95% CL [26]. Before the LHC announced the first hints of the Higgs in 2011, the CKMfitter collaboration performed an extensive fit which in addition to the Gfitter analysis included more flavour observables like e.g. Δm_{B_s} [116], also specializing on $\tan\beta$ and m_{H^+} only. After the Higgs discovery the general interest in the 2HDM increased: The question arose whether the detected boson was the SM Higgs or a Higgs particle of a different model, possibly followed by the observation of further Higgs bosons. Furthermore, the measured Higgs signal strengths could be used as constraints of the 2HDM parameters. A lot of analyses addressed the compatibility of the discovered Higgs with the light $\mathcal{CP}$-even Higgs eigenstate of 2HDM of various types [48, 119–128]; even the possibilities were discussed that the heavy $\mathcal{CP}$-even [105] or the $\mathcal{CP}$-odd Higgs had been found [129], or that two mass degenerate Higgs particles hide behind the bosonic resonance [106], as already mentioned. When the viability of various 2HDM manifestations was tested, most authors presented their results of scans over the 2HDM parameter space, which, however, strongly depends on the chosen parametrization. For instance in [128], a parameter scan was performed combining Higgs data, some flavour constraints and the ρ parameter related to the oblique parameter T as well as perturbativity and stability. They did not find allowed parameter sets with $\tan\beta > 4$ because they chose a parametrization with disadvantageous scan steps. This shows the crucial virtue of parameter *fits*: In parameter scans one usually scans with predefined steps over the single model parameter ranges, calculates the χ^2 at each point and finally takes the lowest χ^2 as global minimum. But these scans will only find the correct global χ^2_{min} if one of the scan points by chance is the best-fit point, which is highly improbable. Parameter fits, however, use the information about the gradient to converge to the χ^2 minimum, so one cannot miss the global χ^2 minimum.

In my combined fit, I use the following bounds to constrain the 2HDM parameters: positivity of the Higgs potential, stability of the 246 GeV vacuum, perturbativity of the quartic couplings, the EWPO, the light Higgs signal strengths, direct H searches up to 1 TeV, and the measurements of Δm_{B_s} and $\mathcal{B}(\overline{B} \to X_s\gamma)$. The SM parameters were set to their best-fit values from Chapter 3 because they are known to a good precision compared to the 2HDM parameters and are not expected to change sizeably. As in the SM4 case, there was already an existing implementation of the 2HDM in the CKMfitter package for their above-mentioned publication on flavour constraints [116]. But apart from the B_s mixing part, I did not use it because in [116] the only free parameters were $\tan\beta$ and the charged Higgs mass, and in the most general 2HDM of type II further parameters enter the analysis of the Higgs signal strengths and EWPO. A fit with 100 minimizations and a 1D scan

with granularity 20 took CKMfitter a few minutes. Having fixed the SM parameters to their best-fit values, I only have to call the Zfitter routine DIZET once for every fit and once for every scan, so the main source of slow-down of the SM4 fits was avoided here.
I do not show the figures from [108] as they are based on data produced with the *my*Fitter framework and cross-checked by my CKMfitter implementation; the figures in this work stem from my CKMfitter fits and are in some sense the invisible half of our publication. Differences between the publication and this thesis can be traced back to slightly changed inputs in the flavour sector, a different parametrization of the 2HDM (CKMfitter uses the physical basis whereas the original couplings of (5.1) were used in *my*Fitter) and the inclusion of the latest R_b^0 expression in the SM, which changed the SM best-fit values. At the best-fit point, $\chi_{\min}^2 = 91.76$; the corresponding parameter values are

$$m_{H^+} = 387 \text{ GeV}, \quad m_{A^0} = 394 \text{ GeV}, \quad m_{H^0} = 465 \text{ GeV},$$
$$\beta - \alpha = 1.581 = 0.5032\pi, \quad \tan\beta = 4.42, \quad \lambda_5 = 0.56$$

Most notably is that $\beta - \alpha$ takes approximately the decoupling limit value of $\frac{\pi}{2}$ at the best-fit point, making the 2HDM and the SM hard to distinguish in low energy observables. Hence, the electroweak precision fit only marginally differs from the SM fit as shown in the deviations list in Fig. 5.5. The signal strength part is a bit more interesting: all bosonic Higgs decays are slightly suppressed in the 2HDM, which could release the tension of the $\mu(H \to WW^*)$ measurements, but on the other hand, more Higgs decays to two photons or Z bosons have been observed than one would expect in the SM, and that is exactly the opposite of the 2HDM prediction, so the corresponding deviations are somewhat increased. (The diminished signal strength can also be seen in the one-dimensional observable predictions of the Higgs decays to neutral bosons in App. B.) Although I also use the two mentioned flavour observables, I do not show their deviation because they are zero due to the theoretical errors involved. Furthermore, they do not contribute to the total $\chi_{\min}^2$ of the best-fit point.
To further investigate how much $\beta - \alpha$ can deviate from $\frac{\pi}{2}$, I show a scan over the $\tan\beta$-$(\beta - \alpha)$ plane in Fig. 5.6(a). One important feature is that $\tan\beta$ is only constrained from below by the Δm_{B_s} measurement, and only because I impose $m_{H^+} < 10$ TeV. At one standard deviation, $\beta - \alpha$ cannot depart from $\frac{\pi}{2}$ by more than 0.02π, independent of $\tan\beta$. For $\tan\beta < 0.5$, $\beta - \alpha$ is basically fixed to the decoupling value. This is due to the flavour observables, which can only compensate the large low $\tan\beta$ contributions with a heavy H^+. This in turn entails heavy neutral Higgs masses because of the EWPO, and we obtain the decoupling limit. If $\tan\beta$ is larger than 3, a second branch appears, and $\beta - \alpha$ can be smaller than 0.4π. This branch, however, which is characterized by comparably small heavy Higgs masses, is excluded at 1σ by the same observables that force $\beta - \alpha$ to the decoupling limit for small $\tan\beta$. For large $\tan\beta$, this strip also approaches the $\beta - \alpha = \frac{\pi}{2}$ limit. In the plane of the coupling ratios r_g^{2HDM} and r_γ^{2HDM} in Fig. 5.6(b), the branch directly corresponds to the disjoint region at the lower right, which features an enhanced ggF Higgs production and at the same time a suppression of diphoton decays. Opposed to this, the 1σ region prefers SM like Higgs couplings, because $\beta - \alpha = \frac{\pi}{2}$ is equivalent to $r_i^{\text{2HDM}} = 1$ for all i (compare Table 5.1).
In Fig. 5.7(a) I show the $\tan\beta$-m_{H^+} plane, compared to Fig. 5.3 and Fig. 5.4(b) only for

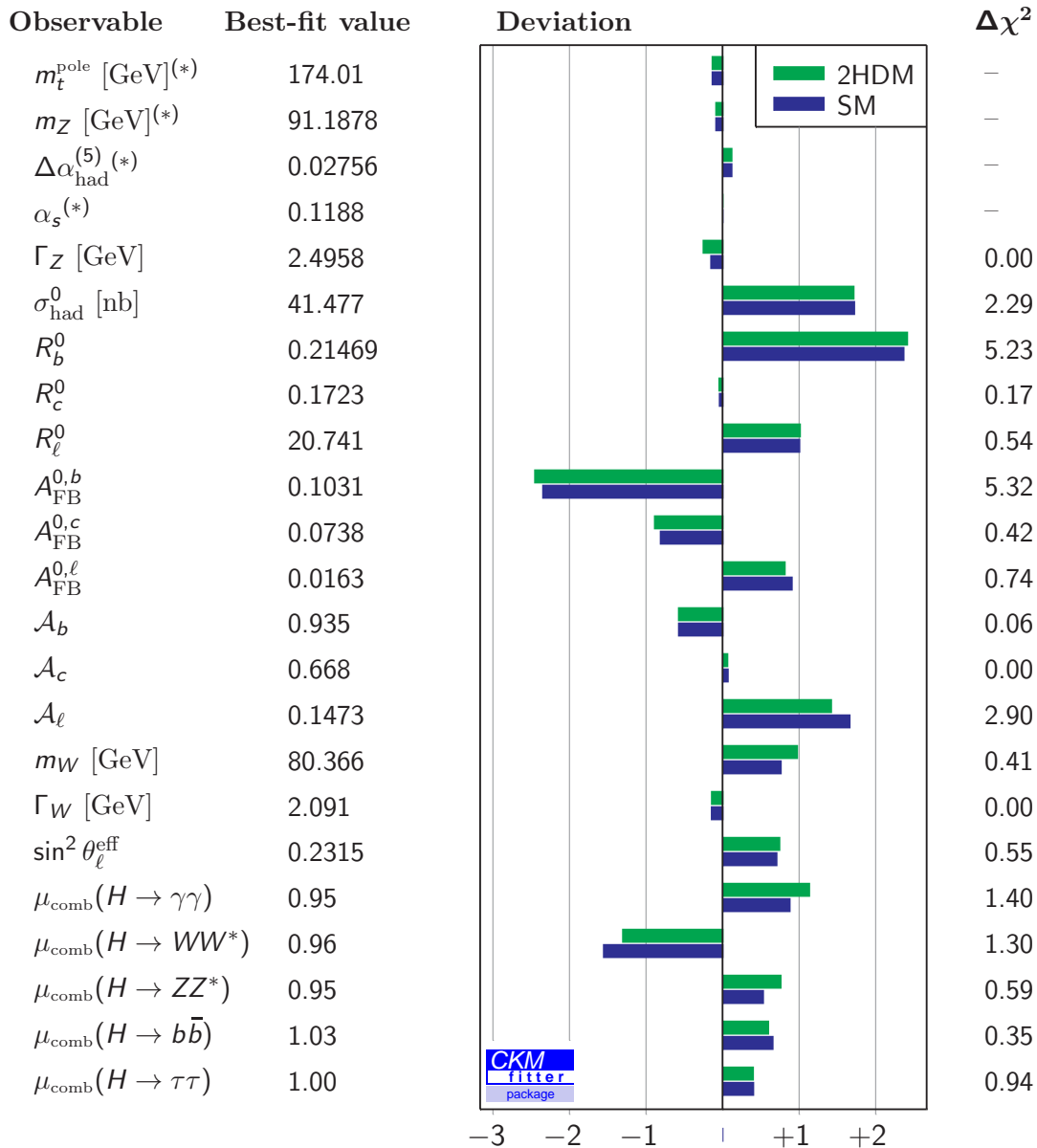| Observable	Best-fit value	Deviation	$\Delta\chi^2$
m_t^{pole} [GeV]$^{(*)}$	174.01		$-$
m_Z [GeV]$^{(*)}$	91.1878		$-$
$\Delta\alpha_{\text{had}}^{(5)\,(*)}$	0.02756		$-$
$\alpha_s^{(*)}$	0.1188		$-$
Γ_Z [GeV]	2.4958		0.00
σ_{had}^0 [nb]	41.477		2.29
R_b^0	0.21469		5.23
R_c^0	0.1723		0.17
R_ℓ^0	20.741		0.54
$A_{\text{FB}}^{0,b}$	0.1031		5.32
$A_{\text{FB}}^{0,c}$	0.0738		0.42
$A_{\text{FB}}^{0,\ell}$	0.0163		0.74
$\mathcal{A}_b$	0.935		0.06
$\mathcal{A}_c$	0.668		0.00
$\mathcal{A}_\ell$	0.1473		2.90
m_W [GeV]	80.366		0.41
Γ_W [GeV]	2.091		0.00
$\sin^2\theta_\ell^{\text{eff}}$	0.2315		0.55
$\mu_{\text{comb}}(H \to \gamma\gamma)$	0.95		1.40
$\mu_{\text{comb}}(H \to WW^*)$	0.96		1.30
$\mu_{\text{comb}}(H \to ZZ^*)$	0.95		0.59
$\mu_{\text{comb}}(H \to b\bar{b})$	1.03		0.35
$\mu_{\text{comb}}(H \to \tau\tau)$	1.00		0.94

Figure 5.5: Deviations of the EWPO and the Higgs signal strengths from the best-fit point in the 2HDM (green) and in the SM (blue). $^{(*)}$ The first four parameters have been treated as fixed in the fit, so their 2HDM deviations are the ones from the SM fit.
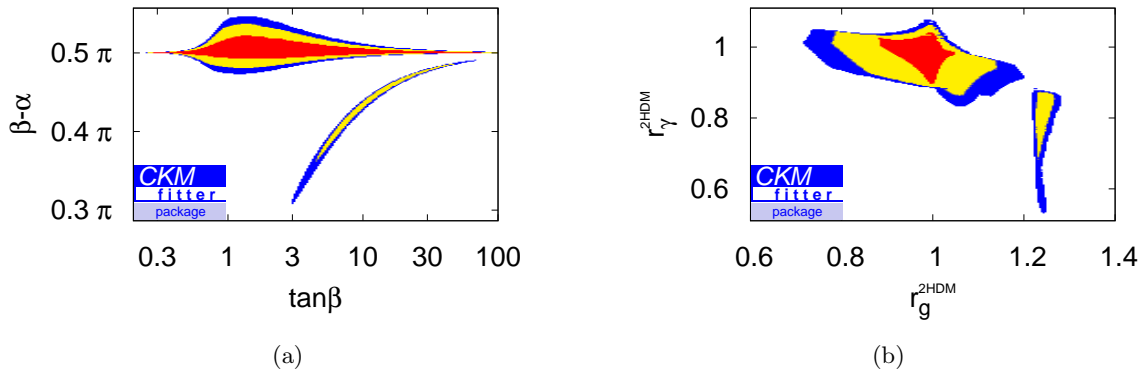
Figure 5.6: Large regions in the $\tan\beta$-$(\beta-\alpha)$ plane are excluded (a). The lower branch is excluded at 1σ. It corresponds to the right area in the $r_g^{2\mathrm{HDM}}$-$r_\gamma^{2\mathrm{HDM}}$ plane (b).

small charged Higgs masses. The flavour observables cut away low $\tan\beta$ and low m_{H^+} regions. If $\tan\beta < 1$, the charged Higgs has to be heavier than 600 GeV at 95% CL.

Scans over the heavy 2HDM masses can be found in Fig. 5.7(b)-(d). One can see that large mass splittings are disfavoured; especially in the high mass regions, perturbative quartic couplings force the masses of the heavy Higgs particles to be relatively close to each other. In combination with constraints for the low mass scenarios like the flavour observables, this allows us to exclude certain on-shell decays for m_{H^0} larger than 715 GeV: the possibility that an H^0 can decay into two charged Higgs bosons is excluded at 3σ, which can be seen in Fig. 5.7(d), and its decay into two A^0 is also excluded at 3σ, compare Fig. 5.7(b). Both decays can be ruled out at 1σ independent of the 2HDM masses. Moreover, 2HDM realizations where the H^0 and the A^0 are simultaneously lighter than 250 GeV are excluded at two standard deviation; $m_{A^0} < 200$ GeV is disfavoured at 1σ. The heavy $\mathcal{CP}$-even Higgs mass is not constrained from below. If we chose 4π as a more conservative perturbativity bound on the quartic couplings, the mass splittings can be larger by 250 GeV [108].

As already mentioned, the SM is nested in the 2HDM. However, the assumption of linear behaviour of the Higgs signal strengths is only an approximation since their errors are still sizeable. And especially the flavour observables are not Gaussian distributed, because they have large theoretical uncertainties. As all experimental data pushes the 2HDM towards its decoupling limit, i.e. the SM, it is useless to calculate the p-value of the SM: it will be one.

The next step could be the inclusion of further flavour observables to examine the large $\tan\beta$ regions. As the (semi-)tauonic B decay measurements cannot be explained in the framework of the 2HDM of type II, it would be interesting to consider a more general model of type III, where flavour-changing neutral currents can occur at tree level.

As a final remark about the 2HDM, I want to mention that there have been analyses which combine the idea of a fourth fermion generation with an additional Higgs doublet [130, 131]. The signal strengths, which essentially ruled out the SM4, have to be reinterpreted in these scenarios. For example, due to supplementary Higgs loops in this combined model the diphoton decay would not necessarily be suppressed like it was the case in the SM4.
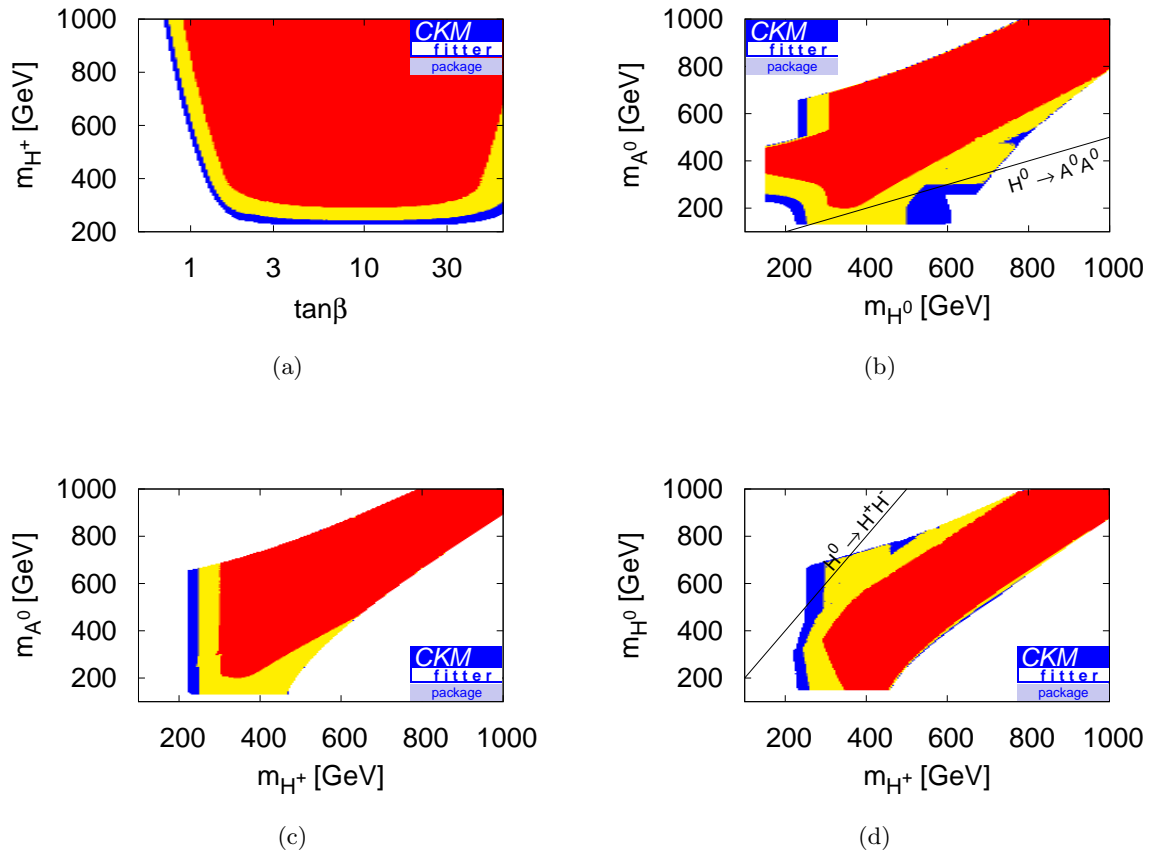
Figure 5.7: Light charged Higgs bosons and low $\tan\beta$ values are excluded by a combination of flavour observables (a). The allowed heavy Higgs mass values are shown in the m_{H^0}-m_{A^0} plane (b), the m_{H^+}-m_{A^0} plane (c) and the m_{H^+}-m_{H^0} plane (d). $m_{A^0} > 200$ GeV and $m_{H^+} > 290$ GeV at 1σ. The magnitude of potential mass splittings decreases with heavier Higgs masses. The decays $H^0 \to A^0 A^0$ and $H^0 \to H^+ H^-$ can be excluded at 1σ and for $m_{H^0} > 715$ GeV even at 3σ.

If perturbative heavy fermions were to be found at the LHC (to which there are no indications at the moment), it would mean at the same time that some other part of the SM Lagrangian needs to be modified – the most obvious choice would then probably be the Higgs sector.

CHAPTER 6

Conclusions

In this thesis I have presented comprehensive analyses of the viable parameter regions of the Standard Model of particle physics and two of its extensions: the Standard Model with four fermion generations and the Two-Higgs-Doublets model of type II. I have performed global fits which show that the SM is compatible with electroweak precision data and the Higgs signal strengths, the SM4 is excluded by the experimental results at more than 5σ, and that in the 2HDM, despite the fit preferring the decoupling limit where it mimics the SM, neutral Higgs boson masses below 200 GeV are still allowed.

The Higgs discovery announced on 4th July 2012 means that for the first time we are equipped with direct measurements of *all* SM parameters. In that sense one could say that the SM is complete now. After that date, we accomplished the first global SM fit to EWPO and Higgs data [12]. Almost all observables of the EWPO and the Higgs signal strengths are in good agreement with the SM; the *b* quark forward-backward asymmetry and the decay width ratio R_b^0 have the largest deviations. If the combined Higgs mass input is included in the fit, the *W* boson mass and the top quark mass receive shifts which are sizeable compared to their experimental uncertainties from their measured central values.

The same observables which corroborate the SM are in conflict with the SM4 hypothesis. Most notably, the signal strength of Higgs decays to two photons, which should approximately vanish in the SM4, has a deviation of 6σ. Also the signal strength of $H \to b\bar{b}$ decays is expected to be suppressed in the SM4, yet the measurements seem to favour the SM expectation, and the SM4 deviation is almost 3σ. The best-fit neutrino mass is required to be lighter than $m_H/2$, such that the invisible decay $H \to \nu_4\nu_4$ is possible. Even then fewer tauonic Higgs decays than expected in the SM4 have been observed. The EWPO fit prefers no mixing between the fourth generation and the SM quarks, and it demands small mass splittings in the $SU(2)$ fermion doublets, so the best-fit mass of the fourth generation charged lepton is almost as low as allowed by direct searches. This also holds for the fourth generation quarks: the SM4 particles do not decouple, and the higher their masses the larger is the effect on the discussed observables. This non-nestedness makes it difficult to reliably determine the *p*-value. However, exactly this property enables us to rule out a fourth fermion generation. For this purpose, we have used the newly developed program *my*Fitter to carry out a likelihood ratio test comparing the SM and the SM4. With the data that was publicly available shortly after the announcement of the Higgs discovery, we could exclude the SM4 with a *p*-value of $1.1 \cdot 10^{-7}$ corresponding to 5.3σ [12]. With the latest Higgs search data, the *p*-value is expected to be even smaller. After the Higgs discovery, the interest in the SM4 dropped almost immediately. The rise and fall

of the SM4 in the last decade is illustrated in Fig. 6.1, which can be approximated by the very same asymmetric Gaussian p.d.f. that we know already from Fig. 2.1(b), assuming an offset of 7. Like in the introduction I display the publication density function of articles containing the expressions "fourth generation", "4th generation", "fourth family", or "4th family" in their title [11]. Fig. 6.1 shows the number of papers released within the last ten years ordered by the year of publication. While the slope seemed to be an exponential at the beginning (dashed line), the publication rate reached a maximum in the year 2011 and has been receding since then. (The 2013 data shaded in grey were extrapolated assuming a constant distribution over the year.)
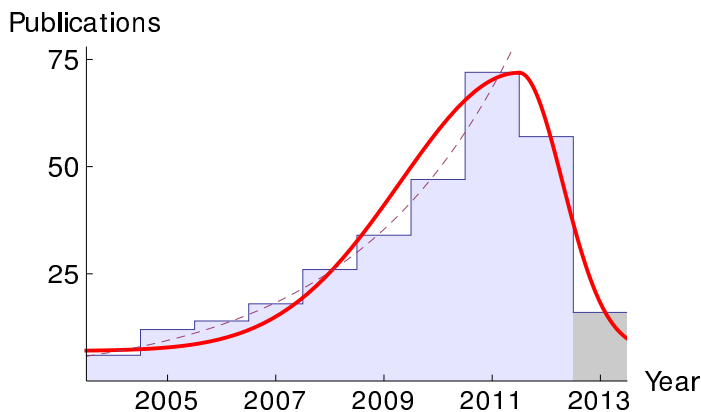
Figure 6.1: Distribution of SM4 publications over the last decade.

In contrast to the SM4, the 2HDM and the SM are nested, so that one can only exclude the parameter regions of the 2HDM which exhibit a fundamentally different phenomenology than the SM. In order to analyze these regions, I implemented the 2HDM of type II with soft Z_2 breaking and with perturbativity, positivity and stability conditions into CKMfitter. Additionally to the EWPO and Higgs signal strengths I also included the flavour-changing neutral current observables $\mathcal{B}(\overline{B} \to X_s\gamma)$ and Δm_{B_s} in the fit because they severely constrain low mass regions of the parameter space. The discovered Higgs boson is interpreted as the lighter $\mathcal{CP}$-even mass eigenstate throughout and its signal strengths are treated similar to the SM4. The heavy $\mathcal{CP}$-even mass eigenstate was constrained by the non-observation of $H \to ZZ$ decays between $150\,\mathrm{GeV}$ and $1\,\mathrm{TeV}$. The result of the fit is that the decoupling limit is preferred. While low $\tan\beta$ and m_{H^+} values are excluded by the flavour observables, perturbativity and the EWPO delimit the mass splittings of the heavy Higgs particles. Only for an intermediate $\tan\beta$ range $\beta - \alpha$ is allowed to deviate substantially from the decoupling value $\frac{\pi}{2}$, but these shifts are excluded at 1σ. The decays $H^0 \to H^+H^-$ and $H^0 \to A^0A^0$ are excluded at 3σ, if the H^0 is heavier than $715\,\mathrm{GeV}$. The results have been published in [108]. Furthermore, I have performed scans predicting the EWPO and the Higgs signal strengths in the three models, which can be found in Appendix B.

The main message of the evaluated LHC data from 2011 and 2012 is that the SM is now complete and confirmed to an unprecedented extent. Many physicists hope that the next LHC run, which will start in 2015 with an increased centre-of-mass energy, reveals unexpected signatures, maybe even the discovery of new particles. It will certainly provide

us with constraints on many models beyond the SM. However, to determine their viability or even to state an exclusion, it is indispensable to perform statistically correct analyses. The methodology and the tools developed for this thesis can be used to study a wide class of these new physics models.

APPENDIX A

Inputs

In this appendix I list all numerical inputs that were used for the fits in this thesis. First of all, I present the data that were important for the SM fit in Chapter 3. It is followed by a discussion of the Higgs observables, which are crucial for the SM4 fits in Chapter 4, but also for the other two models. Finally, the numerical values for the flavour observables that were used as constraints in Chapter 5 are shown. For all observables, I give the central input value and the errors as well as the source. The first error is always the statistical uncertainty – in some cases they are asymmetric –, and the second is the systematic uncertainty, if any.

As far as the CKM matrix elements are concerned, I rely on the values from the Particle Data Book. Yet especially for the SM4 part one needs to be careful not to include any inputs basing on 3×3 unitarity of V. For example $|V_{tb}| = 1$ is a valid approximation in the SM and in the 2HDM, because we know to good precision that $|V_{ub}|$ and $|V_{cb}|$ are small and the unitarity relation is $|V_{ub}|^2 + |V_{cb}|^2 + |V_{tb}|^2 = 1$. But this relation does not necessarily hold in the SM4, so I chose the tree-level values below and let the fitter parts of the respective model account for unitarity. A CKMfitter look-up table for the unitarity triangle angle γ was used to constrain the $\mathcal{CP}$ phase(s).

Quantity	Input value	Source
$|V_{ud}|$	0.97425 ± 0.00022	[132]
$|V_{us}|$	0.2252 ± 0.0009	[13]
$|V_{ub}|$	$4.15 \cdot 10^{-3} \pm 0.49 \cdot 10^{-3}$	[13]
$|V_{cd}|$	0.230 ± 0.011	[13]
$|V_{cs}|$	$0.98 \pm 0.01 \pm 0.10$	[13]
$|V_{cb}|$	$40.9 \cdot 10^{-3} \pm 1.1 \cdot 10^{-3}$	[13]
$|V_{tb}|$	0.89 ± 0.07	[13]
γ	CKMfitter fit	[133]

Table A.1: CKM matrix inputs.

The EWPO fits presented in Sect. 3.2 and 3.3, and also the SM4 and 2HDM fits are based on the following experimental values, mainly stemming from the LEP detectors and SLD:

Quantity	Input value	Source
m_t^{pole}	$173.18 \pm 0.56 \pm 0.75$ GeV	[134]
m_Z	91.1876 ± 0.0021 GeV	[13]
$\Delta\alpha_{\mathrm{had}}^{(5)}$	0.02757 ± 0.00010	[27]
α_s	$0.1202 \pm 0.0006 \pm 0.0021$	[28]
Γ_Z	2.4952 ± 0.0023 GeV	[24]
σ_{had}^0	41.541 ± 0.037 nb	[13]
R_b^0	0.21629 ± 0.00066	[24]
R_c^0	0.1721 ± 0.0030	[24]
R_ℓ^0	20.767 ± 0.025	[24]
$A_{\mathrm{FB}}^{0,b}$	0.0992 ± 0.0016	[24]
$A_{\mathrm{FB}}^{0,c}$	0.0707 ± 0.0035	[24]
$A_{\mathrm{FB}}^{0,\ell}$	0.0171 ± 0.0010	[24]
$\mathcal{A}_b$	0.923 ± 0.020	[24]
$\mathcal{A}_c$	0.670 ± 0.027	[24]
$\mathcal{A}_\ell$	0.1499 ± 0.0018	[24, 49]
m_W	$80.385 \pm 0.015 \pm 0.004$ GeV	[135, 136]
Γ_W	2.085 ± 0.042 GeV	[137]
$\sin^2\theta_\ell^{\mathrm{eff}}$	0.2324 ± 0.0012	[24]

Table A.2: EWPO inputs.

The systematic uncertainty for m_W was adopted from [136] like in the Gfitter publication [49], but the systematic error on $\sin^2\theta_\ell^{\mathrm{eff}}$ was neglected in this work, since its magnitude is less than 4% of the statistical error. During the last stage of this work, a new combination of Tevatron top mass measurements was released: $m_t^{\mathrm{pole}} = 173.20 \pm 0.51 \pm 0.71$ GeV [138]. Compared to the above value used for my fits, the central value stays approximately the same and the errors decrease slightly; however, I do not expect that the improved uncertainties fundamentally change the results presented in this thesis. Some of the Z pole observables are correlated; their inverse covariance matrix entries are displayed in Table A.3.

	M_Z	Γ_Z	σ^0_{had}	R^0_ℓ	$A^{0,\ell}_{FB}$
M_Z	1	−0.02	−0.05	0.03	0.06
Γ_Z		1	−0.30	0	0
σ^0_{had}			1	0.18	0.01
R^0_ℓ				1	−0.06
$A^{0,\ell}_{FB}$					1

	$A^{0,c}_{FB}$	$A^{0,b}_{FB}$	A_c	A_b	R^0_c	R^0_b
$A^{0,c}_{FB}$	1	0.15	0.04	−0.02	−0.06	0.07
$A^{0,b}_{FB}$		1	0.01	0.06	0.04	−0.10
A_c			1	0.11	−0.06	0.04
A_b				1	0.04	−0.08
R^0_c					1	−0.18
R^0_b						1

Table A.3: Correlations between Z and leptonic observables and between b and c precision measurements at LEP [24].

The W mass and decay width are also correlated, but this correlation is only small, and since the values for the two observables originate from different experiments, I neglect it. The last missing input on the SM fit was the Higgs mass. I use a combination of the following LHC measurements:

Quantity	Input value	Source
$m_H^{\mathrm{ATLAS}}(H \to \gamma\gamma)$	$126.8 \pm 0.2 \pm 0.7$ GeV	[139]
$m_H^{\mathrm{CMS}}(H \to \gamma\gamma)$	$125.4 \pm 0.5 \pm 0.6$ GeV	[140]
$m_H^{\mathrm{ATLAS}}(H \to ZZ)$	$124.3^{+0.6}_{-0.5} \pm 0.4$ GeV	[141]
$m_H^{\mathrm{CMS}}(H \to ZZ)$	$125.8 \pm 0.5 \pm 0.2$ GeV	[107]

Table A.4: Mass measurements for the bosonic resonance around 126 GeV. The combination yields $m_H = 125.96^{+0.18}_{-0.19}$.

But not only the reconstructed invariant mass of the (light $\mathcal{CP}$-even) Higgs boson is of importance, also other information like the relative occurrence of decay products compared to the SM expectation are relevant; this is expressed by the collection of signal strengths in Fig. A.1 which represents the status after the Moriond 2013 conferences.

The upper index denotes the data set the measured signal strength relies on. "T" stands for the complete evaluated Tevatron data of up to $10\,\mathrm{fb}^{-1}$. "$A7$" and "$A8$" are the publicly available ATLAS signal strengths obtained at $\sqrt{s} = 7\,\mathrm{TeV}$ and at $\sqrt{s} = 8\,\mathrm{TeV}$, respectively; "$C7$" and "$C8$" label the corresponding measurements by the CMS detector. The Higgs decay products $XX^{(*)}$ are indicated by the bracket ($H \to XX$), where $X \in \{\gamma, \tau, W, Z\}$. For signal strengths characterized by the decay $H \to b\bar{b}$ I assumed that only vector boson associated production plays a role (except for $\mu^{C7}(t\bar{t}H \to t\bar{t}b\bar{b})$, where exclusively $t\bar{t}$ associated production is important), therefore I explicitly list the associated particles. $\mu^{A8}(H \to \tau\tau)$, $\mu^{A8}(H \to ZZ)$, $\mu^{C8}(VH \to Vb\bar{b})$, the tauonic signal strengths of CMS at $\sqrt{s} = 8\,\mathrm{TeV}$ and $\mu^{C8}(H \to ZZ)$ were reconstructed from the combined values in the quoted publications using Equations (2.2) and (2.3) and our knowledge of the 7 TeV data. The tags of the tauonic decays measured at CMS denote the reconstructed final states additional to the τ pair. $H \to \gamma\gamma$ events were separated into up to fourteen categories, which were provided by the detector collaborations together with the corresponding percentage contributions. I refer to the related publications for further explanation. This figure represents the situation at the beginning of May 2013; the latest CMS updates in the middle of May 2013 have not been included. Even if there are correlations between Higgs signal strengths, I could not take them into account because they were not provided by the detector collaborations.

Since we do not know the production mechanism of the individual Higgs candidate events, I chose to use percentage contributions. If they are not given directly, one can derive them from the efficiencies via Eq. (4.1). For the tauonic Higgs decays at CMS the percentage contributions were derived using the summed efficiencies of the five decay sub-channels $\mu\tau_h$, $e\tau_h$, $e\mu$, $\mu\mu$ and $\tau_h\tau_h$ (where τ_h is a τ lepton decaying into hadrons); they can be found in Table A.5. Whereas the ggF and VBF ("$qq \to H$") dominated production parts are explicitly given in [151], the three less important production channels are subsumed under the tag "$qq \to Ht\bar{t}$ or VH"; they were split to the channels defined in Sect. 3.3 according to the relative occurrence from Fig. 3.3. Same efficiencies at 7 and 8 TeV were assumed.

		ggF	VBF	WH	ZH	ttH
CMS	0/1 jet	0.808	0.119	0.042	0.024	0.008
	VBF	0.245	0.742	0.007	0.004	0.001

Table A.5: Percentage contributions as defined in equation (4.1) for the $H \to \tau\tau$ signal strengths derived from the efficiencies in [151].

$\mu^{\mathrm{T}}(VH \to Vb\bar{b}) = 1.59^{+0.69}_{-0.72}$ [38]
$\mu^{\mathrm{T}}(H \to \gamma\gamma) = 5.97^{+3.39}_{-3.12}$ [38]
$\mu^{\mathrm{T}}(H \to \tau\tau) = 1.68^{+2.28}_{-1.68}$ [38]
$\mu^{\mathrm{T}}(H \to WW) = 0.94^{+0.85}_{-0.83}$ [38]
$\mu^{\mathrm{A7}}(VH \to Vb\bar{b}) = 0.481 \pm 2.185$ [142]
$\mu^{\mathrm{A7}}(H \to \gamma\gamma)_{\mathrm{jj}} = 2.896 \pm 1.887$ [143]
$\mu^{\mathrm{A7}}(H \to \gamma\gamma)_{\mathrm{cch}} = -3.665 \pm 1.916$ [143]
$\mu^{\mathrm{A7}}(H \to \gamma\gamma)_{\mathrm{ccl}} = 5.276 \pm 2.554$ [143]
$\mu^{\mathrm{A7}}(H \to \gamma\gamma)_{\mathrm{crh}} = -0.675^{+2.845}_{-2.816}$ [143]
$\mu^{\mathrm{A7}}(H \to \gamma\gamma)_{\mathrm{crl}} = 2.779^{+1.945}_{-1.916}$ [143]
$\mu^{\mathrm{A7}}(H \to \gamma\gamma)_{\mathrm{ct}} = 0.370^{+3.628}_{-3.599}$ [143]
$\mu^{\mathrm{A7}}(H \to \gamma\gamma)_{\mathrm{uch}} = 0.022^{+1.887}_{-1.916}$ [143]
$\mu^{\mathrm{A7}}(H \to \gamma\gamma)_{\mathrm{ucl}} = 0.602 \pm 1.422$ [143]
$\mu^{\mathrm{A7}}(H \to \gamma\gamma)_{\mathrm{urh}} = 10.936 \pm 3.657$ [143]
$\mu^{\mathrm{A7}}(H \to \gamma\gamma)_{\mathrm{url}} = 1.967 \pm 1.597$ [143]
$\mu^{\mathrm{A7}}(H \to \tau\tau) = 0.407^{+1.630}_{-2.037}$ [142]
$\mu^{\mathrm{A7}}(H \to WW) = 0.0^{+0.6}_{-0.6}$ [144]
$\mu^{\mathrm{A7}}(H \to ZZ) = 1.185^{+1.222}_{-0.815}$ [142]
$\mu^{\mathrm{A8}}(VH \to Vb\bar{b}) = 1.0 \pm 0.9 \pm 1.1$ [145]
$\mu^{\mathrm{A8}}(H \to \gamma\gamma)_{\mathrm{lept}} = 2.711^{+1.980}_{-1.657}$ [139]
$\mu^{\mathrm{A8}}(H \to \gamma\gamma)_{\mathrm{cch}} = 2.005^{+1.519}_{-1.258}$ [139]
$\mu^{\mathrm{A8}}(H \to \gamma\gamma)_{\mathrm{ccl}} = 1.391^{+1.043}_{-0.951}$ [139]
$\mu^{\mathrm{A8}}(H \to \gamma\gamma)_{\mathrm{crh}} = 1.299^{+1.320}_{-1.274}$ [139]
$\mu^{\mathrm{A8}}(H \to \gamma\gamma)_{\mathrm{crl}} = 2.220^{+1.166}_{-0.997}$ [139]
$\mu^{\mathrm{A8}}(H \to \gamma\gamma)_{\mathrm{ct}} = 2.818^{+1.688}_{-1.596}$ [139]
$\mu^{\mathrm{A8}}(H \to \gamma\gamma)_{\mathrm{lhmjj}} = 2.772^{+1.780}_{-1.381}$ [139]
$\mu^{\mathrm{A8}}(H \to \gamma\gamma)_{\mathrm{lmjj}} = 0.332^{+1.734}_{-1.458}$ [139]
$\mu^{\mathrm{A8}}(H \to \gamma\gamma)_{\not{E}_{\mathrm{T}}} = 2.987^{+2.716}_{-2.164}$ [139]
$\mu^{\mathrm{A8}}(H \to \gamma\gamma)_{\mathrm{thmjj}} = 1.621^{+0.829}_{-0.675}$ [139]
$\mu^{\mathrm{A8}}(H \to \gamma\gamma)_{\mathrm{uch}} = 0.962^{+1.090}_{-0.936}$ [139]
$\mu^{\mathrm{A8}}(H \to \gamma\gamma)_{\mathrm{ucl}} = 0.885^{+0.721}_{-0.706}$ [139]
$\mu^{\mathrm{A8}}(H \to \gamma\gamma)_{\mathrm{urh}} = 2.711^{+1.350}_{-1.151}$ [139]
$\mu^{\mathrm{A8}}(H \to \gamma\gamma)_{\mathrm{url}} = 2.527^{+0.921}_{-0.783}$ [139]
$\mu^{\mathrm{A8}}(H \to \tau\tau) = 0.756^{+0.775}_{-0.745}$ [142, 146]
$\mu^{\mathrm{A8}}(H \to WW) = 1.26 \pm 0.35$ [144]
$\mu^{\mathrm{A8}}(H \to ZZ) = 1.603^{+0.423}_{-0.459}$ [141, 142]
$\mu^{\mathrm{C7}}(t\bar{t}H \to t\bar{t}b\bar{b}) = -0.729^{+2.018}_{-1.853}$ [147]
$\mu^{\mathrm{C7}}(VH \to Vb\bar{b}) = 0.588^{+1.235}_{-1.153}$ [147]
$\mu^{\mathrm{C7}}(H \to \gamma\gamma)_{\mathrm{u0}} = 3.832^{+2.042}_{-1.671}$ [140]
$\mu^{\mathrm{C7}}(H \to \gamma\gamma)_{\mathrm{u1}} = 0.193^{+1.002}_{-0.965}$ [140]
$\mu^{\mathrm{C7}}(H \to \gamma\gamma)_{\mathrm{u2}} = 0.045 \pm 1.262$ [140]
$\mu^{\mathrm{C7}}(H \to \gamma\gamma)_{\mathrm{u3}} = 1.493 \pm 1.634$ [140]
$\mu^{\mathrm{C7}}(H \to \gamma\gamma)_{\mathrm{jj}} = 4.203^{+2.339}_{-1.782}$ [140]
$\mu^{\mathrm{C7}}(H \to \tau\tau)_{0/1\,\mathrm{jet}} = 1.000^{+1.441}_{-1.400}$ [147]
$\mu^{\mathrm{C7}}(H \to \tau\tau)_{\mathrm{VBF}} = -1.718^{+1.318}_{-1.153}$ [147]
$\mu^{\mathrm{C7}}(H \to \tau\tau)_{\mathrm{VH}} = 0.671^{+4.076}_{-3.047}$ [147]
$\mu^{\mathrm{C7}}(H \to WW) = 0.726^{+0.417}_{-0.412}$ [148]
$\mu^{\mathrm{C7}}(H \to ZZ) = 0.671^{+0.700}_{-0.494}$ [147]
$\mu^{\mathrm{C8}}(VH \to Vb\bar{b}) = 1.584^{+0.771}_{-0.704}$ [147, 149]
$\mu^{\mathrm{C8}}(H \to \gamma\gamma)_{\mathrm{u0}} = 2.198^{+0.928}_{-0.817}$ [140]
$\mu^{\mathrm{C8}}(H \to \gamma\gamma)_{\mathrm{u1}} = 0.045 \pm 0.705$ [140]
$\mu^{\mathrm{C8}}(H \to \gamma\gamma)_{\mathrm{u2}} = 0.304 \pm 0.483$ [140]
$\mu^{\mathrm{C8}}(H \to \gamma\gamma)_{\mathrm{u3}} = -0.327^{+0.817}_{-0.854}$ [140]
$\mu^{\mathrm{C8}}(H \to \gamma\gamma)_{\mathrm{e}} = -0.661^{+2.785}_{-1.968}$ [140]
$\mu^{\mathrm{C8}}(H \to \gamma\gamma)_{\mathrm{jj\,loose}} = 0.824^{+1.077}_{-1.002}$ [140]
$\mu^{\mathrm{C8}}(H \to \gamma\gamma)_{\mathrm{jj\,tight}} = 0.304^{+0.668}_{-0.594}$ [140]
$\mu^{\mathrm{C8}}(H \to \gamma\gamma)_{\not{E}_{\mathrm{T}}} = 1.938^{+2.599}_{-2.339}$ [140]
$\mu^{\mathrm{C8}}(H \to \gamma\gamma)_{\mu} = 0.416^{+1.819}_{-1.411}$ [140]
$\mu^{\mathrm{C8}}(H \to \tau\tau)_{0/1\,\mathrm{jet}} = 1.109^{+0.416}_{-0.417}$ [147, 150]
$\mu^{\mathrm{C8}}(H \to \tau\tau)_{\mathrm{VBF}} = 2.375^{+0.674}_{-0.703}$ [147, 150]
$\mu^{\mathrm{C8}}(H \to \tau\tau)_{\mathrm{VH}} = 0.780^{+1.613}_{-1.723}$ [147, 150]
$\mu^{\mathrm{C8}}(H \to WW) = 0.647^{+0.225}_{-0.221}$ [148]
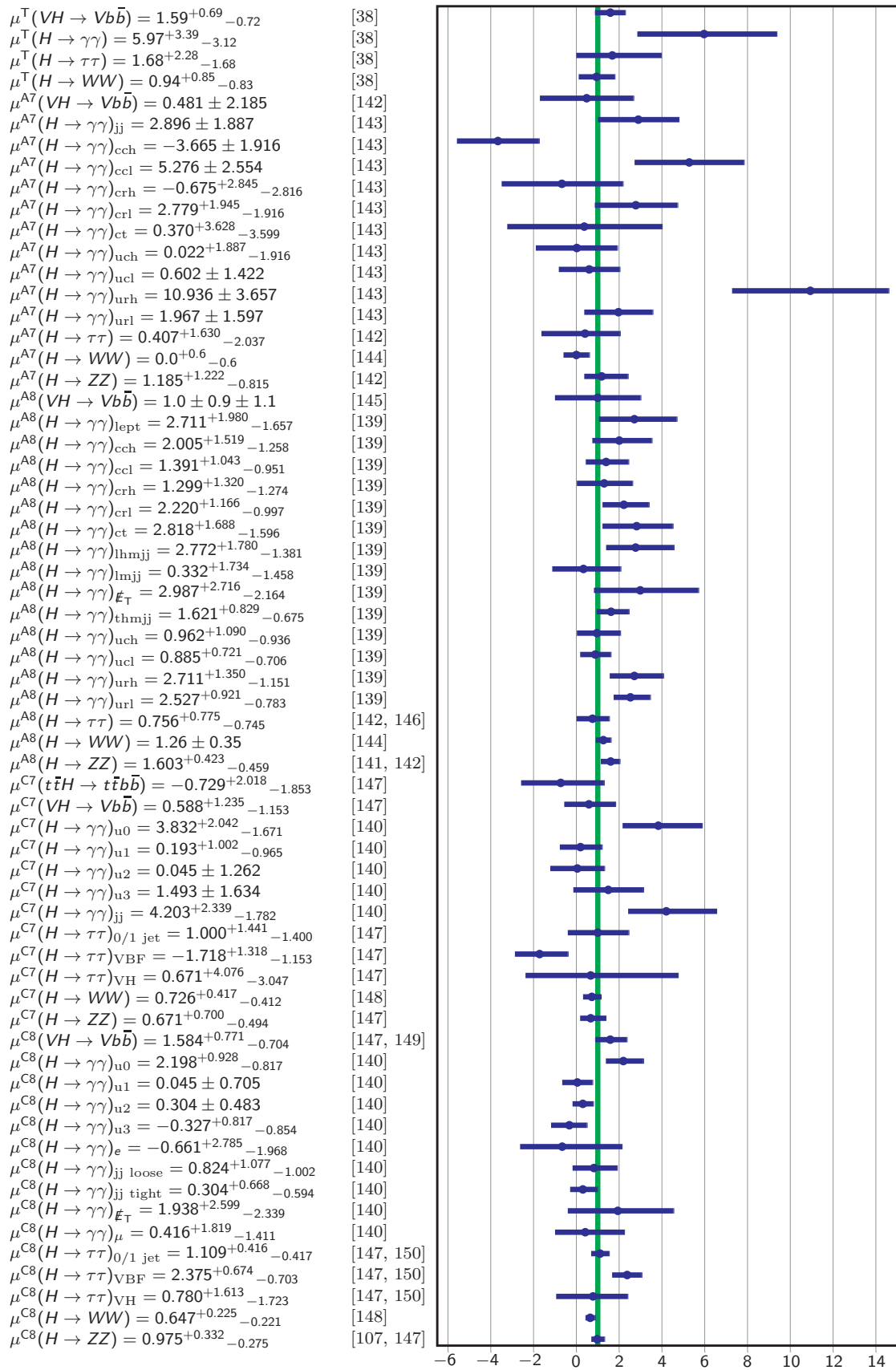$\mu^{\mathrm{C8}}(H \to ZZ) = 0.975^{+0.332}_{-0.275}$ [107, 147]

Figure A.1: Individual signal strengths measured by D∅, CDF, ATLAS and CMS (status April 2013 after the Moriond conferences). The combination yields $\mu_{\mathrm{comb}} = 1.007^{+0.099}_{-0.098}$ and is depicted by the green band. A similar figure can be found in [108].

In the diphoton decay channel, percentage contributions for both, the 7 and 8 TeV data set are stated in the respective ATLAS and CMS publications. They are listed in Table A.6. The different tags correspond to the sub-channels in Fig. A.1.

		ggF	VBF	WH	ZH	ttH
ATLAS 7 TeV						
	jj	0.225	0.767	0.004	0.002	0.001
	cch	0.666	0.153	0.100	0.057	0.025
	ccl	0.928	0.040	0.019	0.010	0.002
	crh	0.653	0.160	0.110	0.059	0.018
	crl	0.928	0.038	0.020	0.011	0.002
	ct	0.894	0.052	0.033	0.017	0.003
	uch	0.665	0.157	0.099	0.057	0.024
	ucl	0.929	0.040	0.018	0.010	0.002
	urh	0.654	0.161	0.108	0.061	0.018
	url	0.928	0.039	0.020	0.011	0.002
ATLAS 8 TeV						
	lept	0.022	0.006	0.632	0.154	0.186
	cch	0.789	0.126	0.043	0.027	0.015
	ccl	0.936	0.040	0.013	0.009	0.002
	crh	0.777	0.130	0.052	0.030	0.011
	crl	0.932	0.041	0.016	0.010	0.001
	ct	0.907	0.055	0.022	0.013	0.002
	lhmjj	0.450	0.541	0.005	0.003	0.001
	lmjj	0.481	0.030	0.297	0.172	0.019
	$\not{E}_\mathrm{T}$	0.041	0.005	0.357	0.476	0.121
	thmjj	0.238	0.760	0.001	0.001	0.000
	uch	0.793	0.126	0.041	0.025	0.014
	ucl	0.937	0.040	0.014	0.008	0.002
	urh	0.781	0.133	0.047	0.028	0.011
	url	0.932	0.040	0.016	0.010	0.001

		ggF	VBF	WH	ZH	ttH
CMS 7 TeV						
	u0	0.614	0.168	0.121	0.066	0.031
	u1	0.876	0.062	0.036	0.020	0.005
	u2	0.913	0.044	0.025	0.014	0.003
	u3	0.913	0.044	0.026	0.015	0.002
	jj	0.268	0.725	0.004	0.002	0.000
CMS 8 TeV						
	u0	0.729	0.116	0.082	0.047	0.026
	u1	0.835	0.084	0.045	0.026	0.010
	u2	0.916	0.045	0.023	0.013	0.004
	u3	0.925	0.039	0.021	0.012	0.003
	e	0.011	0.004	0.502	0.285	0.198
	jj loose	0.470	0.509	0.011	0.006	0.005
	jj tight	0.207	0.789	0.002	0.001	0.001
	$\not{E}_\mathsf{T}$	0.220	0.026	0.407	0.230	0.117
	μ	0.000	0.002	0.504	0.286	0.208

Table A.6: Percentage contributions from [139, 140, 152].

If neither percentage contributions nor efficiencies were provided by the detector collaborations, I used the relative occurrences as listed in Fig. 3.3. (In the case of the $H \rightarrow b\bar{b}$ signal strengths, I set all other contributions to zero.) They can be found in Table A.7.

		ggF	VBF	WH	ZH	ttH
Tevatron		0.748	0.058	0.118	0.073	0.003
Tevatron	VH only	0.000	0.000	0.619	0.381	0.000
LHC 7 TeV		0.875	0.070	0.032	0.018	0.005
LHC 7 TeV	VH only	0.000	0.000	0.644	0.356	0.000
LHC 8 TeV		0.875	0.071	0.031	0.017	0.006
LHC 8 TeV	VH only	0.000	0.000	0.638	0.362	0.000

Table A.7: Percentage contributions as defined in equation (4.1) as extracted from [42, 43].
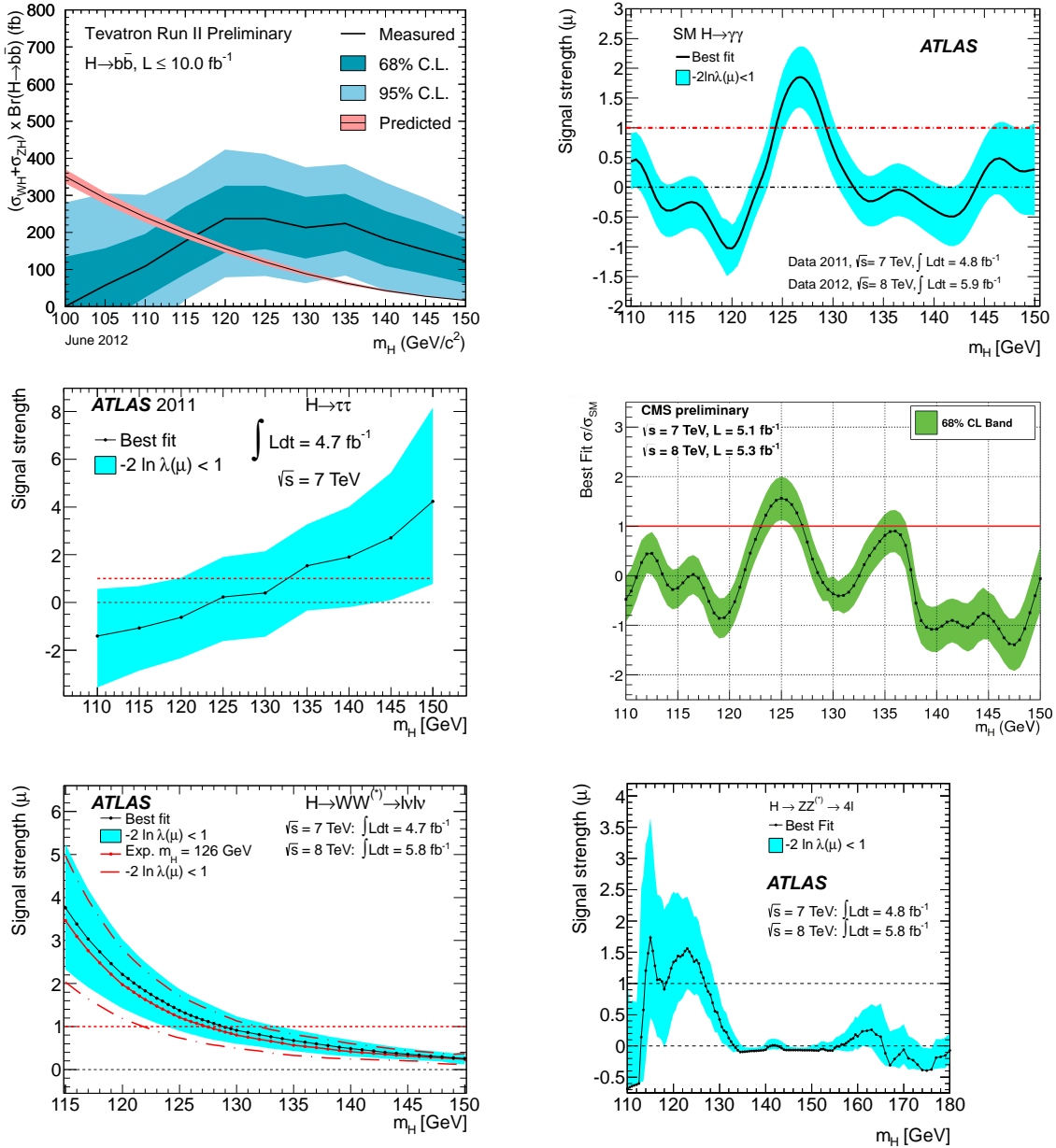
Figure A.2: Higgs signal strengths as functions of m_H after the summer conferences in 2012. They stem from the CDF, DØ, ATLAS and CMS detectors [4, 142, 153, 154] and serve as inputs for the Higgs mass scan in Fig. 4.2(b). (The Tevatron combination was normalized to the red SM expectation.

In Fig. 4.2(b), I show the explicit Higgs mass dependence of the SM and SM4 fits to the signal strength that were publicly available after the Higgs discovery in July 2012. They are based on the digitalized plots shown in Fig. A.2.

In the 2HDM fits information on non-observation of heavy Higgs bosons were included. I digitalised the CMS signal strength exclusion plot for the $H \to ZZ$ decay (Fig. A.3) and extrapolated the data up to 10 TeV in order to ameliorate the convergence of the fit minimization. I did not take into account the update published in May 2013 [155]. Instead of the actually observed exclusion limits, I use the expected limits because above 150 GeV, both lines agree within 2σ and I want to prevent the fit from being sensitive to background fluctuations.
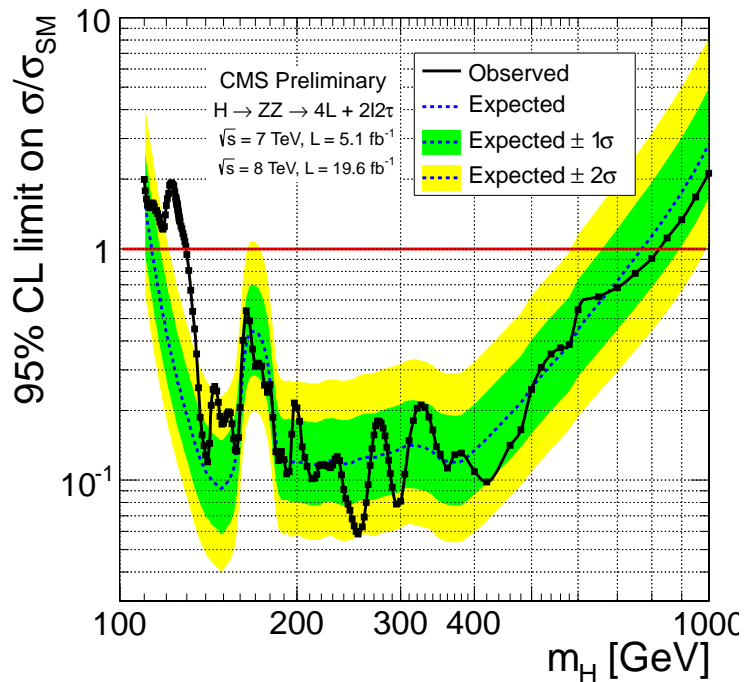
Figure A.3: An H^0 lighter than about 800 GeV can be excluded at 95% CL by CMS searches in $H \to ZZ$ decays [107].

Furthermore, the SM Higgs decay branching ratios are of major importance. Since uncertainties on them are already included in the experimental signal strength errors, I only need to take the fixed central values from [42]. (Some of the values were already shown in Fig. 3.3; here I list them ordered by magnitude.)

$\mathcal{B}(H \to b\bar{b})$	0.561	$\mathcal{B}(H \to c\bar{c})$	0.0283
$\mathcal{B}(H \to WW^*)$	0.231	$\mathcal{B}(H \to \gamma\gamma)$	$2.28 \cdot 10^{-3}$
$\mathcal{B}(H \to gg)$	0.0848	$\mathcal{B}(H \to Z\gamma)$	$1.62 \cdot 10^{-3}$
$\mathcal{B}(H \to \tau\tau)$	0.0615	$\mathcal{B}(H \to \mu\mu)$	$2.14 \cdot 10^{-4}$
$\mathcal{B}(H \to ZZ^*)$	0.0289		

Table A.8: Branching ratios of a Higgs boson with a mass of 126 GeV [42].

Finally, the inputs for the flavour observables $\mathcal{B}(\overline{B} \to X_s\gamma)$ and Δm_{B_s}, which I need for the 2HDM fit, are presented in Table A.9. The inputs for $\mathcal{B}(\overline{B} \to X_s\gamma)$ were fixed for the parametrization; their systematic errors are accounted for by an additional theoretical error on the observable.

Quantity	Input value	Source
Δm_{B_s}	$17.768 \pm 0.023 \pm 0.006 \hbar\,\mathrm{ps}^{-1}$	[111]
G_F	$1.16638 \cdot 10^{-5}\,\mathrm{GeV}^{-2}$	[13]
f_{B_s}	$225 \pm 0 \pm 4\,\mathrm{GeV}$	[133, 156]
η_B	$0.5510 \pm 0 \pm 0.0022$	[116, 157]
$\hat{B}_s$	$1.322 \pm 0.040 \pm 0.035$	[133, 158]
m_{B_s}	$5.367\,\mathrm{GeV}$	[13]
$\overline{m}_t$	$166.6\,\mathrm{GeV}$	SM fit
$\mathcal{B}(\overline{B} \to X_s\gamma)$	$(3.43 \pm 0.21 \pm 0.55) \cdot 10^{-4}$	[117, 118, 159]
$\mathcal{B}(\overline{B} \to X_c e\bar{\nu})_{\mathrm{exp}}$	0.1061	[118]
C	0.580	[118]

Table A.9: Flavour inputs

APPENDIX B

Prediction fits

The larger the deviation of an observable, the larger is its potential to exclude a specific model. In this appendix I want to illustrate the individual impact of all observables used in this thesis on the three discussed models. In the following plots, the one-dimensional scans over all important observables are shown with the corresponding naive p-value as defined in (2.9): the blue curves show the SM prediction, the red ones the SM4 prediction, and the green ones the 2HDM prediction. Furthermore, the experimental values are shown at the 1σ level ($p \approx 0.31$) with systematic and statistical errors, where the former correspond to the inner error bars and the latter to the outer error bars.
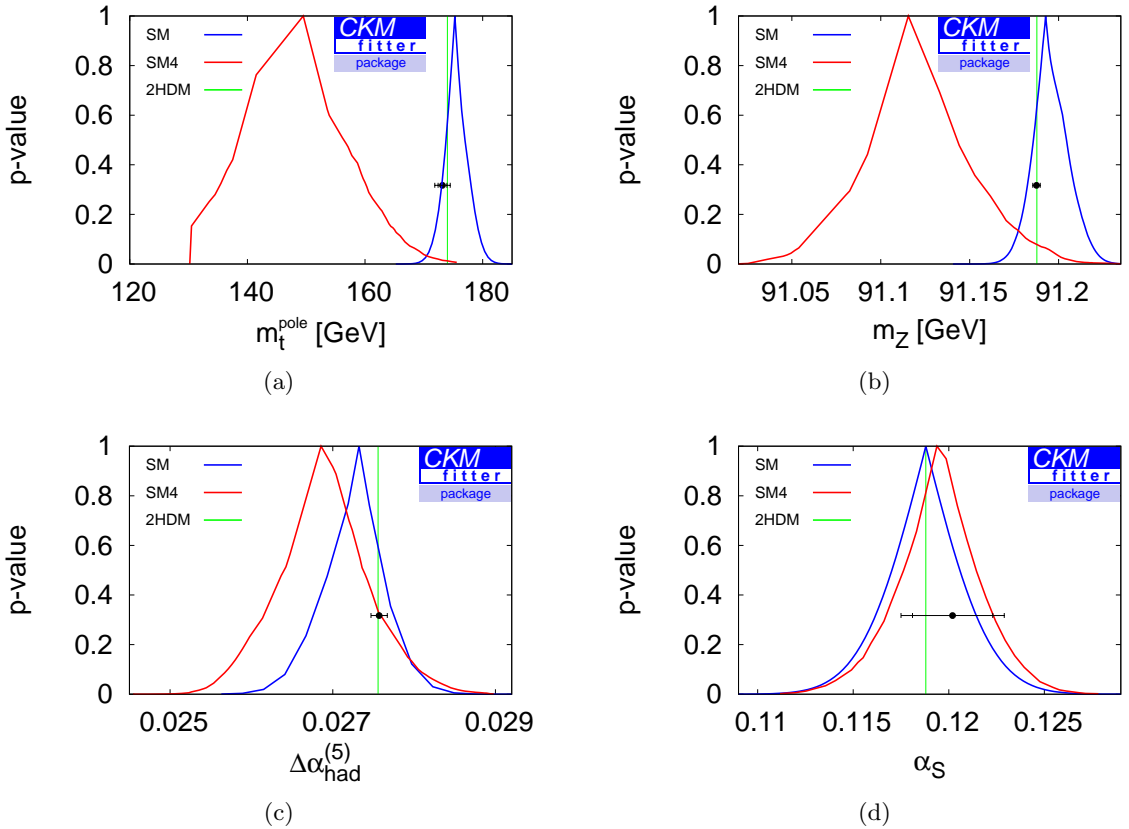
Figure B.1: p-value scans predicting m_t^{pole}, m_Z, $\Delta\alpha_{\text{had}}^{(5)}$ and α_s in the SM and in the SM4.
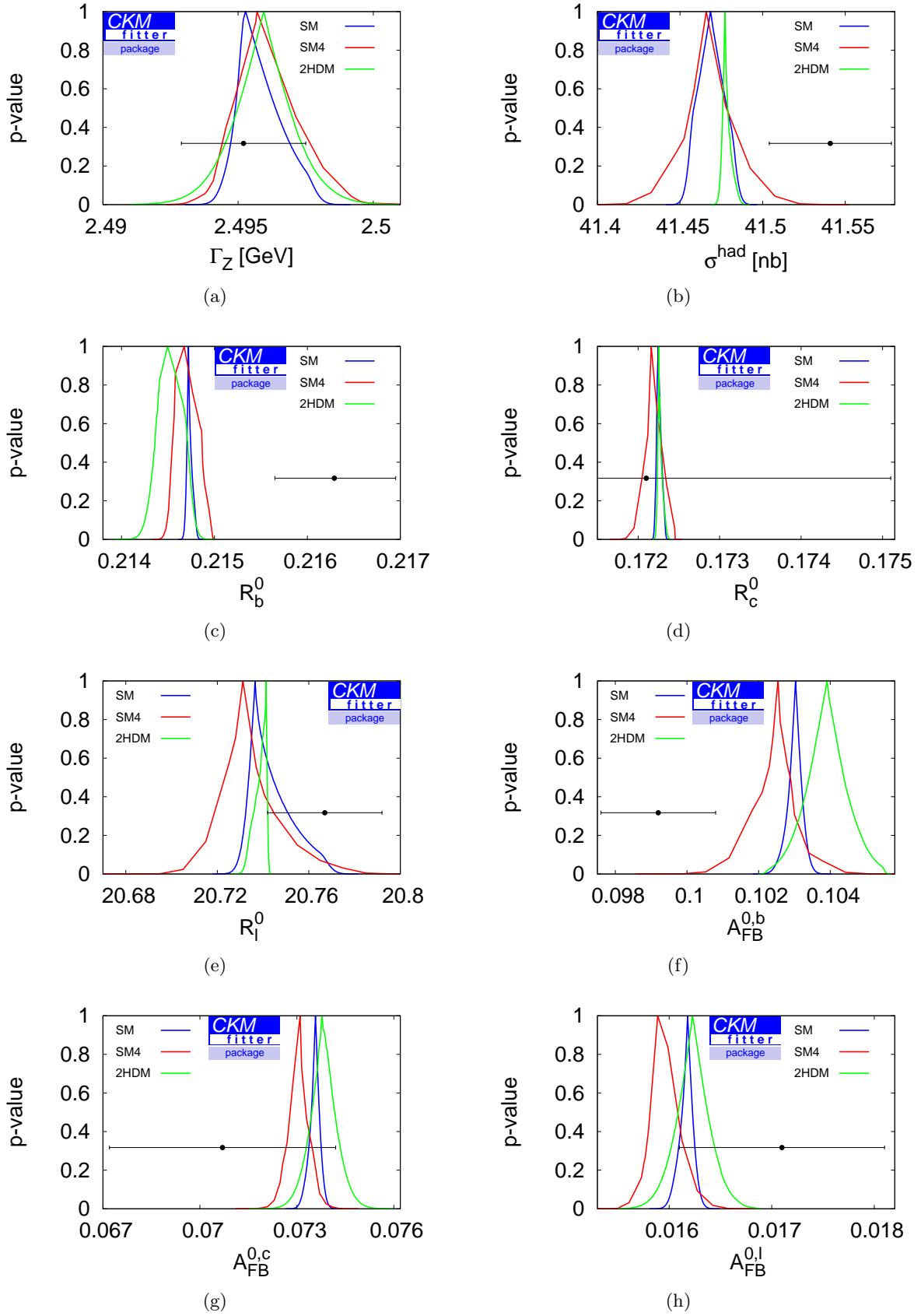
Figure B.2: p-value scans predicting Γ_Z, σ^0_{had}, R^0_b, R^0_c, R^0_ℓ, $A^{0,b}_{FB}$, $A^{0,c}_{FB}$ and $A^{0,\ell}_{FB}$ in the SM, in the SM4 and in the 2HDM.
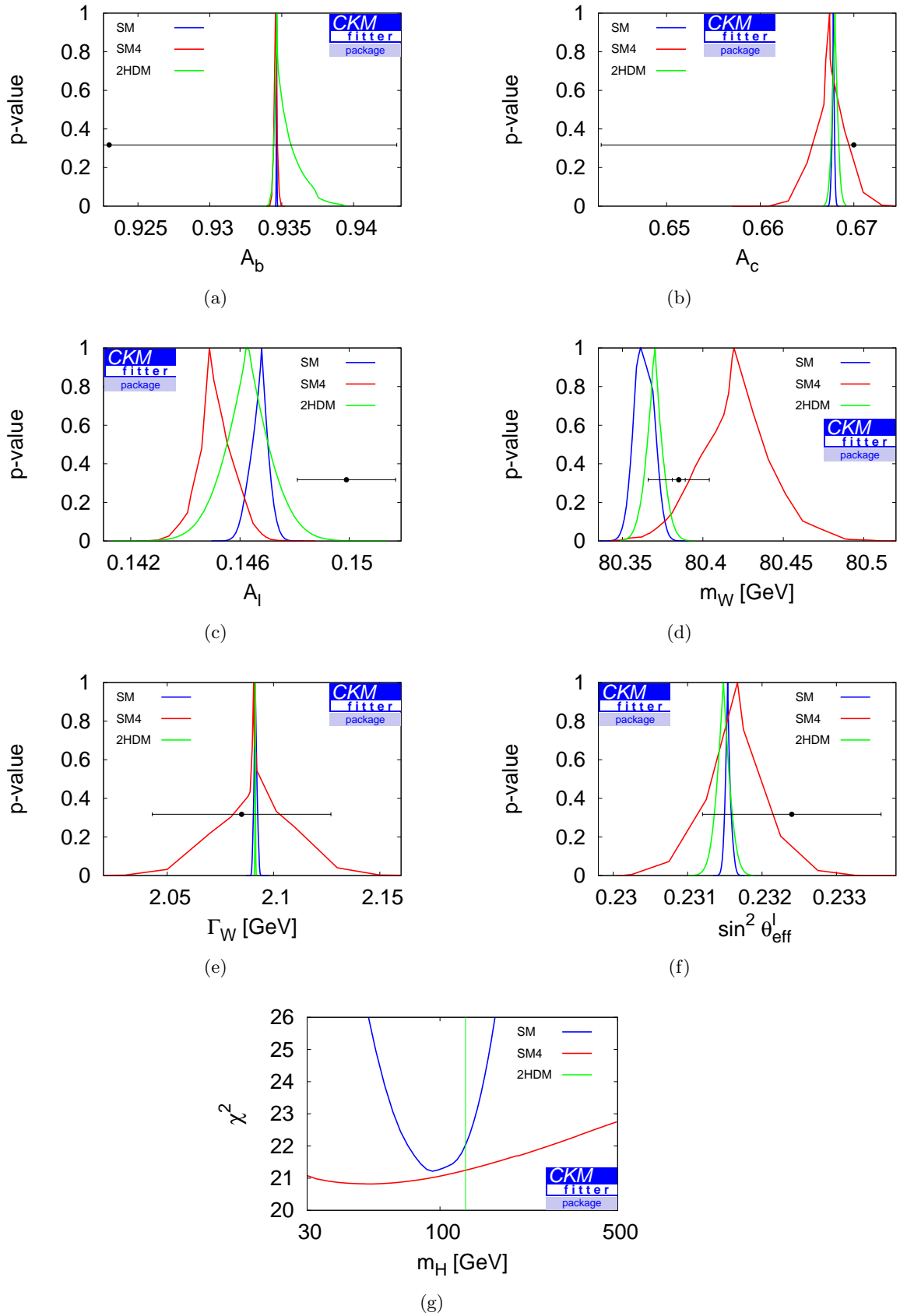
Figure B.3: p-value scans predicting $\mathcal{A}_b$, $\mathcal{A}_c$, $\mathcal{A}_\ell$, m_W, Γ_W and $\sin^2\theta_\ell^{\text{eff}}$ in the SM, in the SM4 and in the 2HDM, and a χ^2 scan of the Higgs mass prediction by the EWPO in the respective models.
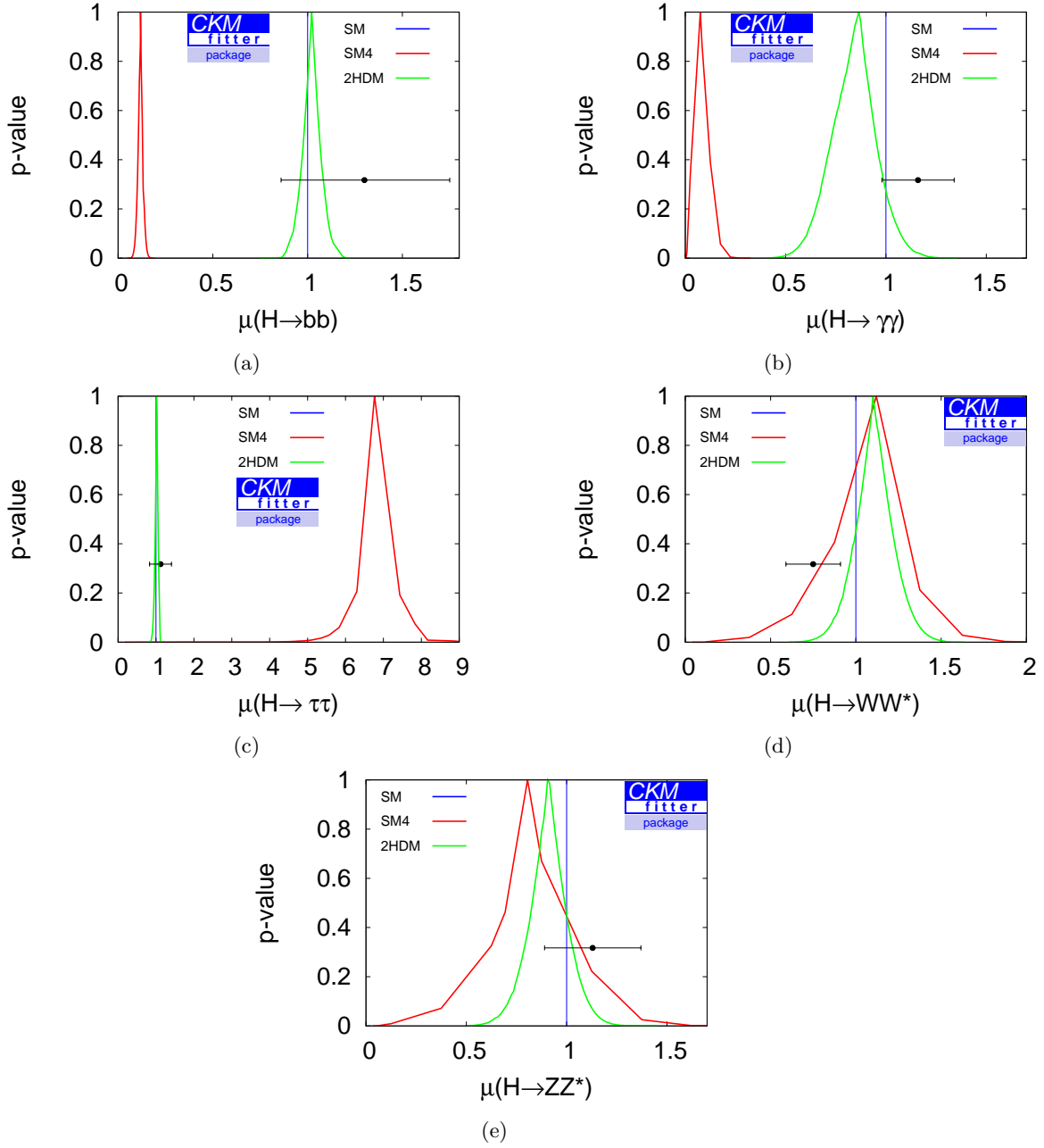
Figure B.4: *p*-value scans predicting the combined Higgs signal strengths in the SM4 and in the 2HDM.

All SM predictions of the EWPO largely agree with the predicted 1σ confidence intervals of the Bayesian analysis by Ciuchini et al. [50]. The top quark pole mass prediction in the SM4 features remarkably small allowed values. Due to technical reasons, I required $m_t^{\text{pole}} > 130$ GeV, so the p-value vanishes at that point; however, a top mass below 130 GeV would be allowed at 95% CL. For σ_{had}^0, R_b^0, $A_{\text{FB}}^{0,b}$ and $\mathcal{A}_\ell$, which were introduced in Sect. 3.2, none of the prediction fits agrees at one standard deviation with the experiment. The fits of R_c^0, $\mathcal{A}_b$ and $\mathcal{A}_c$ show that the measurements are less precise than the predictions, so only a limited range of the 1σ interval is shown. However, in some models the observables might be important constraints. A good example is Γ_W, for which the SM prediction is within a narrow interval, but in the SM4, the W decay width is allowed to deviate sizeably from the SM value. In the 2HDM fits, the SM parameters from (3.5) were fixed to the SM best-fit values (not to the SM predictions!) as mentioned in Chapter 5. Without Higgs discovery data, the Higgs mass fit of the SM4 prefers lighter values for m_H than the SM fit does. Around the measured value of the Higgs mass, the χ_{min}^2 of the SM4 is slightly lower than the one of the SM.All signal strength predictions agree well with the SM and with the 2HDM. The fermionic and the diphoton Higgs decays interpreted in the SM4 are incompatible with the measured signal strength values. Here, the prediction scans reveal complementary information to the deviations Fig. 4.3: $\mu(H \to \tau\tau)$ features a best-fit deviation smaller than one. However, its prediction is in conflict with the best-fit value of 1.34. Without tauonic Higgs decay measurements, the best-fit parameters are completely different. The fourth generation neutrino mass is pushed to $m_H/2$, which changes all Higgs decay branching ratios sizeably; $m_{t'}$ and $m_{b'}$ are at the upper end of their allowed range. In the complete SM4 fit, $\mu(H \to \tau\tau)$ is as small as possible, which in turn requires a high invisible Higgs decay probability. Shifting m_{ν_4} to 56.7 GeV suppresses the Higgs branching ratio to τ leptons by a factor of five. The reduction of the $\mu(H \to \tau\tau)$ deviation is compensated by large deviations of $\mu(H \to \gamma\gamma)$ and $\mu(H \to b\bar{b})$, however, the tauonic Higgs decay observables exhibit the largest $\Delta\chi^2$, even larger than the ones of the diphoton decay observables.

APPENDIX C

2HDM relations

There are different parametrizations of the 2HDM of type II (see for instance [94]). Starting from the quadratic and quartic couplings from the Lagrangian (5.1), I want to list the relations connecting m_{ij} and λ_i to the parameters that I used in my fits, i.e. the four physical Higgs masses m_{h^0}, m_{H^0}, m_{A^0}, m_{H^+}, the vacuum expectation value v, the quartic coupling λ_5, and the two mixing angles α and β.

$$m_{11}^2 = -\frac{1}{2}\left[m_{H^0}^2\cos^2\alpha + m_{h^0}^2\sin^2\alpha + \left(m_{H^0}^2 - m_{h^0}^2\right)\cos\alpha\sin\alpha\tan\beta\right] + \frac{\tan^2\beta\left(m_{A^0}^2 + v^2\lambda_5\right)}{1 + \tan^2\beta}$$

$$m_{22}^2 = -\frac{1}{2}\left[m_{H^0}^2\sin^2\alpha + m_{h^0}^2\cos^2\alpha + \left(m_{H^0}^2 - m_{h^0}^2\right)\frac{\cos\alpha\sin\alpha}{\tan\beta}\right] + \frac{m_{A^0}^2 + v^2\lambda_5}{1 + \tan^2\beta}$$

$$m_{12}^2 = \frac{\tan\beta}{1 + \tan^2\beta}\left(m_{A^0}^2 + v^2\lambda_5\right)$$

$$\lambda_1 = \frac{1}{v^2}\left[\left(1 + \tan^2\beta\right)\left(m_{H^0}^2\cos^2\alpha + m_{h^0}^2\sin^2\alpha\right) - \tan^2\beta\left(m_{A^0}^2 + v^2\lambda_5\right)\right]$$

$$\lambda_2 = \frac{1}{v^2\tan^2\beta}\left[\left(1 + \tan^2\beta\right)\left(m_{h^0}^2\cos^2\alpha + m_{H^0}^2\sin^2\alpha\right) - m_{A^0}^2 - v^2\lambda_5\right]$$

$$\lambda_3 = \frac{1 + \tan^2\beta}{v^2\tan^2\beta}\cos\alpha\sin\alpha\left(m_{H^0}^2 - m_{h^0}^2\right) - \frac{m_{A^0}^2 - 2m_{H^+}^2}{v^2} - \lambda_5$$

$$\lambda_4 = \frac{2(m_{A^0}^2 - m_{H^+}^2)}{v^2} + \lambda_5$$

APPENDIX D

External programs and parallelization with CKMfitter

In this appendix, I want to elaborate on the possibilities of adding external programs to the CKMfitter package and parallelizing two-dimensional CKMfitter scans, which I developed in the last two years.

D.1   External programs

When I wanted to use the `Zfitter` subroutine `DIZET` to calculate electroweak precision observables in the SM, I encountered a problem that was new to CKMfitter users: up to this point, everybody had added theoretical formulae as analytic expressions. Fortunately, one can switch off the analytic gradient for the global minimum searches in CKMfitter, such that the minimization routine can be used even for numerical input. (As mentioned in Sect. 2.4, the minimization is performed by a Fortran part.) So I had to establish an interface that linked `DIZET` to the CKMfitter code. For this purpose, I had to assign on Mathematica level one Fortran function for each of the EWPO, from which in turn I called `DIZET` with a given set of parameters. The `Zfitter` subroutine returns all EWPO values at once, so I interposed a query that tests whether the input parameters have changed since the last call of `DIZET`, and if not only reads the stored values from the last call. As we have 14 EWPO, this yields approximately a factor of $1/14$ in run time because the `DIZET` call is the bottleneck of the fits.

Generalizing this interface, I provided a method to include any external programs to the CKMfitter package. Only a few months later, when I wanted to add the Higgs signal strengths to the SM4 fits, I decided to use `HDecay` to calculate the Higgs decay width and the branching ratios. Although it was not possible to link `HDecay` directly like I did with `DIZET`, I ran `HDecay` for many parameter values and collected its output in look-up tables. (Neglecting flavour mixing, the relevant SM4 parameters are the fourth generation fermion masses and the Higgs mass; thus, the corresponding tables have five parameter dimensions.) With the help of an interpolation algorithm provided by Martin Wiebusch, I was now able to connect these tables to predefined observables in the code, following the same pattern as in the EWPO case.

D.2 Parallelization

As discussed in Sect. 2.4, I wrote a parallelization program for two-dimensional scans with CKMfitter. If the granularity for a scan is N and supposed one is equipped with N processors, this program called `parallelize` can speed up the scan time by a factor of $1/N$. (Note that the *fit* time of the initial global minimization is not affected. So if a complete scan is dominated by the first fit, the parallelization will not ameliorate the run time.) The two-dimensional 2HDM scans in Chapter 5, for instance, have a granularity of 200. With the run time of a one-dimensional fit of up to 50 minutes, I saved up to one week for each plot, even though some of the 1D fits did not converge properly, and I had to re-run them.

`parallelize` is a simple bash script. One needs to hard-code the path leading to a generic job description for the cluster computer ("qsub script") as well as the command that sends the qsub script to the computing cluster. CKMfitter stores input data, theory expressions and job instructions in different files; the latter are called *analysis cards* and are the only files that `parallelize` needs to access: it reads the relevant job parameters such as the granularity, the scan quantities and their ranges from the specified analysis card and creates N subdirectories in the working directory. Each of these new directories is provided with its own analysis card, in which the 2D scan has been changed to a 1D scan by setting one of the scan quantities to a fixed value. This value is different for each subdirectory. Moreover, each subdirectory gets its own modified qsub script. If successful, `parallelize` then submits all N jobs to the cluster. (Several security queries such as a maximal allowed granularity and syntax checks along this procedure have been implemented.)

When all parallelized jobs have finished, we need to unite all data from the subfolders. For that purpose, I wrote a second bash script, called `unify`. The crux of the unification is the correct calculation of the (naive) p-value. If we combined all one-dimensional scan points by simply concatenating the data files, we would get at least N points with an assigned p-value of 1 because every 1D scan has been normalized to its own χ^2 minimum. So the relevant information are the χ^2 values. `unify` finds the global χ^2_{min} in all data files and subsequently re-calculates the p-value for all scan points. At the end, `ckmgnuplot` is called, which is another bash script written by Andreas Menzel and myself to visualize CKMfitter data using the open source plotting program `gnuplot`. (`unify` can be called if at least one of the N parallelized jobs has finished – in that case a fake p-value of -1 is assigned to the missing data points, which is converted into white space by `ckmgnuplot`.) The drawback of the parallelization is that for the constrained scan fits at the individual scan points, CKMfitter cannot resort to the information of all neighbouring scan points. Hence, some of the 1D scan fits may not converge to its global minimum; in the resulting plot one gets a few "streaks" from one-dimensional scans where the minimum has obviously not been found. In order to cope with this, I additionally wrote the short bash script `redo` that saves the old data files and restarts on request single 1D scans. `unify` has been modified such that it automatically merges the old and the new data file and for every scan point takes the smaller χ^2 value. Making use of the three parallelization tools, CKMfitter users can save a lot of time; the scripts are available on the CKMfitter software system.

List of Figures

Bibliography

[1] P. W. Higgs, "BROKEN SYMMETRIES AND THE MASSES OF GAUGE BOSONS", *Phys.Rev.Lett.* **13** (1964) 508–509.

[2] F. Englert and R. Brout, "BROKEN SYMMETRY AND THE MASS OF GAUGE VECTOR MESONS", *Phys.Rev.Lett.* **13** (1964) 321–323.

[3] G. Guralnik, C. Hagen, and T. Kibble, "GLOBAL CONSERVATION LAWS AND MASSLESS PARTICLES", *Phys.Rev.Lett.* **13** (1964) 585–587.

[4] **ATLAS Collaboration**, G. Aad *et al.*, "Observation of a New Particle in the Search for the Standard Model Higgs Boson with the ATLAS Detector at the LHC", *Phys.Lett.* **B716** (2012) 1–29, `arXiv:1207.7214`, additional auxiliary plots on the website.

[5] **CMS Collaboration**, S. Chatrchyan *et al.*, "Observation of a new boson at a mass of 125 GeV with the CMS experiment at the LHC", *Phys.Lett.* **B716** (2012) 30–61, `arXiv:1207.7235`.

[6] W.-S. Hou, "Source of *CP* Violation for the Baryon Asymmetry of the Universe", *Chin.J.Phys.* **47** (2009) 134, `arXiv:0803.1234`.

[7] W.-S. Hou, M. Nagashima, and A. Soddu, "Enhanced $K_L \to \pi^0 \nu \bar{\nu}$ from Direct *CP* Violation in $B \to K\pi$ with Four Generations", *Phys.Rev.* **D72** (2005) 115007, `arXiv:hep-ph/0508237`.

[8] A. Soni, A. K. Alok, A. Giri, R. Mohanta, and S. Nandi, "The fourth family: a simple explanation for the observed pattern of anomalies in *B-CP* asymmetries", *Phys.Lett.* **B683** (2010) 302–305, `arXiv:0807.1971`.

[9] S. Raby and G. B. West, "A FOURTH GENERATION NEUTRINO WITH A STANDARD HIGGS SCALAR SOLVES BOTH THE SOLAR NEUTRINO AND DARK MATTER PROBLEMS", *Phys.Lett.* **B202** (1988) 47.

[10] H.-S. Lee, Z. Liu, and A. Soni, "Neutrino dark matter candidate in fourth generation scenarios", *Phys.Lett.* **B704** (2011) 30–35, `arXiv:1105.3490`.

[11] INSPIRE HEP Search. `http://www.inspirehep.net`, 9/5/2013.

[12] O. Eberhardt, G. Herbert, H. Lacker, A. Lenz, A. Menzel, U. Nierste, and M. Wiebusch, "Impact of a Higgs boson at a mass of 126 GeV on the standard model with three and four fermion generations", *Phys.Rev.Lett.* **109** (2012) 241802, `arXiv:1209.1101`.

[13] **Particle Data Group**, J. Beringer *et al.*, "Review of Particle Physics", *Phys.Rev.* **D86** (2012) 010001.

[14] A. Höcker, H. Lacker, S. Laplace, and F. Le Diberder, "A NEW APPROACH TO A GLOBAL FIT OF THE CKM MATRIX", *Eur.Phys.J.* **C21** (2001) 225–259, `arXiv:hep-ph/0104062`.

[15] M. Wiebusch, "Numerical Computation of p-values with myFitter", `arXiv:1207.1446`, accepted by *Comput.Phys.Commun.*

[16] L. Lyons, "Bayes and Frequentism: a particle physicist's perspective", *Contemporary Physics* **54** (2013), no. 1, 1–16, `arXiv:1301.1273`.

[17] S. S. Wilks, "THE LARGE-SAMPLE DISTRIBUTION OF THE LIKELIHOOD RATIO FOR TESTING COMPOSITE HYPOTHESES", *Ann. Math. Statist.* **9-1** (1938) 060062.

[18] M. Böhm, A. Denner, and H. Joos, "Gauge theories of the strong and electroweak interaction", Vieweg+Teubner Verlag, Stuttgart, Leipzig, Wiesbaden, 3rd rev. ed., 2001.

[19] S. Novaes, "Standard Model: An Introduction", published in: "Particles and fields. Proceedings, 10th Jorge André Swieca Summer School, Sao Paulo, Brazil, February 6-12, 1999", `arXiv:hep-ph/0001283`.

[20] N. Cabibbo, "UNITARY SYMMETRY AND LEPTONIC DECAYS", *Phys.Rev.Lett.* **10** (1963) 531–533.

[21] M. Kobayashi and T. Maskawa, "CP-Violation in the Renormalizable Theory of Weak Interaction", *Prog.Theor.Phys.* **49** (1973) 652–657.

[22] C. Wu, E. Ambler, R. Hayward, D. Hoppes, and R. Hudson, "Experimental Test of Parity Conservation in Beta Decay", *Phys.Rev.* **105** (1957) 1413–1414.

[23] J. Christenson, J. Cronin, V. Fitch, and R. Turlay, "EVIDENCE FOR THE 2π DECAY OF THE K_2^0 MESON", *Phys.Rev.Lett.* **13** (1964) 138–140.

[24] **ALEPH Collaboration, DELPHI Collaboration, L3 Collaboration, OPAL Collaboration, SLD Collaboration, LEP Electroweak Working Group, SLD Electroweak Group, SLD Heavy Flavour Group**, S. Schael *et al.*, "Precision Electroweak Measurements on the Z Resonance", *Phys.Rept.* **427** (2006) 257–454, `arXiv:hep-ex/0509008`.

[25] Interactive Tevatron timeline. `http://www.fnal.gov/pub/tevatron/milestones/interactive-timeline.html`, 22/6/2013.

[26] **The Gfitter Group**, H. Flächer, M. Goebel, J. Haller, A. Höcker, K. Mönig, and J. Stelzer, "Revisiting the Global Electroweak Fit of the Standard Model and Beyond with Gfitter", *Eur.Phys.J.* **C60** (2009) 543–583, arXiv:0811.0009.

[27] M. Davier, A. Höcker, B. Malaescu, and Z. Zhang, "Reevaluation of the Hadronic Contributions to the Muon $g - 2$ and to $\alpha(M_Z^2)$", *Eur.Phys.J.* **C71** (2011) 1515, arXiv:1010.4180.

[28] P. Baikov, K. Chetyrkin, and J. H. Kuhn, "Hadronic Z- and τ-Decays in Order α_s^4", *Phys.Rev.Lett.* **101** (2008) 012002, arXiv:0801.1821.

[29] D. Y. Bardin, M. S. Bilenky, T. Riemann, M. Sachwitz, and H. Vogt, "DIZET – ELECTROWEAK ONE-LOOP CORRECTIONS FOR $e^+ + e^- \to f^+ + f^-$ AROUND THE Z^0 PEAK", *Comput.Phys.Commun.* **59** (1990) 303–312.

[30] D. Y. Bardin, P. Christova, M. Jack, L. Kalinovskaya, A. Olchevski, *et al.*, "ZFITTER v.6.21. A Semi-Analytical Program for Fermion Pair Production in $e^+ e^-$ Annihilation", *Comput.Phys.Commun.* **133** (2001) 229–395, arXiv:hep-ph/9908433.

[31] A. Arbuzov, M. Awramik, M. Czakon, A. Freitas, M. Grunewald, *et al.*, "ZFITTER: a semi-analytical program for fermion pair production in $e^+ e^-$ annihilation, from version 6.21 to version 6.42", *Comput.Phys.Commun.* **174** (2006) 728–758, arXiv:hep-ph/0507146.

[32] A. Freitas and Y.-C. Huang, "Electroweak two-loop corrections to $sin^2\theta_{\text{eff}}^{b\bar{b}}$ and R_b using numerical Mellin-Barnes integrals", *JHEP* **1208** (2012) 050, arXiv:1205.0299.

[33] M. E. Peskin and T. Takeuchi, "New Constraint on a Strongly Interacting Higgs Sector", *Phys.Rev.Lett.* **65** (1990) 964–967.

[34] M. E. Peskin and T. Takeuchi, "Estimation of oblique electroweak corrections", *Phys.Rev.* **D46** (1992) 381–409.

[35] M. Veltman, "Second Threshold in Weak Interactions", *Acta Phys.Polon.* **B8** (1977) 475.

[36] **LEP Working Group for Higgs boson searches, ALEPH Collaboration, DELPHI Collaboration, L3 Collaboration, OPAL Collaboration**, R. Barate *et al.*, "Search for the Standard Model Higgs Boson at LEP", *Phys.Lett.* **B565** (2003) 61–75, arXiv:hep-ex/0306033.

[37] **CDF Collaboration, D0 Collaboration**, T. Aaltonen *et al.*, "Combination of Tevatron searches for the standard model Higgs boson in the $W + W-$ decay mode", *Phys.Rev.Lett.* **104** (2010) 061802, arXiv:1001.4162.

[38] **D0 Collaborations**, CDF, "Higgs Boson Studies at the Tevatron", arXiv:1303.6346.

[39] **ATLAS Collaboration**, "ATLAS Note CONF-2013-034".
http://cds.cern.ch/record/1528170, 23/6/2013.

[40] **ATLAS Collaboration**, "ATLAS Note CONF-2013-040".
http://cds.cern.ch/record/1542341, 23/6/2013.

[41] **CMS Collaboration**, "CMS Physics Analysis Summary HIG-13-005".
http://cds.cern.ch/record/1542387, 23/6/2013.

[42] **LHC Higgs Cross Section Working Group**.
https://twiki.cern.ch/twiki/bin/view/LHCPhysics/CrossSections,
22/6/2013.

[43] J. Baglio and A. Djouadi, "Predictions for Higgs production at the Tevatron and
the associated uncertainties", *JHEP* **1010** (2010) 064, arXiv:1003.4266.

[44] **LHC Higgs Cross Section Working Group**, S. Dittmaier, C. Mariotti,
G. Passarino, R. Tanaka, *et al.*, "Handbook of LHC Higgs cross sections: 2.
Differential Distributions", arXiv:1201.3084.

[45] A. Azatov, R. Contino, D. Del Re, J. Galloway, M. Grassi, *et al.*, "Determining
Higgs couplings with a model-independent analysis of $h \to \gamma\gamma$", *JHEP* **1206** (2012)
134, arXiv:1204.4817.

[46] M. Klute, R. Lafaye, T. Plehn, M. Rauch, and D. Zerwas, "Measuring Higgs
Couplings from LHC Data", *Phys.Rev.Lett.* **109** (2012) 101801, arXiv:1205.2699.

[47] J. Espinosa, C. Grojean, M. Mühlleitner, and M. Trott, "First Glimpses at Higgs'
face", *JHEP* **1212** (2012) 045, arXiv:1207.1717.

[48] D. Carmi, A. Falkowski, E. Kuflik, T. Volansky, and J. Zupan, "Higgs After the
Discovery: A Status Report", *JHEP* **1210** (2012) 196, arXiv:1207.1718.

[49] M. Baak, M. Goebel, J. Haller, A. Höcker, D. Kennedy, *et al.*, "The Electroweak
Fit of the Standard Model after the Discovery of a New Boson at the LHC",
Eur.Phys.J. **C72** (2012) 2205, arXiv:1209.2716.

[50] M. Ciuchini, E. Franco, S. Mishima, and L. Silvestrini, "Electroweak Precision
Observables, New Physics and the Nature of a 126 GeV Higgs Boson",
arXiv:1306.4644.

[51] M. S. Chanowitz, M. Furman, and I. Hinchliffe, "WEAK INTERACTIONS OF
ULTRA HEAVY FERMIONS", *Phys.Lett.* **B78** (1978) 285.

[52] M. S. Chanowitz, M. Furman, and I. Hinchliffe, "WEAK INTERACTIONS OF
ULTRA HEAVY FERMIONS (II)", *Nucl.Phys.* **B153** (1979) 402.

[53] A. Denner, S. Dittmaier, A. Muck, G. Passarino, M. Spira, *et al.*, "Higgs
production and decay with a fourth Standard-Model-like fermion generation",
Eur.Phys.J. **C72** (2012) 1992, arXiv:1111.6395.

[54] A. Sakharov, "Violation of *CP* invariance, *C* asymmetry, and baryon asymmetry of the universe", *Pisma Zh.Eksp.Teor.Fiz.* **5** (1967) 32–35.

[55] A. J. Buras, B. Duling, T. Feldmann, T. Heidsieck, C. Promberger, *et al.*, "Patterns of flavour violation in the presence of a fourth generation of quarks and leptons", *JHEP* **1009** (2010) 106, `arXiv:1002.2126`.

[56] **ATLAS Collaboration**, G. Aad *et al.*, "Search for pair production of heavy top-like quarks decaying to a high-p_T W boson and a b quark in the lepton plus jets final state at $\sqrt{s} = 7$ TeV with the ATLAS detector", *Phys.Lett.* **B718** (2013) 1284–1302, `arXiv:1210.5468`.

[57] **CMS Collaboration**, S. Chatrchyan *et al.*, "Search for heavy quarks decaying into a top quark and a W or Z boson using lepton + jets events in pp collisions at $\sqrt{s} = 7$ TeV", *JHEP* **01** (2013) 154, `arXiv:1210.7471`.

[58] **CMS Collaboration**, S. Chatrchyan *et al.*, "Combined search for the quarks of a sequential fourth generation", *Phys.Rev.* **D86** (2012) 112003, `arXiv:1209.1062`.

[59] **L3 Collaboration**, P. Achard *et al.*, "Search for Heavy Neutral and Charged Leptons in e^+e^- Annihilation at LEP", *Phys.Lett.* **B517** (2001) 75–85, `arXiv:hep-ex/0107015`.

[60] **DELPHI Collaboration**, P. Abreu *et al.*, "Searches for heavy neutrinos from Z decays", *Phys.Lett.* **B274** (1992) 230–238.

[61] M. Bobrowski, A. Lenz, J. Riedl, and J. Rohrwild, "How much space is left for a new family of fermions?", *Phys.Rev.* **D79** (2009) 113006, `arXiv:0902.4883`.

[62] B. Pontecorvo, "Mesonium and anti-mesonium", *Sov.Phys.JETP* **6** (1957) 429.

[63] Z. Maki, M. Nakagawa, and S. Sakata, "Remarks on the Unified Model of Elementary Particles", *Prog.Theor.Phys.* **28** (1962) 870–880.

[64] B. Pontecorvo, "Neutrino Experiments and the Problem of Conservation of Leptonic Charge", *Sov.Phys.JETP* **26** (1968) 984–988.

[65] P. Gerhold, K. Jansen, and J. Kallarackal, "Higgs boson mass bounds in the presence of a very heavy fourth quark generation", *JHEP* **1101** (2011) 143, `arXiv:1011.1648`.

[66] J. Bulava, K. Jansen, and A. Nagy, "Constraining a fourth generation of quarks: non-perturbative Higgs boson mass bounds", *Phys.Lett.* **B723** (2013) 95–99, `arXiv:1301.3416`.

[67] H.-J. He, N. Polonsky, and S. Su, "Extra Families, Higgs Spectrum and Oblique Corrections", *Phys.Rev.* **D64** (2001) 053004, `arXiv:hep-ph/0102144`.

[68] G. D. Kribs, T. Plehn, M. Spannowsky, and T. M. Tait, "Four Generations and Higgs Physics", *Phys.Rev.* **D76** (2007) 075016, `arXiv:0706.3718`.

[69] O. Eberhardt, A. Lenz, and J. Rohrwild, "Less space for a new family of fermions", *Phys.Rev.* **D82** (2010) 095006, `arXiv:1005.3505`.

[70] **Particle Data Group**, C. Amsler *et al.*, "Review of Particle Physics", *Phys.Lett.* **B667** (2008) 1–1340.

[71] P. González, J. Rohrwild, and M. Wiebusch, "Electroweak Precision Observables in a Fourth Generation Model with General Flavour Structure", *Eur.Phys.J.* **C72** (2012) 2007, `arXiv:1105.3434`.

[72] T. Hahn and M. Pérez-Victoria, "Automatized One-Loop Calculations in four and D dimensions", *Comput.Phys.Commun.* **118** (1999) 153–165, `arXiv:hep-ph/9807565`.

[73] T. Hahn, "Generating Feynman Diagrams and Amplitudes with *FeynArts* 3", *Comput.Phys.Commun.* **140** (2001) 418–431, `arXiv:hep-ph/0012260`.

[74] T. Hahn and M. Rauch, "News from FormCalc and LoopTools", *Nucl.Phys.Proc.Suppl.* **157** (2006) 236–240, `arXiv:hep-ph/0601248`.

[75] V. A. Khoze, "Comment on an invisible Higgs boson and 50 GeV neutrino", `arXiv:hep-ph/0105069`.

[76] A. Djouadi, J. Kalinowski, and M. Spira, "HDECAY: a Program for Higgs Boson Decays in the Standard Model and its Supersymmetric Extension", *Comput.Phys.Commun.* **108** (1998) 56–74, `arXiv:hep-ph/9704448`.

[77] A. Djouadi and P. Gambino, "QCD corrections to Higgs boson self-energies and fermionic decay widths", *Phys.Rev.* **D51** (1995) 218–228, `arXiv:hep-ph/9406431`.

[78] A. Djouadi and P. Gambino, "Leading electroweak correction to Higgs boson production at proton colliders.", *Phys.Rev.Lett.* **73** (1994) 2528–2531, `arXiv:hep-ph/9406432`.

[79] G. Passarino, C. Sturm, and S. Uccirati, "Complete Electroweak Corrections to Higgs production in a Standard Model with four generations at the LHC", *Phys.Lett.* **B706** (2011) 195–199, `arXiv:1108.2025`.

[80] J. Gunion, D. W. McKay, and H. Pois, "A MINIMAL FOUR-FAMILY SUPERGRAVITY MODEL", *Phys.Rev.* **D53** (1996) 1616–1647, `arXiv:hep-ph/9507323`.

[81] J. Gunion and S. Geer, "PROGRESS IN SSC HIGGS PHYSICS: REPORT OF THE HIGGS WORKING GROUP", published in: "Proceedings of the 'Workshop on Physics at Current Accelerators and the Supercollider', eds. J. Hewett, A. White, and D. Zeppenfeld, Argonne National Laboratory, 2-5 June (1993)", `arXiv:hep-ph/9310333`.

[82] **Particle Data Group**, C. Caso *et al.*, "Review of particle physics", *Eur.Phys.J.* **C3** (1998) 1–794.

[83] P. H. Frampton, P. Hung, and M. Sher, "Quarks and Leptons Beyond the Third Generation.", *Phys.Rept.* **330** (2000) 263, `arXiv:hep-ph/9903387`.

[84] V. Novikov, L. Okun, A. N. Rozanov, and M. Vysotsky, "Extra generations and discrepancies of electroweak precision data", *Phys.Lett.* **B529** (2002) 111–116, `arXiv:hep-ph/0111028`.

[85] V. Novikov, L. Okun, A. N. Rozanov, and M. Vysotsky, "Mass of the higgs versus fourth generation masses", *JETP Lett.* **76** (2002) 127–130, `arXiv:hep-ph/0203132`.

[86] M. S. Chanowitz, "Bounding CKM Mixing with a Fourth Family", *Phys.Rev.* **D79** (2009) 113008, `arXiv:0904.3570`.

[87] J. Erler and P. Langacker, "Precision Constraints on Extra Fermion Generations", *Phys.Rev.Lett.* **105** (2010) 031801, `arXiv:1003.3211`.

[88] A. Djouadi and A. Lenz, "Sealing the fate of a fourth generation of fermions", *Phys.Lett.* **B715** (2012) 310–314, `arXiv:1204.1252`.

[89] E. Kuflik, Y. Nir, and T. Volansky, "Implications of Higgs Searches on the Four Generation Standard Model", `arXiv:1204.1975`.

[90] M. Buchkremer, J.-M. Gérard, and F. Maltoni, "Closing in on a perturbative fourth generation", *JHEP* **1206** (2012) 135, `arXiv:1204.5403`.

[91] O. Eberhardt, A. Lenz, A. Menzel, U. Nierste, and M. Wiebusch, "Status of the fourth fermion generation before ICHEP2012: Higgs data and electroweak precision observables", *Phys.Rev.* **D86** (2012) 074014, `arXiv:1207.0438`.

[92] O. Eberhardt, G. Herbert, H. Lacker, A. Lenz, A. Menzel, U. Nierste, and M. Wiebusch, "Joint analysis of Higgs decays and electroweak precision observables in the Standard Model with a sequential fourth generation", *Phys.Rev.* **D86** (2012) 013011, `arXiv:1204.3872`.

[93] T. Lee, "A Theory of Spontaneous T Violation", *Phys.Rev.* **D8** (1973) 1226–1239.

[94] J. F. Gunion and H. E. Haber, "The CP-conserving two-Higgs-doublet model: the approach to the decoupling limit", *Phys.Rev.* **D67** (2003) 075019, `arXiv:hep-ph/0207010`.

[95] G. Branco, P. Ferreira, L. Lavoura, M. Rebelo, M. Sher, *et al.*, "Theory and phenomenology of two-Higgs-doublet models", *Phys.Rept.* **516** (2012) 1–102, `arXiv:1106.0034`.

[96] S. L. Glashow and S. Weinberg, "Natural conservation laws for neutral currents", *Phys.Rev.* **D15** (1977) 1958.

[97] J. F. Donoghue and L. F. Li, "Properties of charged Higgs bosons", *Phys.Rev.* **D19** (1979) 945.

[98] A. Djouadi, "The anatomy of electroweak symmetry breaking Tome II: The Higgs bosons in the Minimal Supersymmetric Model", *Phys.Rept.* **459** (2008) 1–241, `arXiv:hep-ph/0503173`.

[99] A. Barroso, P. Ferreira, I. Ivanov, and R. Santos, "Metastability bounds on the two Higgs doublet model", *JHEP* **1306** (2013) 045, `arXiv:1303.5098`.

[100] U. Nierste and K. Riesselmann, "Higgs Sector Renormalization Group in the $\overline{\mathsf{MS}}$ and OMS Scheme: The Breakdown of Perturbation Theory for a Heavy Higgs", *Phys.Rev.* **D53** (1996) 6638–6652, `arXiv:hep-ph/9511407`.

[101] **ALEPH Collaboration**, A. Heister *et al.*, "Search for charged Higgs bosons in e^+e^- collisions at energies up to $\sqrt{s} = 209$ GeV", *Phys.Lett.* **B543** (2002) 1–13, `arXiv:hep-ex/0207054`.

[102] W. Hollik, "Non-Standard Higgs Bosons in $SU(2) \times U(1)$ Radiative Corrections", *Z.Phys.* **C32** (1986) 291.

[103] W. Hollik, "Radiative corrections with two Higgs doublets at LEP/SLC and HERA", *Z.Phys.* **C37** (1988) 569.

[104] H. E. Haber and H. E. Logan, "Radiative Corrections to the $Zb\bar{b}$ Vertex and Constraints on Extended Higgs Sectors", *Phys.Rev.* **D62** (2000) 015011, `arXiv:hep-ph/9909335`.

[105] P. Ferreira, R. Santos, M. Sher, and J. P. Silva, "Could the LHC two-photon signal correspond to the heavier scalar in two-Higgs-doublet models?", *Phys.Rev.* **D85** (2012) 035020, `arXiv:1201.0019`.

[106] P. Ferreira, R. Santos, H. E. Haber, and J. P. Silva, "Mass-degenerate Higgs bosons at 125 GeV in the Two-Higgs-Doublet Model", *Phys.Rev.* **D87** (2013) 055009, `arXiv:1211.3131`.

[107] **CMS Collaboration**, "CMS Physics Analysis Summary HIG-13-002". `http://cds.cern.ch/record/1523767`, 23/6/2013.

[108] O. Eberhardt, U. Nierste, and M. Wiebusch, "Status of the two-Higgs-doublet model of type II", *JHEP* **1307** (2013) 118, `arXiv:1305.1649`.

[109] A. Crivellin, C. Greub, and A. Kokulu, "Explaining $B \to D\tau\nu$, $B \to D^*\tau\nu$ and $B \to \tau\nu$ in a two Higgs doublet model of type III", *Phys.Rev.* **D86** (2012) 054014, `arXiv:1206.2634`.

[110] **D0 Collaboration**, V. Abazov *et al.*, "Direct Limits on the B_s^0 Oscillation Frequency", *Phys.Rev.Lett.* **97** (2006) 021802, `arXiv:hep-ex/0603029`.

[111] **LHCb collaboration**, R. Aaij *et al.*, "Precision measurement of the B_s^0-$\overline{B}_s^0$ oscillation frequency with the decay $B_s^0 \to D_s^-\pi^+$", *New J.Phys.* **15** (2013) 053021, `arXiv:1304.4741`.

[112] L. Abbott, P. Sikivie, and M. B. Wise, "Constraints on charged-Higgs-boson couplings", *Phys.Rev.* **D21** (1980) 1393.

[113] G. Branco, A. Buras, and J.-M. Gérard, "*CP* VIOLATION IN MODELS WITH TWO- AND THREE-SCALAR DOUBLETS", *Nucl.Phys.* **B259** (1985) 306.

[114] C. Geng and J. N. Ng, "Charged-Higgs-boson effect in B_d^0-$\overline{B}_d^0$ mixing, $K \to \pi\nu\bar{\nu}$ decay, and rare decays of B mesons", *Phys.Rev.* **D38** (1988) 2857.

[115] A. J. Buras, P. Krawczyk, M. E. Lautenbacher, and C. Salazar, "B^0–$\overline{B}^0$ MIXING, *CP* VIOLATION, $K^+ \to \pi^+\nu\bar{\nu}$ AND $B \to K\gamma X$ IN A TWO-HIGGS-DOUBLET MODEL", *Nucl.Phys.* **B337** (1990) 284–312.

[116] O. Deschamps, S. Descotes-Genon, S. Monteil, V. Niess, S. T'Jampens, *et al.*, "The Two Higgs Doublet Model of Type II facing flavour physics data", *Phys.Rev.* **D82** (2010) 073012, `arXiv:0907.5135`.

[117] T. Hermann, M. Misiak, and M. Steinhauser, "$\overline{B} \to X_s\gamma$ in the Two Higgs Doublet Model up to Next-to-Next-to-Leading Order in QCD", *JHEP* **1211** (2012) 036, `arXiv:1208.2788`.

[118] M. Misiak and M. Steinhauser, "NNLO QCD Corrections to the $\overline{B} \to X_s\gamma$ Matrix Elements Using Interpolation in m_c", *Nucl.Phys.* **B764** (2007) 62–82, `arXiv:hep-ph/0609241`.

[119] P. Ferreira, R. Santos, M. Sher, and J. P. Silva, "Implications of the LHC two-photon signal for two-Higgs-doublet models", *Phys.Rev.* **D85** (2012) 077703, `arXiv:1112.3277`.

[120] L. Basso, A. Lipniacka, F. Mahmoudi, S. Moretti, P. Osland, *et al.*, "Probing the charged Higgs boson at the LHC in the CP-violating type-II 2HDM", *JHEP* **1211** (2012) 011, `arXiv:1205.6569`.

[121] H. Cheon and S. K. Kang, "Constraining parameter space in type-II two-Higgs doublet model in light of a 125 GeV Higgs boson", `arXiv:1207.1083`.

[122] A. Drozd, B. Grzadkowski, J. F. Gunion, and Y. Jiang, "Two-Higgs-Doublet Models and Enhanced Rates for a 125 GeV Higgs", *JHEP* **1305** (2013) 072, `arXiv:1211.3580`.

[123] C.-Y. Chen and S. Dawson, "Exploring Two Higgs Doublet Models Through Higgs Production", *Phys. Rev. D* **87** (2013) 055016, `arXiv:1301.0309`.

[124] A. Celis, V. Ilisie, and A. Pich, "LHC constraints on two-Higgs doublet models", *JHEP* **1307** (2013) 053, `arXiv:1302.4022`.

[125] P. P. Giardino, K. Kannike, I. Masina, M. Raidal, and A. Strumia, "The universal Higgs fit", `arXiv:1303.3570`.

[126] B. Grinstein and P. Uttayarat, "Carving Out Parameter Space in Type-II Two Higgs Doublets Model", *JHEP* **1306** (2013) 094, `arXiv:1304.0028`.

[127] A. Barroso, P. Ferreira, R. Santos, M. Sher, and J. P. Silva, "2HDM at the LHC - the story so far", `arXiv:1304.5225`.

[128] B. Coleppa, F. Kling, and S. Su, "Constraining Type II 2HDM in Light of LHC Higgs Searches", `arXiv:1305.0002`.

[129] G. Burdman, C. E. Haluch, and R. D. Matheus, "Is the LHC observing the pseudoscalar state of a two-Higgs-doublet model?", *Phys.Rev.* **D85** (2012) 095016, `arXiv:1112.3961`.

[130] S. Bar-Shalom, S. Nandi, and A. Soni, "Two Higgs doublets with 4th generation fermions - models for TeV-scale compositeness", *Phys.Rev.* **D84** (2011) 053009, `arXiv:1105.6095`.

[131] N. Chen and H.-J. He, "LHC Signatures of Two-Higgs-Doublets with Fourth Family", *JHEP* **1204** (2012) 062, `arXiv:1202.3072`.

[132] J. Hardy and I. Towner, "Superallowed $0^+ \to 0^+$ nuclear β decays: A new survey with precision tests of the conserved vector current hypothesis and the standard model", *Phys.Rev.* **C79** (2009) 055502, `arXiv:0812.1202`.

[133] Private communication with the CKMfitter group.

[134] **CDF Collaboration, D0 Collaboration**, T. Aaltonen *et al.*, "Combination of the top-quark mass measurements from the Tevatron collider", *Phys.Rev.* **D86** (2012) 092003, `arXiv:1207.1069`.

[135] **Tevatron Electroweak Working Group, CDF Collaboration, D0 Collaboration**, "2012 Update of the Combination of CDF and D0 Results for the Mass of the W Boson", `arXiv:1204.0042`.

[136] M. Awramik, M. Czakon, A. Freitas, and G. Weiglein, "Precise prediction for the W-boson mass in the standard model", *Phys.Rev.* **D69** (2004) 053006, `arXiv:hep-ph/0311148`.

[137] **Tevatron Electroweak Working Group**, "Combination of CDF and D0 Results on the Width of the W boson", `arXiv:1003.2826`.

[138] **Tevatron Electroweak Working Group, D0 Collaborations**, CDF, "Combination of CDF and DØ results on the mass of the top quark using up to 8.7 fb^{-1} at the Tevatron", `arXiv:1305.3929`.

[139] **ATLAS Collaboration**, "ATLAS Note CONF-2013-012". `http://cds.cern.ch/record/1523698`, 23/6/2013.

[140] **CMS Collaboration**, "CMS Physics Analysis Summary HIG-13-001". `http://cds.cern.ch/record/1530524`, 23/6/2013.

[141] **ATLAS Collaboration**, "ATLAS Note CONF-2013-013". `http://cds.cern.ch/record/1523699`, 23/6/2013.

[142] **ATLAS Collaboration**, G. Aad *et al.*, "Combined search for the Standard Model Higgs boson in *pp* collisions at $\sqrt{s} = 7$ TeV with the ATLAS detector", *Phys.Rev.* **D86** (2012) 032003, `arXiv:1207.0319`.

[143] **ATLAS Collaboration**, "ATLAS Note CONF-2012-091, Fig. 14". `http://cds.cern.ch/record/1460410`, 23/6/2013.

[144] **ATLAS Collaboration**, "ATLAS Note CONF-2013-030". `http://cds.cern.ch/record/1527126`, 23/6/2013.

[145] **ATLAS Collaboration**, "ATLAS Note CONF-2012-161". `http://cds.cern.ch/record/1493625`, 23/6/2013.

[146] **ATLAS Collaboration**, "ATLAS Note CONF-2012-160". `http://cds.cern.ch/record/1493624`, 23/6/2013.

[147] **CMS Collaboration**, "CMS Physics Analysis Summary HIG-12-020". `http://cds.cern.ch/record/1460438`, 23/6/2013.

[148] **CMS Collaboration**, "CMS Physics Analysis Summary HIG-13-003". `http://cds.cern.ch/record/1523673`, 23/6/2013.

[149] **CMS Collaboration**, "CMS Physics Analysis Summary HIG-12-045". `http://cds.cern.ch/record/1494149`, 23/6/2013.

[150] **CMS Collaboration**, "CMS Physics Analysis Summary HIG-13-004". `http://cds.cern.ch/record/1528271`, 23/6/2013.

[151] **CMS Collaboration**, "CMS Physics Analysis Summary HIG-12-043". `http://cds.cern.ch/record/1493615`, 23/6/2013.

[152] **ATLAS Collaboration**, "ATLAS Note CONF-2012-091, Table 6". `http://cds.cern.ch/record/1460410`, 23/6/2013.

[153] **Tevatron New Physics Higgs Working Group, CDF Collaboration, D0 Collaboration**, "Updated Combination of CDF and D0 Searches for Standard Model Higgs Boson Production with up to 10.0 fb^{-1} of Data", `arXiv:1207.0449`.

[154] **CMS Collaboration**, "CMS Physics Analysis Summary HIG-12-015". `http://cds.cern.ch/record/1460419`, 23/6/2013.

[155] **CMS Collaboration**, "CMS Physics Analysis Summary HIG-13-014". `http://cds.cern.ch/record/1546776`, 23/6/2013.

[156] C. McNeile, C. Davies, E. Follana, K. Hornbostel, and G. Lepage, "High-Precision f_{B_s} and HQET from Relativistic Lattice QCD", *Phys.Rev.* **D85** (2012) 031503, `arXiv:1110.4510`.

[157] A. J. Buras, M. Jamin, and P. H. Weisz, "LEADING AND NEXT-TO-LEADING QCD CORRECTIONS TO ε-PARAMETER AND B^0–$\overline{B}^0$ MIXING IN THE PRESENCE OF A HEAVY TOP QUARK", *Nucl.Phys.* **B347** (1990) 491–536.

[158] **HPQCD Collaboration**, E. Gámiz, C. T. Davies, G. P. Lepage, J. Shigemitsu, and M. Wingate, "Neutral B Meson Mixing in Unquenched Lattice QCD", *Phys.Rev.* **D80** (2009) 014503, `arXiv:0902.1815`.

[159] Heavy Flavor Averaging Group. `http://www.slac.stanford.edu/xorg/hfag/rare/`, 23/6/2013.

Acknowledgements

I would like to thank everybody who supported me and my work in the last years.

First and most all, I would like to thank Ulrich Nierste for the supervision of this thesis. He gave me as much freedom in research as I wanted, but he always took the time for inspiring discussions about physical problems and encouraged me, when I required help. He taught me a lot about the exciting fields of flavour and high energy physics, but also about the academic life.

Next, I want to thank Martin Wiebusch, who patiently advised me in all technical, statistical and physical details that I encountered, and modified his illustrations to fit my notation. I am grateful to Alexander Lenz for his continued support even after my Diploma thesis and his help with my applications. In this context I also want to express my gratitude to Michael Chanowitz.

Also the rest of our little collaboration needs to be mentioned: regular fruitful discussions with Heiko Lacker, Andreas Menzel and Geoffrey Herbert about physical details but also concerning technical topics steadily pushed forward the progress of this work. Moreover, I would like to thank the CKMfitter group, especially Jérôme Charles, for technical support with the CKMfitter package.

I am grateful to Dieter Zeppenfeld, who was my second supervisor and advisor.

I had the privilege to spend the past years at the TTP surrounded by many nice colleagues (also from the ITP), who contributed to a pleasant and productive atmosphere. In particular, I want to thank Markus Bobrowski and Philipp Frings for sharing an office and lots of cake. In many seminars and lectures, I learned a lot about various aspects of high energy physics; I would like to thank Johann Kühn and Matthias Steinhauser, who organized most of them. Thomas Hermann deserves a special mention for providing me with his $b \to s\gamma$ code. Furthermore, he helped together with Peter Marquard and Jens Hoff to maintain our computer system, which constitutes an essential part of the working conditions. I also appreciate Martina Schorn's assistance when she helped me filling in forms.

This thesis would contain many errors if it had not been proofread by Martin Wiebusch, Markus Bobrowski, Alexander Lenz, Andreas Scholz, Elio König and my father. Many thanks to all of them!

Finally, I want to express my deepest gratitude to my family and my friends, who made me the person I am, and especially to my school teachers Gerhard Forster and Trevor Plant, who sparked my enthusiasm for physics and thus made me the physicist I am.